

# Experimental & CFD Analysis of Fixed Bed Heat Transfer for Ethylene Epoxidation

---

A Major Qualifying Project Report

Submitted to the Faculty of the  
WORCESTER POLYTECHNIC INSTITUTE

in partial fulfillment of the requirements for the  
Degree of Bachelor of Science  
In Chemical Engineering

By

Edward Chau \_\_\_\_\_

Jason Krug \_\_\_\_\_

Date: April 2010

Approved:

\_\_\_\_\_  
Dr. Anthony G. Dixon, Advisor

## **Abstract**

In this study, we conducted experiments and simulations to analyze the heat transfer phenomena in fixed bed tubes jacketed for cooling water flow. These experiments studied the cooling of heated air flowing at varying Reynolds numbers through three columns of different diameter. The experimental results were compared to those acquired by a Computational Fluid Dynamic (CFD) simulation of a similar system. With the CFD validated by experiment, we then studied the heat transfer of ethylene epoxidation in a cooled tube by simulation.

## Executive Summary

In this study, heat transfer effects of cooled packed tubes were explored using both an experimental method and computer simulation. Our experiments studied the effect of varying column diameter and flow rate on heat transfer through a tower jacketed for cooling water flow. These experiments produced results similar to prior experiments, and we concluded that more radial heat transfer occurs with smaller column diameter, though other parameters are functions of flow rate and superficial velocity.

In order to show that our computer simulation produced meaningful results, simulation data was compared to experimental data of similar conditions. Our simulations had similar trends to those of the experiments, with some error which could be attributed to differences between the experimental conditions and those of the computational model. The simulations were concluded to be a satisfactory method to analyze heat transfer.

Once validated, our simulation was used to study the heat transfer effects of a reaction occurring within the computational model. Ethylene epoxidation is an exothermic reaction that occurs only on the surface of the silver catalyst particles, and these conditions were coded into our simulation. The model output expected results, with heat being generated on the surface of the particles, and the cooled wall maintaining a nearly constant temperature in the fluid.

## Table of Contents

Abstract .....	i
Executive Summary .....	ii
List of Figures .....	v
List of Tables .....	vi
Introduction .....	1
Background.....	5
Data Acquisition Techniques .....	5
IPPF Model .....	6
Theory behind Dimensionless Parameters .....	10
Experimental Procedure .....	12
Tower Operation .....	18
Safety Considerations.....	19
CFD Methodology .....	20
Experimental Comparison .....	21
Ethylene Epoxidation Reaction.....	23
Experimental Results .....	28
Experimental Dimensionless Temperature Profiles .....	28
Dimensionless Parameters with respect to Reynolds Number .....	31
Experimental to CFD Temperature Profile .....	35
Comparison of Experimental Temperature Output to CFD Output.....	37
Ethylene Oxide Reaction Results.....	39
Conclusions .....	42

Nomenclature.....	43
Greek letters.....	44
Subscripts.....	44
Bibliography.....	45
Appendix.....	46
Ethylene Epoxidation Reaction Kinetics.....	46
Reaction Enthalpy.....	49
Diffusivity.....	51
Spherical Particle Diameter.....	52
Reynolds Number.....	52
Dimensionless Temperature vs. Dimensionless Radial Position.....	53
First Bed Height.....	53
All Bed Heights.....	61
Heat Transfer Parameters vs. $Re$ .....	69
Combined $kr/k_f$ , $Nu_w$ .....	75
Experimental Temperature Profile.....	76
Comparison of Experimental T-Profile to CFD.....	77

## List of Figures

Figure 1: Ethylene Epoxidation on Silver Catalyst Mechanism (Sachtler et al., 1981).....	1
Figure 2: Various Techniques Utilized for Obtaining Radial Temperature Profiles (Thomeo et al., 2004).....	5
Figure 3: Schematic of Laboratory Apparatus.....	12
Figure 4: Schematic of Thermocouple Cross .....	14
Figure 5: Screenshot of DMM Scan .....	15
Figure 6: Screenshot of DMM Config .....	16
Figure 7: Screenshot of 120° Segment of Packing .....	20
Figure 8: Dimensionless Temperature Profile Parabolic Fit for $\frac{3}{8}$ " ceramic rings in the 2 inch column, with a Reynolds Number of 878 at the First Bed Height.....	28
Figure 9: Dimensionless Temperature Profile Parabolic Fit for $\frac{3}{8}$ " ceramic rings in the 3 inch column, with a Reynolds Number of 464 at the First Bed Height.....	28
Figure 10: Dimensionless Temperature Profile Parabolic Fit for $\frac{3}{8}$ " ceramic rings in the 4 inch column, with a Reynolds Number of 296 at the First Bed Height.....	29
Figure 11: Dimensionless Temperature Profile Fit for $\frac{3}{8}$ " ceramic rings in the 2 inch column, with a Reynolds Number of 464 at Various Bed Heights .....	29
Figure 12: Dimensionless Temperature Profile Parabolic Fit for $\frac{3}{8}$ " ceramic rings in the 4 inch column, at various Reynolds Numbers .....	30
Figure 13: Radial Peclet Number with respect to Reynolds Number for $\frac{3}{8}$ " ceramic rings in the 2 inch column .....	31
Figure 14: Radial Peclet Number with respect to Reynolds Number for $\frac{3}{8}$ " ceramic rings in the 3 inch column .....	31
Figure 15: Radial Peclet Number with respect to Reynolds Number for $\frac{3}{8}$ " ceramic rings in the 4 inch column .....	32
Figure 16: $Nu_w$ with respect to Reynolds Number for $\frac{3}{8}$ " ceramic rings in Various Cooled Tube Diameters.....	32
Figure 17: $kr/k_f$ with respect to Reynolds Number for $\frac{3}{8}$ " ceramic rings in Various Cooled Tube Diameters.....	33
Figure 18: Biot Number with respect to Reynolds Number for $\frac{3}{8}$ " ceramic rings in the 2 inch column.....	34

Figure 19: Temperature Profile Parabolic Fit for 3/8" ceramic rings in the 2 inch column, at various bed heights.....	35
Figure 20: Temperature Contour of Top and Bottom for 4"-6" for AirOnlyrxn.cas with No Reaction.....	36
Figure 21: Temperature Contour of Particle 2 and Symmetry Boundaries for AirOnlyrxn.cas with No Reaction .....	36
Figure 22: Temperature Profile Comparison of Experimental and CFD for the 4" - 6" bed depth, in the 2 inch column .....	37
Figure 23: Temperature Profile Comparison of Experimental and CFD for the 6" - 8" bed depth, in the 2 inch column .....	37
Figure 24: Temperature Profile Comparison of Experimental and CFD for the 8"-10" bed depth, in the 2 inch column .....	38
Figure 25: Temperature Contour of Top and Bottom of 2 inch packing for the EthyleneOxidern.cas .....	40
Figure 26: Temperature Contour of Particle 2 and Symmetry Boundaries for the EthyleneOxidern.cas .....	40

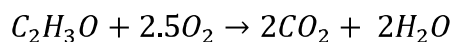
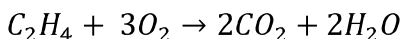
## List of Tables

Table 1: Maximum Air Flow Rate as a Function of Pressure .....	13
Table 2: Thermocouple Radial Positions .....	14
Table 3: List of Experimental Runs for various Re .....	17
Table 4: List of Constants for Ethylene Epoxidation.....	23
Table 5: Reaction Rates of Ethylene Epoxidation .....	39

## Introduction

Ethylene oxide is one of the top chemicals produced in the United States, with approximately 6.78 billion pounds produced in 1994, in the US alone (Minahan et al., 1996). The epoxidation of ethylene to create ethylene oxide is common to the chemical industry due to the importance of ethylene oxide. Ethylene oxide serves as an intermediate to various products, such as ethylene glycol, and polyethylene-oxide. Ethylene glycol is a primary ingredient in antifreeze and polyethylene-oxide can be used as a detergent additive. Ethylene oxide's reactivity allows it to be used as a reactant, but its reactivity also limits its ability to be shipped for danger of explosion and toxicity. The product is usually produced on the site and pumped directly to neighboring consumers e.g. glycol plant. (Turton et al., 2009)

The reactions are as follows:



Reaction 1 is the epoxidation of ethylene and reaction 2 is the complete combustion of ethylene. These two reactions are considered to be parallel and dependent on the species' interaction with the catalyst. Depending on the conditions, the third reaction, oxidation of ethylene oxide, may occur with a much lower rate compared to reactions 1 and 2 (Lafarga et al., 2000)

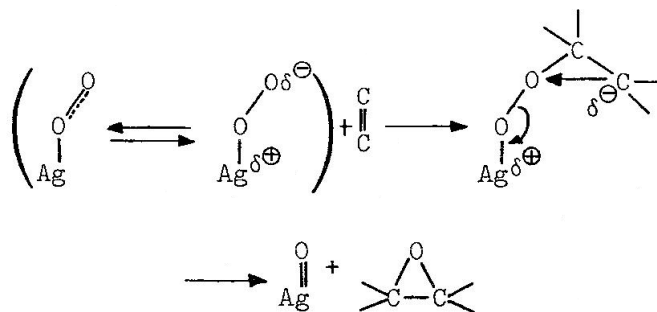


Figure 1: Ethylene Epoxidation on Silver Catalyst Mechanism (Sachtler et al., 1981)

The catalyst used for this reaction is silver on an inert support (Alumina). The first catalyst used for ethylene epoxidation was a “supported catalyst with silver deposited on ceramic substrate,” (Porcelli et al., 1981) Silver is unique because it allows oxygen to adsorb onto it. These weak oxygen-to-silver bonds allow the formation of ethylene oxide when reacted with ethylene. A hypothesis of the mechanism is shown in Figure 1.

Large catalyst particles are generally favored, due to a reduced pressure drop thus a reduction in power consumption. The catalyst’s productivity can be improved through “selection of support, use of alkaline promoters, chlorine containing compounds as feed additives and optimal distribution of catalyst in pellets.” (Lafarga et al., 2000) Ethylene oxide selectivity has increased from 68% to 80% due to advancements in the industrial process. A large part of this increase is due the addition of alkali promoters to the catalyst (Minahan et al., 1996)

Although alkali promoter and catalyst size are both important aspects to achieving a high selectivity/conversion of ethylene oxide, this variable will not be examined in this study.

Kinetic expressions adapted from Stoukides and Pavlou, by Turton, et al. are as follows:

$$r_1 = \frac{1.96 \exp\left(-\frac{2400}{RT}\right) p_{ethylene}}{1 + 0.00098 \exp\left(\frac{11,200}{RT}\right) p_{ethylene}}$$

$$r_2 = \frac{0.0936 \exp\left(-\frac{6400}{RT}\right) p_{ethylene}}{1 + 0.00098 \exp\left(\frac{11,200}{RT}\right) p_{ethylene}}$$

$$r_3 = \frac{0.42768 \exp\left(-\frac{6200}{RT}\right) p_{ethylene\ oxide}^2}{1 + 0.000033 \exp\left(\frac{21200}{RT}\right) p_{ethylene\ oxide}^2}$$

Stoukides and Pavlou studied the effects of ethylene oxidation using an Ag catalyst film which was deposited on the flat bottom of an 8% yttria stabilized tube with a cross sectional area

of 2 cm<sup>2</sup> (1985). Turton modified the kinetics for industrial use, for an excess amount of O<sub>2</sub>, air only (2009).

It can be observed from the reaction rates that the partial pressure of ethylene influences the reaction rate of ethylene oxide formation. Partial pressure of ethylene oxide does influence the reaction rate of the third reaction, but it is not very relevant due to a negligible reaction rate. Although these were the kinetic expressions used in our study, various other rate expressions have been reported in literature. A study of Turton's kinetics along with his specified conditions was conducted utilizing Fluent 6.3.

Because ethylene epoxidation is highly exothermic, the reaction is carried out commercially in a cooled wall tubular packed bed reactor. It is imperative to control the temperature in the packed bed in order "to maintain selectivity, to prevent catalyst deactivation or runaway," (Borman et al, 1992). Ethylene oxide has greater selectivity at lower temperatures, but slower reactions rates (Zomerdijk et al., 1981). High temperatures can lead to favoring of reactions 2 and 3 as well due to enough energy to overcome the activation energies of reactions 2 and 3. That is why when designing a cooled tube reactor; the diameter and heat transfer parameters and temperature profiles of the tubes are examined. Properly designed models can save both time and money due to longer lasting life for the tubes and less repairs.

In order to study the effects of ethylene epoxidation in cooled tubes, Computational Fluid Dynamics (CFD) is utilized. Improvements in computational speed and memory and software have allowed CFD to solve for flow and energy balances numerically. The use of CFD in simulating fixed bed reactors allow for flow profiles to be established, and used in simulating reactions. CFD has been used in the past for fixed bed heated tubes (Nijemeisland, 2000) as well

as the simulation of endothermic reactions such as methane steam reforming (MSR). It is our goal to extend this method to exothermic reactions.

Prior to altering the supplied C file for the exothermic reaction of ethylene epoxidation, the CFD has to be verified experimentally. This was done for airflow with no reaction, using  $\frac{3}{8}$ " ceramic rings. Although Turton, et al. utilized spherical catalyst particles, cylindrical rings were used in this study. Borman et al. used industrial ringed shaped silver on  $\alpha$ -alumina catalyst, in his experimental study of selective oxidation of ethane in cooled tubular packed reactors (1992).

Although its effect will not be studied, an increase in the inner diameter of the ring, leads to a decrease in pore length for diffusion, thus increasing mass transfer rate. This increases the effectiveness, but reduces the reaction rate per unit volume of reactor as well because of less catalyst area. The  $\frac{3}{8}$ " ceramic rings are packed to the desired height in the experimental column, and radial temperature are recorded at each height. Temperature profile of the column and the CFD are compared in order to validate use the CFD for ethylene epoxidation.

## Background

### Data Acquisition Techniques

In order to design optimal packed bed reactors, temperature profiles need to be examined.

There are four common techniques for measuring radial temperature profiles.

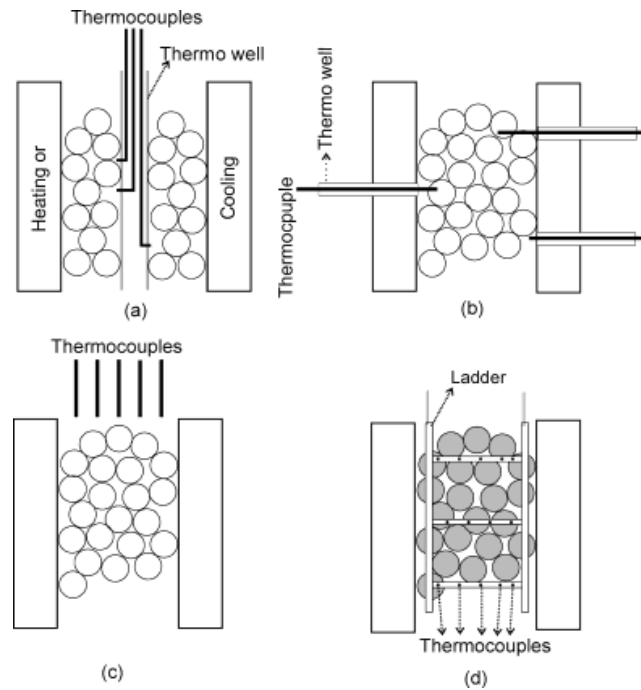


**Figure 2: Various Techniques Utilized for Obtaining Radial Temperature Profiles: a) Axial thermo-well, b) Radial thermo-well, c) Thermocouples above the bed, d) Ladder frame (Thomeo et al., 2004).**

Axial thermo well utilizes a method in which the thermo well is placed longitudinally through the center of the bed. The thermo well contains several thermocouples with tips at various radial and axial positions. Meant to be used for small diameter tubes, the axial thermo well allows several temperature profiles to be recorded simultaneously. This method however, disrupts the structure of the bed as well as the heat transfer. (Thomeo et al., 2004)

The radial thermo well method has wells located at various heights and radial positions, with each one containing one or more thermocouples. Like the axial thermo-well, this method allows temperature sampling to be conducted simultaneously in a single test. But like the axial thermo-well, this technique disrupts the structure of the bed. (Thomeo et al., 2004)

The thermocouples above the bed is the most commonly used technique. A group of thermocouples at various radial and angular positions rest slightly above the packing. Height above packing varies with user; some say 3-6mm while others say 5-10mm. This technique requires more time because the temperatures profiles require to be taken at various heights rather than simultaneously. The setback to using this technique is that by increasing the bed height and adding more packing, one may disrupt the previous bed structure and compromise measurements. (Thomeo et al., 2004) Our analysis of cooled wall packed tubes utilizes the thermocouples above the bed technique.

The ladder frame method utilizes a ladder like structure which supports a set of thermocouples at many axial, radial and angular positions. This allows temperature profiles to be conducted simultaneously. Like the other techniques this method's flaw also lies in the disruption of the bed structure. (Thomeo et al., 2004)

### **IPPF Model**

The IPPF model requires a number of assumptions (Borkink et al., 1993):

- System at steady state
- System considered to be pseudo-homogeneous
- No axial dispersion of heat
- No free convection of heat
- No reaction occurs
- No heat radiation
- No pressure drop through the packed bed
- No radial variation of the superficial gas velocity
- Constant wall temperature

- Physical property of gas and solid independent of temperature

Because of heat loss in the calming section, which will be described in detail later, the IPPF model utilizes the temperature at the initial bed height as the inlet and compares it to subsequent bed heights.

The IPPF model is derived from the dimensionless energy balance:

$$GC_p \frac{\partial T}{\partial z} = k_r \left( \frac{\partial^2 T}{\partial r^2} + \frac{1}{r} \frac{\partial T}{\partial r} \right) \quad (1)$$

The boundary conditions are as follows:

$$T = T_{z,o}(r) \text{ at } z = z_o \quad (2a)$$

$$\frac{\partial T}{\partial r} = 0 \text{ at } r = 0 \quad (2b)$$

$$-k_r \frac{\partial T}{\partial r} = h_w(T - T_w) \text{ at } r = R \quad (2c)$$

The energy balance and boundary conditions are made dimensionless with these definitions:

$$\vartheta = \frac{(T - T_w)}{(T_o - T_w)} \quad (3)$$

$$y = \frac{r}{R} \quad (4)$$

$$x = z/R \quad (5)$$

$$Pe_R = \frac{GC_p R}{k_r} \quad (6)$$

$$Bi = \frac{h_w R}{k_r} \quad (7)$$

In this case, using the first measurement height at  $z=z_o$  as the inlet temperature, we get:

$$\zeta = \frac{z/L - z_o/L}{1 - z_o/L} \quad (8a)$$

$$\frac{\partial \zeta}{\partial z} = \frac{1}{L} \frac{1}{1 - z_o/L} \quad (8b)$$

So:

$$\frac{\partial T}{\partial z} = \frac{\partial T}{\partial \zeta} \frac{\partial \zeta}{\partial z} = \frac{1}{L} \frac{1}{1 - z_o/L} \frac{\partial T}{\partial \zeta} \quad (9)$$

Substitute into Eq. 1 to obtain:

$$GC_p \frac{1}{L} \frac{1}{1 - z_o/L} \frac{\partial \vartheta}{\partial \zeta} = k_r \frac{1}{R^2} \left( \frac{\partial^2 \vartheta}{\partial y^2} + \frac{1}{y} \frac{\partial \vartheta}{\partial y} \right) \quad (10)$$

Solving for  $\frac{\partial \vartheta}{\partial \zeta}$ :

$$\frac{\partial \vartheta}{\partial \zeta} = \frac{k_r L}{GC_p R^2} \left( 1 - \frac{z_o}{L} \right) \left( \frac{\partial^2 \vartheta}{\partial y^2} + \frac{1}{y} \frac{\partial \vartheta}{\partial y} \right) \quad (11)$$

Define:

$$Bo_{h,r}^\theta = \frac{GC_p R^2}{k_r L} \quad (12)$$

$$\theta = \frac{\vartheta}{\vartheta_o} \quad (13)$$

Where:

$$\vartheta_o = \frac{(T|_{r=o} - T_w)}{(T_o - T_w)} \quad (14)$$

Gives:

$$\frac{\partial \theta}{\partial \zeta} = \frac{1}{Bo_{h,r}^\theta} \left( 1 - \frac{z_o}{L} \right) \left( \frac{\partial^2 \theta}{\partial y^2} + \frac{1}{y} \frac{\partial \theta}{\partial y} \right) \quad (15)$$

With boundary condition:

$$-k_r \frac{\partial T}{\partial r} = h_w (T - T_w) \quad (16)$$

This can be made dimensionless into:

$$-k_r \frac{1}{R} \frac{\partial \vartheta}{\partial y} = h_w \vartheta \quad (17)$$

This may be reduced to the following:

$$\frac{\partial \vartheta}{\partial y} + Bi\vartheta = 0 = \frac{\partial \theta}{\partial y} + Bi\theta \quad (18, 19)$$

Assume a parabolic profile at  $z = z_o$ :

$$T = T|_{r=0} + A'r^2 \quad (20)$$

Where  $A' < 0$  for cooling.

$$\frac{(T - T_o)}{(T_w - T_o)} = \frac{(T|_{r=0} - T_w)}{(T_o - T_w)} + \frac{A'}{T_o - T_w} R^2 y^2 \quad (21)$$

$$\vartheta = \vartheta_o + \frac{A'R^2}{T_o - T_w} y^2 \quad (22)$$

Thus:

$$\theta = \frac{\vartheta}{\vartheta_o} = 1 + \frac{A'R^2}{(T_o - T_w)\vartheta_o} y^2 = 1 - Ay^2 \quad (23)$$

Where A is always as defined:

$$A = \frac{A'R^2}{(T_o - T_w)\vartheta_o} > 0 \quad (24)$$

A series of additional definition and mathematics is conducted with a corrected Bordenstein number of:

$$Bo_{h,r}^{\theta}(\text{corrected}) = \frac{GC_p R^2}{k_r L} \frac{1}{1 - z_o/L} = Bo_{h,r}^{\theta} \frac{1}{1 - z_o/L} \quad (25)$$

Leading to:

$$\vartheta = 1 - 2(1 - \vartheta_o) \sum_{i=1}^{\infty} \left\{ \frac{[(Bi\lambda_i^2 + 4ABi - 2A\lambda_i^2 - ABi\lambda_i^2)J_o(\lambda_i y)]}{\lambda_i^2 [\lambda_i J_o(\lambda_i) + Bi J_i(\lambda_i)]} e^{\left[ -\frac{\lambda_i^2}{Pe_R} (x - x_o) \right]} \right\} \quad (26)$$

$$= 1 - 2(1 - \vartheta_o) \sum_{i=1}^{\infty} \left\{ \frac{(Bi + 4ABi/\lambda_i^2 - 2A - ABi) J_o(\lambda_i y)}{[Bi^2 + \lambda_i^2] J_o(\lambda_i)} e^{\left[ -\frac{\lambda_i^2}{Pe_R} (x - x_o) \right]} \right\} \quad (27)$$

A more detailed derivation is located in Ashman et al.

## Theory behind Dimensionless Parameters

Although the IPPF model defines:

$$\vartheta = \frac{(T - T_w)}{(T_o - T_w)} \quad (28)$$

The Fortran Program defines:

$$\vartheta = \frac{(T - T_o)}{(T_w - T_o)} = 1 - \frac{(T - T_w)}{(T_o - T_w)} \quad (29)$$

From this definition, it is expected for dimensionless temperature to increase with respect to radial position, since the denominator will be constant while thermocouple readings of temperature decrease with respect to radial position.

Reynolds number in the fixed bed is defined as:

$$Re = \frac{v_s \rho d_p}{\mu} \quad (30)$$

As the definition shows, Re is proportional to superficial velocity. It also increases with respect to particle diameter as well. The Re for the columns were calculated in the lab based on a chart indicating the max flow rates. The Re is expected to have a great impact on the heat transfer coefficients to be calculated for.

Peclet number is defined as:

$$Pe_r = \frac{GC_p R}{k_r} \quad (6)$$

But can also be written as:

$$Pe_r = \frac{Re * Pr}{k_r / k_f} \quad (31)$$

The radial Peclet number should increase rapidly with respect to Re at low superficial velocities and flatten out at a constant at higher Reynolds numbers. At low Re, conduction dominates where  $k_r/k_f$  increases with respect to Reynolds number. At high Re, turbulent dispersion dominates and the Peclet number is rearranged as:

$$Pe_r = \frac{Re * Pr}{m * Re + b} \quad (32)$$

Because Re is such a large value, the intercept of b does not have a great impact on the radial Peclet number and it is constant.

The Biot number is defined as:

$$Bi = \frac{h_w R}{k_r} = Nu_w \frac{R/d_p}{k_r / k_f} \quad (33,34)$$

Because  $k_r$  is linearly proportional to Re and the heat transfer coefficient at the wall increases slowly, with respect to Re, it is expected for the Biot number to decrease with respect to increase in Reynolds number. It is also predicted that since the Nusselt number at the wall is approximately  $Re^{0.8}$ , then Biot number should decrease proportionally with respect to Re as well.

The ratio of diameter of tube to diameter of particle is the dimensionless parameter N.

$$N = \frac{2 * R}{d_p} \quad (35)$$

The wall heat transfer coefficient,  $h_w$  and the effective radial thermal conductivity,  $k_r$  are related to one another through the equation of:

$$\frac{1}{U} = \frac{1}{h_w} + \frac{\alpha R}{k_r} \quad (36)$$

U, the overall heat transfer coefficient is dependent of these two variables and as  $h_w$  increases,  $k_r$  decreases and vice versa keeping U at a constant.

## Experimental Procedure

The equipment used in this experiment is shown in the figure below.

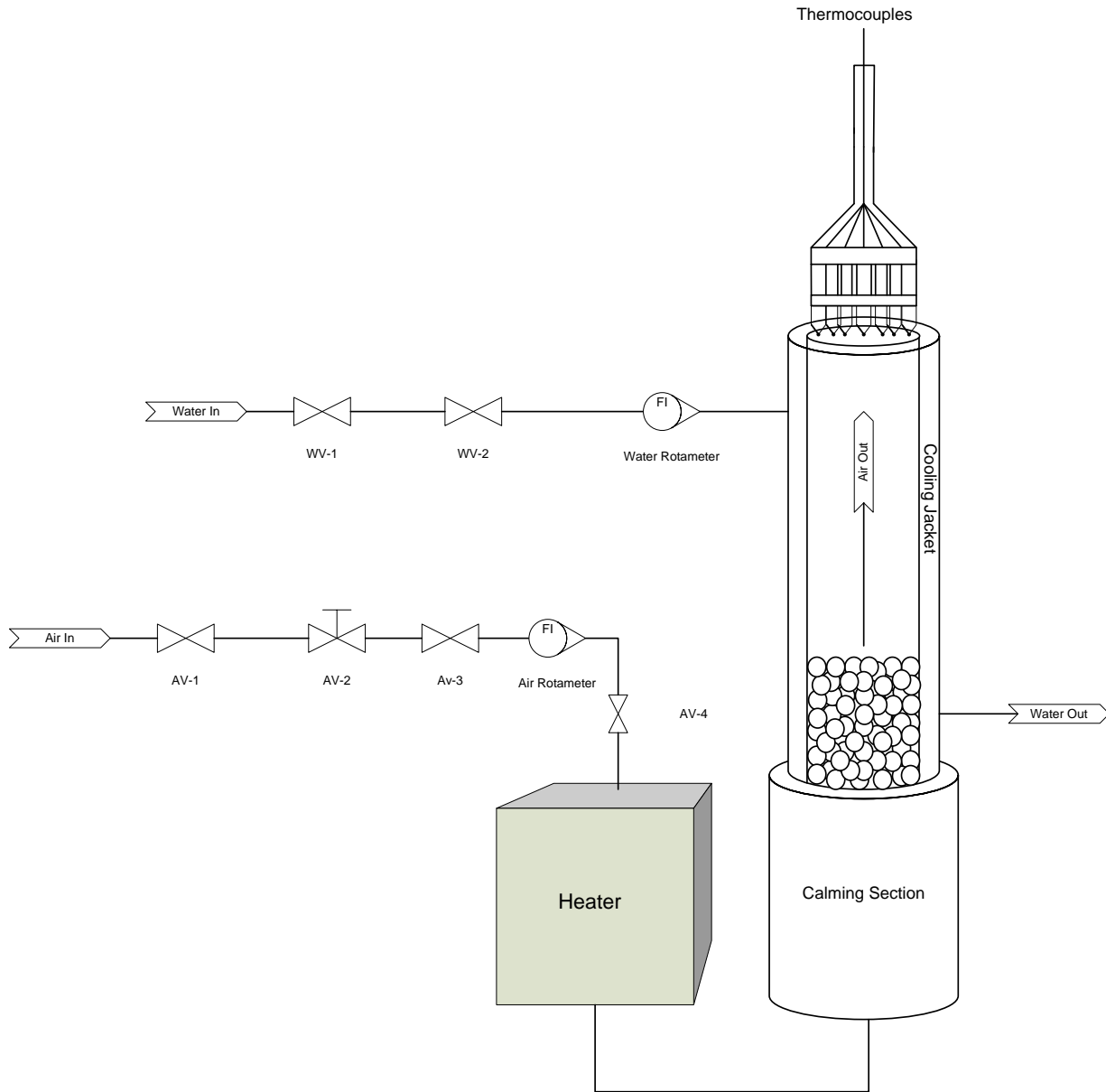


Figure 3: Schematic of Laboratory Apparatus

The column was jacketed to allow for cooling water to flow and remove heat from the heated air stream. A calming section upstream of the column allows for even distribution of air flow. This calming section was filled with  $\frac{1}{4}$  inch nylon spheres, with a steel mesh separating the nylon spheres from the column packing. The columns had inside diameters of 2 inches, 3 inches,

and 4 inches. The columns were packed with  $\frac{3}{8}$  inch one-hole ceramic rings. Packing heights of 4, 6, 8, and 10 inches were studied to evaluate the temperature profile as air progresses through the tower.

The flow rate of water and air was measured by using a rotameter. For air flow, the maximum flow rate was dependent on the pressure of the inlet air. The following list shows the change in maximum flow rate of air with the inlet pressure. For each tower, five different flow rates of air were studied to evaluate how heat transfer is affected by air flow rate.

Pressure (psig)	Flow Rate (CFM)	Pressure (psig)	Flow Rate (CFM)	Pressure (psig)	Flow Rate (CFM)
0	4.90	24	3.02	48	2.37
1	4.73	25	2.98	49	2.30
2	4.60	26	2.94	50	2.34
3	4.46	27	2.91	51	2.32
4	4.34	28	2.88	52	2.30
5	4.23	29	2.84	53	2.28
6	4.13	30	2.80	54	2.27
7	4.03	31	2.78	55	2.25
8	3.94	32	2.75	56	2.23
9	3.86	33	2.72	57	2.22
10	3.78	34	2.69	58	2.21
11	3.70	35	2.67	59	2.19
12	3.64	36	2.64	60	2.18
13	3.57	37	2.61	61	2.16
14	3.51	38	2.59	62	2.15
15	3.45	39	2.56	63	2.13
16	3.39	40	2.54	64	2.12
17	3.34	41	2.52	65	2.10
18	3.28	42	2.49	66	2.09
19	3.23	43	2.47	67	2.08
20	3.19	44	2.45	68	2.07
21	3.15	45	2.43	69	2.05
22	3.10	46	2.41	70	2.04
23	3.06	47	2.39		

Table 1: Maximum Air Flow Rate as a Function of Pressure

Inlet air is heated to 100 °C using a heater controlled by a Micromega CN77000 PID controller. This controller uses a thermocouple to read the temperature of air downstream of the heater. If this temperature is less than 100 °C, the heater will provide more heat, until the

temperature at the thermocouple approaches 100 °C, when the controller would signal the heater to stop heating. Once the temperature at the thermocouple begins to drop again, the heater is signaled to begin heating once more. This process causes an oscillation in the inlet temperature of approximately  $\pm 0.5$  °C.

Temperature at the air outlet was measured using a thermocouple cross. The cross was composed of 8 arms set a 45 degree angles from each other, each with 3 thermocouples, including a center thermocouple. The thermocouples were arranged such that 6 different radii could be measured simultaneously in 4 locations 90 degrees apart. A diagram and table of the thermocouple positions is shown below.

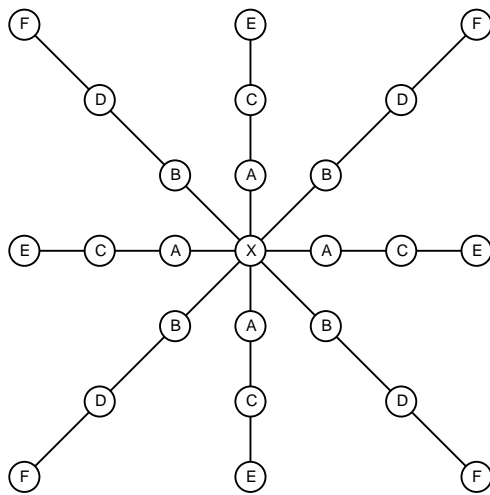


Figure 4: Schematic of Thermocouple Cross

Radial Position	2 inch Column (mm)	3 inch Column (mm)	4 inch Column (mm)
A	9	11.1	10.8
B	12	15.9	20.8
C	15	23.9	31
D	18.5	30.9	39.8
E	21.5	33.3	43.9
F	24	35.4	46.1
X	0	0	0

Table 2: Thermocouple Radial Positions

Temperature readings from the thermocouples were recorded using a Keithley Integra Series 2700 Datalogger. This instrument is capable of collecting up to 200 channels of thermocouple data, of which we used 35, along with other functions which we did not use, such as the digital multi-meter.

The Keithley instrument was connected to a computer running ExceLINX, an add-in for Microsoft Excel. Once ExceLINX is installed to the computer, the relevant sheets may be added to Excel by selecting ExceLINX → DMM Config and DMM Scan. To properly configure the program to record data, the DMM Config and Scan sheets were set as in the screenshots below.

ExceLINX		KEITHLEY A Greater Measure of Confidence	
Task: Scan DMM Channels			
Task	Name	DMM Scan	
	Description		
	Created By	drawde	
	Company	Worcester Polytechnic Institute	
	Date Created	2/13/2010	
	Date Modified	2/13/2010	
	Status/Cmds		
Configuration	Worksheet	DMM Config	
Trigger	Model	Scan	
	Source	Immediate	
	Delay	Auto	sec
	Reading Count	INF	
	Timer		0.1 sec
	Monitor	None	
	Monitor Limits	None	
Data Location	Worksheet	Sheet1	
	Starting Col	A	
	Starting Row	1	
	Organize By	Rows	
	Autoincrement	Use one table	
	Auto Wrap	On	
	Log File		
Data Display	Format	Delimited text (comma)	
	Add Channel Tags	Yes	
	Add Channels	Yes	
	Add Units	No	
	Scroll Display	No	
	Limits	None	
	Timestamp	None	
Update Interval		100 msec	
Task Data			

Figure 5: Screenshot of DMM Scan

Task: Configure Scanning DMM Channels	
Task	Name DMM Config
	Description
	Created By drawde
	Company Worcester Polytechnic Institute
	Date Created 2/13/2010
	Date Modified 2/13/2010
Instrument	Status/Cmds
	Device KE2700_COM1
	Password
	Slot 1 Module M7700
	Slot 2 Module M7700
	Slot 3 Module
	Slot 4 Module
	Slot 5 Module
Front Panel Lockout On	
Setup	Line Sync Off
	Autozero On
	Display Digits 6½
	DCV Input Divider Off
	Open TC Detection On
Limits	Temp Scale °C
	Digital Outputs Off
	Pulse Output Off
	Polarity High
	Duration 60 sec
Master Latch Off	

Channel Scan List																									
Channel			Measurement			Scaling					Alarm Limits			Rep Filter		Sampling		Options							
Enb	List	Tag	Function	Range	Rel	Math	m/ref	b	U	En1	Hi1	Lo1	En2	Hi2	Lo2	Enb	Count	Rate	AC BW	Opt 1	Opt 2	Opt 3	Opt 4		
On	101-120,201-214		TEMP	K	Off	None				Off			Off			Off			SLOW		INT				

Figure 6: Screenshot of DMM Config

To start recording data, “Start” was selected from the “Status/Cmds” menu, followed by pressing enter. The sheet selected under “Worksheet” is where data will be recorded to, beginning at the row in the “Starting Row” option. To stop recording data, “Stop” was selected in the “Status/Cmds” menu, followed by immediately pressing enter. In the sheet recording data, each column shows the temperatures at a thermocouple, with the most recent values at the bottom row.

Runs were performed changing different variables. Three columns were used, with internal diameters of 2 inches, 3 inches, and 4 inches. Each column was run using bed depths of 4 inches, 6 inches, 8 inches, and 10 inches. At every bed depth, runs were made at 5 different Reynolds numbers, with the set dependent on the tower diameter, as shown in the table below.

<b>Tower Diameter (in)</b>	<b>Reynolds Numbers</b>				
2	878	789	693	622	532
3	464	395	330	286	228
4	296	246	199	149	102

**Table 3: List of Experimental Runs for various Re**

## Tower Operation

1. To fill the calming section of the tower, the top section of the tower needed to be unscrewed and removed.
2. The calming section was filled with the nylon spheres and covered with a wire mesh, followed by attaching the top of the tower.
3. Packing was added to the desired height, making sure that the particles are packed tightly to ensure uniform packing density.
  - a. Packing height is determined by subtracting the empty space above the top of the packing from the total height available in the empty tower
4. The thermocouple cross was prepped by adjusting the height of the cross bar such that the bottom of the cross would sit only a couple millimeters above the top of the packing. Also, the tips of the thermocouples were checked to make sure they were all straight (at the proper radius) and at a uniform height.
5. The thermocouple cross was lowered into the tower, making sure to not touch the top of the packing and not to bend the tips of the thermocouples.
6. ExceLINX and the Keithley Multimeter were turned on and configured as described previously.
7. Ensured that all valves are in the closed position, meaning that valves WV 1 and 2 and AV 1 and 3 were perpendicular to their piping and AV 2 was fully counter clockwise.
8. Valve WV 1 was fully opened, followed by opening WV 2 until the water flow rotameter read 80%.
9. AV 1 and AV 3 were fully opened.
10. AV 4 was set to allow for varying air flow within the desired range using only AV 2.
11. AV 2 was opened until the air flow rotameter read the desired value for the current run.

12. The heater was turned on using the Micromega controller.
13. Data was recorded by ExceLINX until the system reached steady state
  - a. Due to the oscillating nature of the heater, 'steady state' was determined to be when the temperatures only oscillated within  $\pm 0.3$  °C. The time it would take to reach steady state was dependent on air flow rate, varying between 1 hour for faster rates and 3 hours for slower rates.
14. The thermocouple cross was rotated 45 degrees within the tower, to allow for a total of 8 different readings at each radius on the cross.
15. Data was recorded once more by ExceLINX, by changing the starting row, to allow the data to be recorded in the same sheet. Data collection was stopped once the system reached steady conditions again.
16. Repeated steps 11 through 15 for each desired air flow rate.
17. To shut the system down, valves were closed in reverse order from how they were opened, and the heater was turned off.

## **Safety Considerations**

When the heater is running, and for at least 15 minutes after shutdown, the heater will be very hot, along with the tubing containing the hot air. Though the heater is insulated, it is recommended that the operator does not touch any part directly connected to the heater while it is running. While running the column, and especially when handling packing, gloves and safety glasses/goggles are recommended as the packing occasionally releases dust particles into the air that can irritate the eyes or get on the operator's hands. The Micromega controller requires air flow to properly control the output of the heater. If there is no air flow, the heater will overheat.

## CFD Methodology

To further analyze heat transfer in cooled tubes, we utilized FLUENT 6.3 CFD software. We were provided case files and a UDF file that would simulate methane steam reforming through a four inch diameter column packed with one inch diameter one-hole cylinders. First, these files were edited to simulate air flow without reaction, for comparison to our experiments. Second, these files were edited to simulate ethylene epoxidation as specified in Turton et al.

The mesh used in this study is a 120 degree segment of a packed tower, two inches high and two inches in radius, with flow traveling in the positive z direction. Particles are arranged such that the bottom and top boundaries are identical, and therefore allow for periodic conditions to be specified when solving for flow. The mesh contains a total of 4,555,433 cells. The internal boundaries of the 120 degree segment are symmetry boundaries to allow for simulating a full tower, though it should be noted that particles penetrating the symmetry boundaries will be mirrored, which would not be indicative of a realistic tower. For this reason, only phenomena around the full particle in the center of the mesh were considered when observing results (Taskin et al., 2007). Below is a screenshot showing the placement of particles in our mesh.

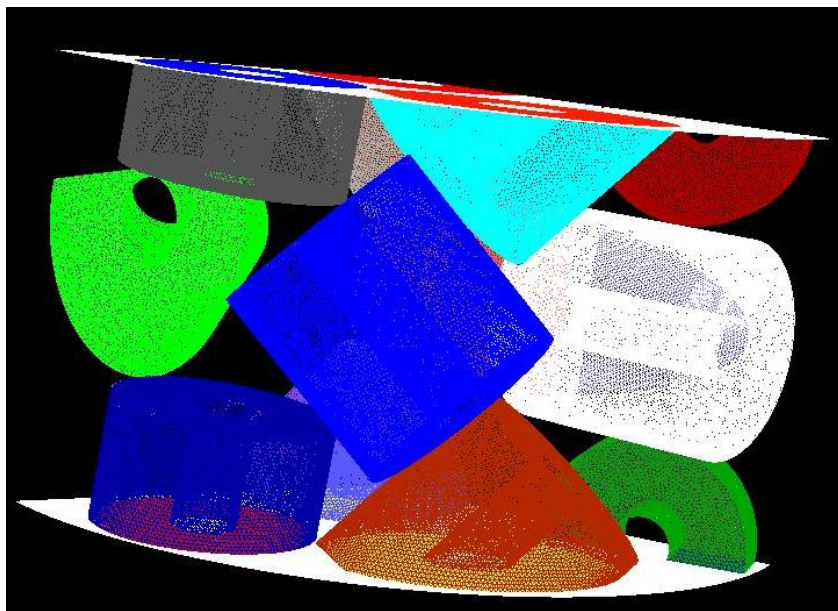


Figure 7: Screenshot of 120° Segment of Packing

Before heat transfer was calculated, a non-uniform flow profile at the bottom boundary was required. The “flow” case would be run, specifying a mass flow rate as a periodic condition, and a profile of velocity vectors, along with  $k$  and  $\omega$  turbulence variables would be generated. This profile would be used in the “reaction” case, which would solve for heat transfer and reaction rates.

The flow and reaction cases were run on a UNIX computer, with the work split between four processors. The time it would take for a case to run was dependent on the number of variables FLUENT was solving and the total number of iterations, from 8 hours for a case solving only for flow and turbulence for 500 iterations, to 48 hours for a case solving for flow and reaction for 2000 iterations. Post-processing was done on the same machines, using only one processor, as certain post-processing tools cannot run using multiple cores.

## Experimental Comparison

Part of our experimental runs included a 2 inch diameter column packed with three-eighth inch one-hole ceramic particles, for an  $N$  value of 5.33. We determined that this value best approximates our CFD model ( $N = 4$ ), and that comparing these two cases could validate our simulation. The 2 inch experimental column was run at heights of 4, 6, 8, and 10 inches, and at Reynolds numbers of 878, 693, and 622. The first changes made to the FLUENT cases were changing the material properties from methane steam reforming compounds to only air, and removing the UDF hooks to allow for simulation of air flow with no reactions. Material properties are adjusted in FLUENT by clicking on Define → Materials and adjusting the constants to the desired values. Mass flow rates through the tower can be set in Define → Periodic Conditions, and FLUENT will iterate for the pressure gradient between the periodic boundaries. For the FLUENT flow case, mass flow rates of 0.001032, 0.000815, and 0.000731

kg/s were set as periodic conditions. These mass flow rates correspond to one third of the total mass flow for each Reynolds number, because the mesh is for one third of a tower. In Solve → Controls → Solution, equations for flow and turbulence were set to be solved by FLUENT. An initial guess of the parameters is set in Solve → Initialize → Initialize, and the program was run for 1000 iterations. The resulting flow and turbulence profile was written using File → Write → Profile and selecting the bottom boundary, and saving the x, y, and z velocities, along with the  $k$  and  $\omega$  values for our turbulence model.

Further changes needed to be made to allow for the heat transfer case to run properly. A UDF file was input that specified an inlet temperature profile. A separate UDF file was generated for each run, each with the appropriate polynomial function describing inlet temperature, generated from our experimental data at the specified Reynolds numbers and 4, 6, and 8 inch tower heights. The flow profile generated in the first case is read by File → Read → Profile and selecting the previously saved bottom profile. Boundary conditions are set in FLUENT in Define → Boundary Conditions, followed by selecting the boundary to be edited. The bottom boundary was set to the flow profile and temperature profile generated above. The cooling wall boundary was set to a constant temperature (approximately 10 degrees Celsius), matching the cooling wall temperature of the similar experiment. The program was set to solve for flow, turbulence, and energy. This case was run for 2000 iterations, and the resulting top temperatures were compared to the 6, 8, and 10 inch profiles from the experimental data.

## Ethylene Epoxidation Reaction

Our ethylene epoxidation reaction specifications were from Stoukides and Pavlou, modified by Turton et al. The reactor specified by Turton et al. has 4,722 ten meter long tubes that are 7.38 centimeters in diameter, packed with 9 millimeter silver catalyst spheres. Cooling water removes 33,101 MJ/hour of heat. The inlet stream to the reactor is at conditions of 240 degrees C and 26.5 bar, at a total flow of 1,023,980 kg/h. The inlet mass fractions were: 0.028667 for ethylene, 0.000278 for ethylene oxide, 0.000545 for water, 0.197938 for oxygen, 0.001363 for carbon dioxide, and 0.771209 for nitrogen.

Similar to the flow case for only air flow, the material properties will need to be changed to contain ethylene, ethylene oxide, water, oxygen, carbon dioxide, and nitrogen. Due to the difference in N value between the textbook example and the CFD model, the mass flow rate set in the periodic conditions was adjusted to keep Reynolds number the same. One third of the mass flow rate for our conditions was determined to be 0.0135 kg/s. This was run for 2000 iterations and the velocity and turbulence variables were written for use in the reaction case.

In order to describe reaction on a catalyst surface, a UDF file was created to describe the complex conditions. First, a list of important constants was defined, as listed in the table below:

Gas Constant (kJ/mol-K)	0.0083144	Pre-exponent factor for $K_{et}$ (kPa <sup>-1</sup> )	$9.8 \cdot 10^{-6}$
$Rho_{S1}$ (Correction Factor)	100	Pre-exponent factor for $K_{eto}$ (kPa <sup>-2</sup> )	$3.3 \cdot 10^{-9}$
$Rho_{S2}$ (Correction Factor)	4000	$\Delta H$ of Reaction 1 (J/kmol)	105140000
Adsorption $\Delta H$ C <sub>2</sub> H <sub>2</sub> (kJ/mol)	-46.8608	$\Delta H$ of Reaction 2 (J/kmol)	1323158000
Adsorption $\Delta H$ C <sub>2</sub> H <sub>2</sub> O (kJ/mol)	-88.7008	$\Delta H$ of Reaction 3 (J/kmol)	1218018000
Activation Energy for R <sub>1</sub> (kJ/mol)	10.0416	Molecular Weight of C <sub>2</sub> H <sub>2</sub>	28.05
Activation Energy for R <sub>2</sub> (kJ/mol)	26.7776	Molecular Weight of C <sub>2</sub> H <sub>2</sub> O	44.05
Activation Energy for R <sub>3</sub> (kJ/mol)	25.9408	Molecular Weight of H <sub>2</sub> O	18.01534
Pre-exponent factor for $k_1$ (kmol/m <sup>3</sup> -s)	$1.96 \cdot 10^{-5}$	Molecular Weight of O <sub>2</sub>	31.9988
Pre-exponent factor for $k_2$ (kmol/m <sup>3</sup> -s)	$9.36 \cdot 10^{-7}$	Molecular Weight of CO <sub>2</sub>	44.00995
Pre-exponent factor for $k_3$ (kmol/m <sup>3</sup> -s)	$4.2768 \cdot 10^{-8}$	Molecular Weight of N <sub>2</sub>	28.0134

Table 4: List of Constants for Ethylene Epoxidation

The first functions of the UDF file defined ‘sources’ of each component due to reaction. Each component of the reaction, except nitrogen, was assigned to a user-defined scalar 0-4. This scalar would return the source defined as:

$$source = (\rho_{s1} * \alpha_1 * r_1 + \rho_{s2} * \alpha_2 * r_2 + \alpha_3 * r_3) * MW$$

where alpha is the stoichiometric coefficient of the component in each respective reaction, and r is the reaction rate in kmol/m<sup>3</sup>(solid)-s. Also required in the UDF is the derivative of the source term with respect to mass fraction and temperature. This is found by:

$$\frac{dS_i}{dY_i} = MW * (\alpha_1 * \rho_{s1} * \frac{dr1}{dPi} + \alpha_2 * \rho_{s2} * \frac{dr2}{dPi} + \alpha_3 * \frac{dr3}{dPi}) * \frac{dPi}{dY_i}$$

The derivatives with respect to partial pressure or mass fraction are found for each component. Below is a list of all the required functions and derivatives, with any omissions equal to zero.

$$ket = AKet * exp(-delhet/(R * T))$$

$$keto = AKeto * exp(-delheto/(R * T))$$

$$DENet = (1 + Pet * ket) * 0.6$$

$$DENeto = (1 + Peto^2 * keto) * 0.6$$

$$k1 = A1 * exp(-E1/(R * T))$$

$$r1 = k1 * Pet / DENet$$

$$k2 = A2 * exp(-E2/(R * T))$$

$$r2 = k2 * Pet / DENet$$

$$k3 = A3 * exp(-E3/(R * T))$$

$$r3 = k3 * Peto^2 / DENeto$$

$$\frac{dP_i}{dY_i} = \frac{P_T * MW_{av}}{MW_i * \left(1 - Y_i * \frac{MW_{av}}{MW_i}\right)}$$

$$\frac{dr_1}{dP_{et}} = (k1/DENet) - (k1 * Pet * ket * 0.6)/DEN^2$$

$$\frac{dr_2}{dP_{et}} = (k2/DENet) - (k2 * Pet * ket * 0.6)/DEN^2$$

$$\frac{dr_3}{dP_{eto}} = ((2 * k3 * Peto)/DENeto) * (1 - Peto^2 * keto * 0.6)/(DENeto)$$

The UDF file also contains a routine that adjusts the built-in mass fraction in the fluid cells to match that calculated by the user-defined scalars.

The next part of the UDF file specified reaction enthalpies. The heat generated by the reactions is specified as:

$$source = (\Delta H_{r1} * \rho_{s1} * r_1 + \Delta H_{r2} * \rho_{s2} * r_2 + \Delta H_{r3} * r_3)$$

with its derivative defined as:

$$dS[eqn] = (\Delta H_{r1} * \rho_{s1} * \frac{dr_1}{dT} + \Delta H_{r2} * \rho_{s2} * \frac{dr_2}{dT} + \Delta H_{r3} * \frac{dr_3}{dT})$$

FLUENT uses some of the functions specified above to solve this, along with the extra functions specified below.

$$\frac{dDENet}{dT} = -0.6 * \left( \frac{Pet * AKet * \Delta H_{et}}{R * T^2} \right) * \exp\left(\frac{\Delta H_{et}}{R * T}\right)$$

$$\frac{dDENeto}{dT} = -0.6 * \left( \frac{Peto^2 * AKeto * \Delta H_{eto}}{R * T^2} \right) * \exp\left(\frac{\Delta H_{eto}}{R * T}\right)$$

$$\frac{dk1}{dT} = k1 * \frac{E1}{R * T^2}$$

$$\frac{dk2}{dT} = k2 * \frac{E2}{R * T^2}$$

$$\frac{dk3}{dT} = k3 * \frac{E3}{R * T^2}$$

$$\frac{dr1}{dT} = (DENet * \frac{dk1}{dT} * Pet - k1 * Pet * \frac{dDENet}{dT})/DENet^2$$

$$\frac{dr2}{dT} = (DENet * \frac{dk2}{dT} * Pet - k2 * Pet * \frac{dDENet}{dT}) / DENet^2$$

$$\frac{dr3}{dT} = (DENeto * \frac{dk3}{dT} * Peto^2 - k3 * Peto^2 * \frac{dDENeto}{dT}) / DENeto^2$$

The UDF file then contains routines that specify the diffusivities of the components, calculated as a combination of Knudsen and bulk diffusion. Knudsen diffusion was defined as:

$$D_{Ki} = 9700 * 1000 * 10^{-8} * \left( \frac{T}{MW_i} \right)^{0.5} \left[ \frac{cm^2}{s} \right]$$

Bulk diffusion was defined as:

$$D_{Bi} = \frac{1}{\frac{\sum_j \left( \frac{y_j - y_i * N_j / N_i}{D_{ij}} \right)}{1 - y_i \sum_j (N_j / N_i)}} \left[ \frac{cm^2}{s} \right]$$

Effective diffusion was defined as:

$$D_{i\_eff} = \frac{\varepsilon}{\tau} * \frac{1}{\left( \frac{1}{D_{Ki}} \right) + \left( \frac{1}{D_{Bi}} \right)} * 10^{-4} \left[ \frac{m^2}{s} \right]$$

Epsilon and tau in the effective diffusion equation represent the porosity and tortuosity of the particle, respectively. For this study, 0.44 was used for porosity and 3.54 for tortuosity. These values were used in the study of methane steam reforming on alumina, and it was assumed that these values do not change for ethylene epoxidation on alumina, for want of better information.

The UDF file contains some post-processing functions, as well. After FLUENT has finished iterating, these functions may be called in the Define → User-Defined → Execute on Demand window. The UDF file can solve for three more parameters, the heat sink, the reaction rates, and the mass flux around the full particle.

The reaction case contains the settings required to simulate ethylene epoxidation. The material properties are set to those of an ethylene, ethylene oxide, water, oxygen, carbon dioxide,

and nitrogen mixture. The wall boundary was set to a heat flux of  $-820 \text{ W/m}^2$ . This value is adjusted from Turton et al. to accommodate the change in reaction extent that occurs because of the change in mass flow rate. The bottom flow profile was set to the flow and turbulence profile from the flow case, and the inlet mass fractions of the components were set to the conditions from Turton et al. A few iterations were done only solving for flow and turbulence variables, followed by a few iterations to include energy, and last, 2000 more iterations included solving for the mass fraction of the components.

## Experimental Results

Experimental data obtained from the cooled columns were compared to data from the previous experiments conducted by Ashman, et al. The past experiments have trends similar to the assumptions made earlier. Previous experiments show a parabolic relationship between Dimensionless Temperature and Dimensionless radial position. The Peclet number is expected to be constant at high Reynolds numbers and the Biot number to decrease proportionally with respect to Re.

### Experimental Dimensionless Temperature Profiles

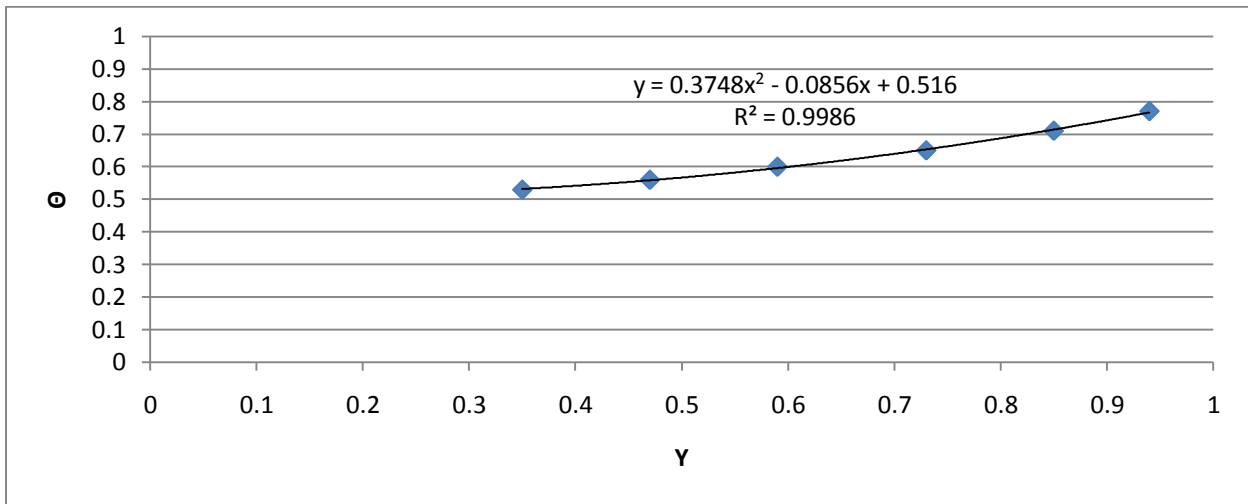


Figure 8: Dimensionless Temperature Profile Parabolic Fit for  $\frac{3}{8}$ " ceramic rings in the 2 inch column, with a Reynolds Number of 878 at the First Bed Height

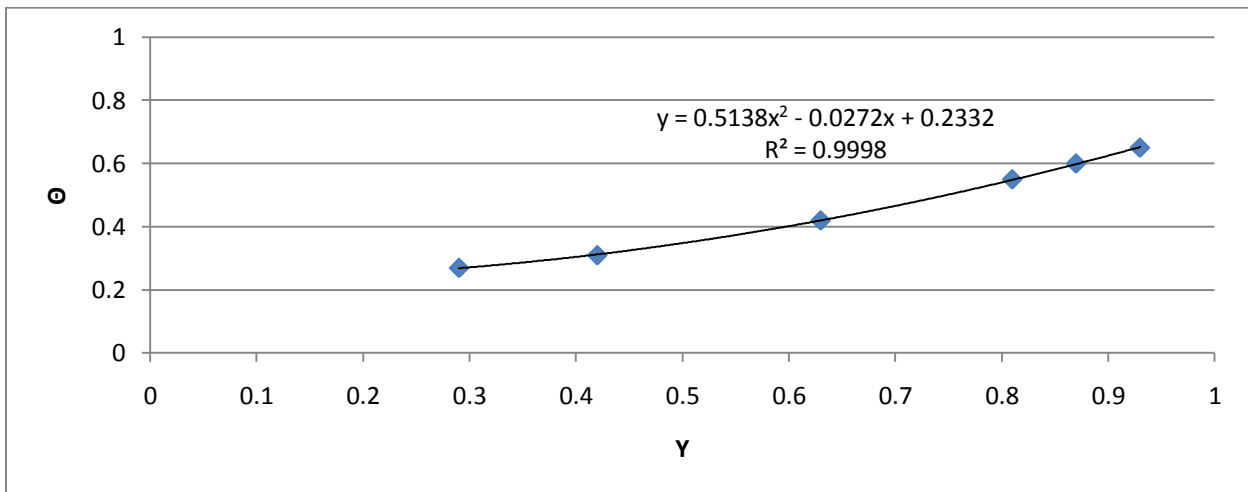


Figure 9: Dimensionless Temperature Profile Parabolic Fit for  $\frac{3}{8}$ " ceramic rings in the 3 inch column, with a Reynolds Number of 464 at the First Bed Height

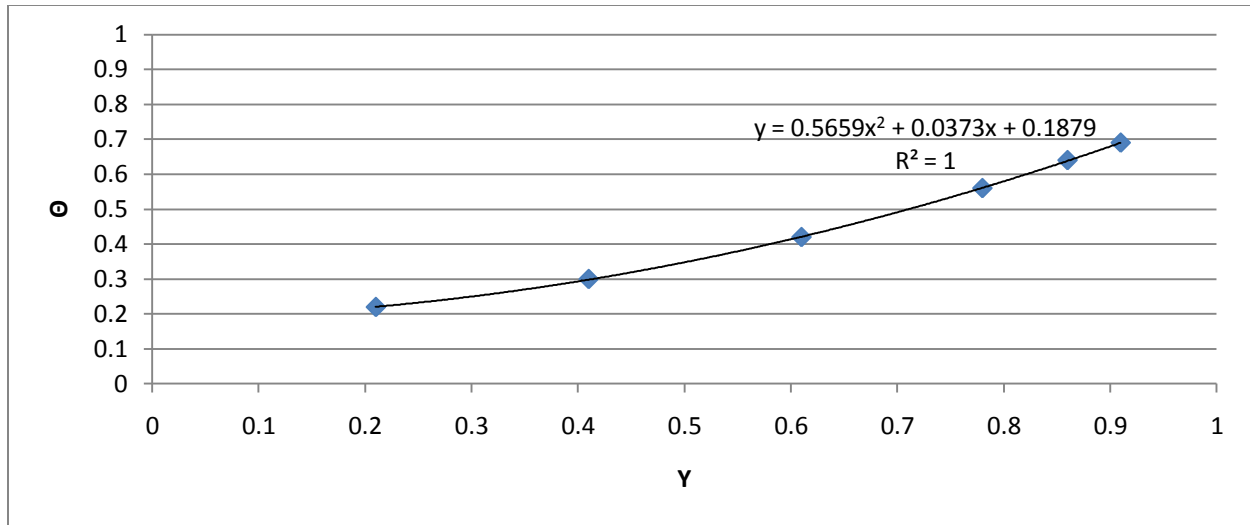


Figure 10: Dimensionless Temperature Profile Parabolic Fit for  $3/8$ " ceramic rings in the 4 inch column, with a Reynolds Number of 296 at the First Bed Height

Similar to previous experiments, the graphs of  $\theta$  vs.  $y$  for each of the three columns show a parabolic trend line. The data shows a very good parabolic fit, with coefficients of determination ( $R^2$ ) close to 1 for all three columns. The data and trend lines support the definition of  $\theta$ , whose denominator is a constant ( $T_w - T_o$ ) and numerator ( $T - T_o$ ) increases as the radial position is close to the wall. This is because the Temperature measured ( $T$ ) decreases as it approaches the cooling jacket. The inlet temperature profile is parabolic and in agreement with IPPF's assumption that it is parabolic at the first bed height.

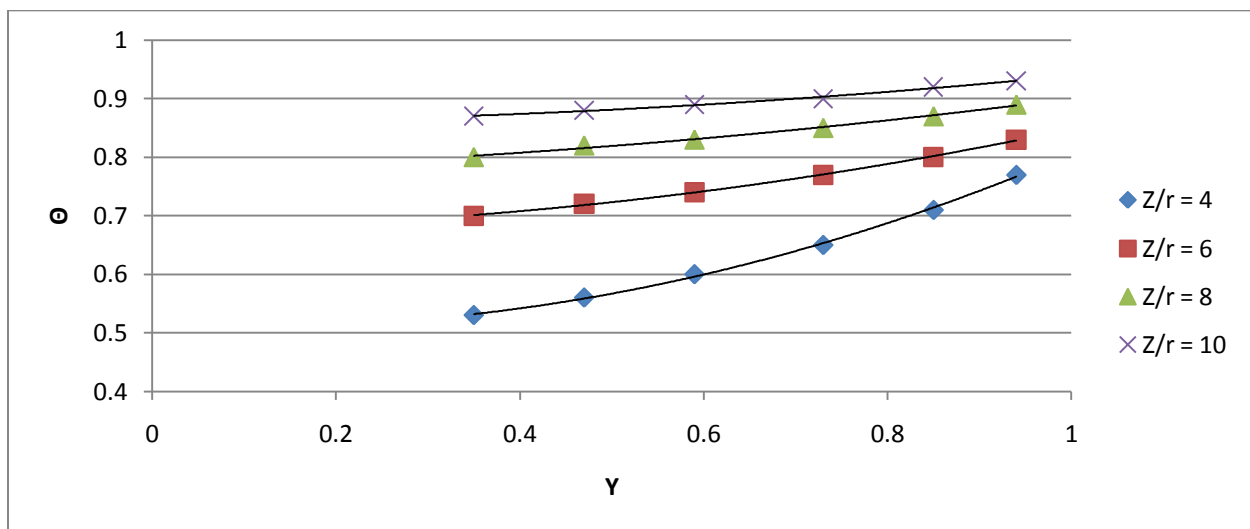
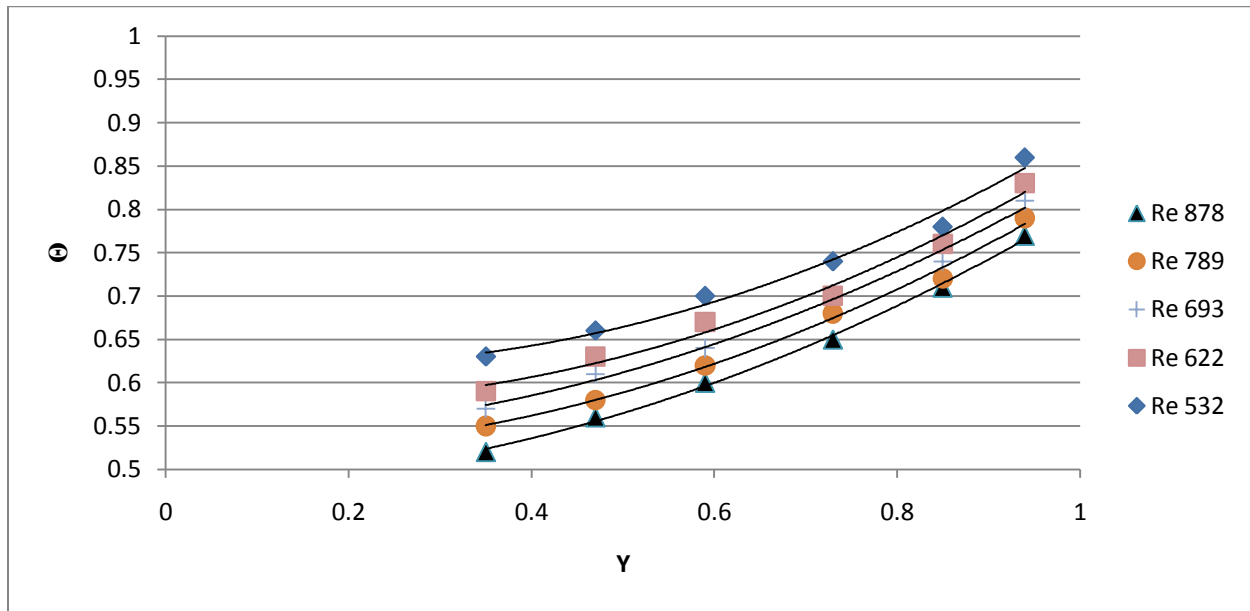


Figure 11: Dimensionless Temperature Profile Fit for  $3/8$ " ceramic rings in the 2 inch column, with a Reynolds Number of 464 at Various Bed Heights

It can be observed in Figure 11 that the dimensionless temperature profile shifts upwards as bed depth increases. This observation agrees with definition for  $\theta$ , where an increase in bed height will decrease the T value and produce a greater value for  $\theta$ . It is also observed as bed depth increases; there is a change among the trend lines. While the first bed depth gave a parabolic curve, the trend lines that follow shifts towards a more linear representation. This is in agreement with the IPPF model which only assumes that the first bed height is parabolic.



**Figure 12: Dimensionless Temperature Profile Parabolic Fit for  $\frac{3}{8}$ " ceramic rings in the 2 inch column, at various Reynolds Numbers**

Figure 12 depicts the trend lines at the first bed depth in the 2 inch column, for various values of Reynolds number. The trend looks similar, with only a difference in the intercept. The difference in intercepts may be attributed to the difference in superficial velocities. It can be observed from the graph that the stream with the greater superficial velocity was able to retain more heat.

## Dimensionless Parameters with respect to Reynolds Number

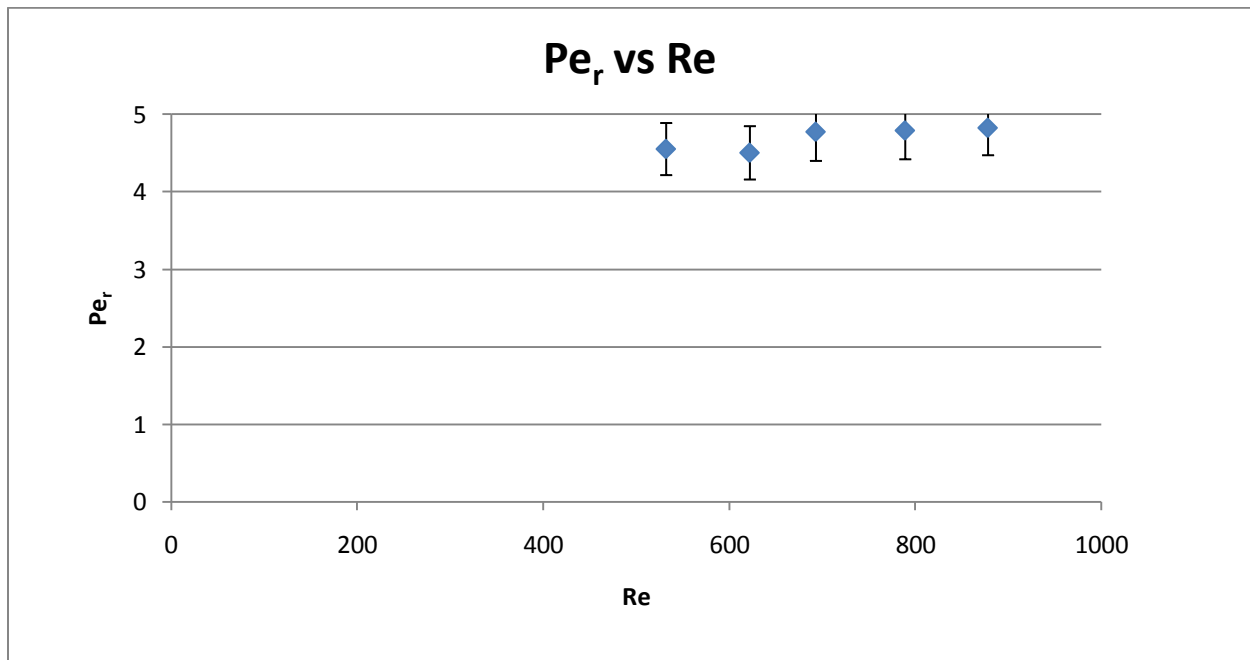


Figure 13: Radial Peclet Number with respect to Reynolds Number for  $\frac{3}{8}$ " ceramic rings in the 2 inch column

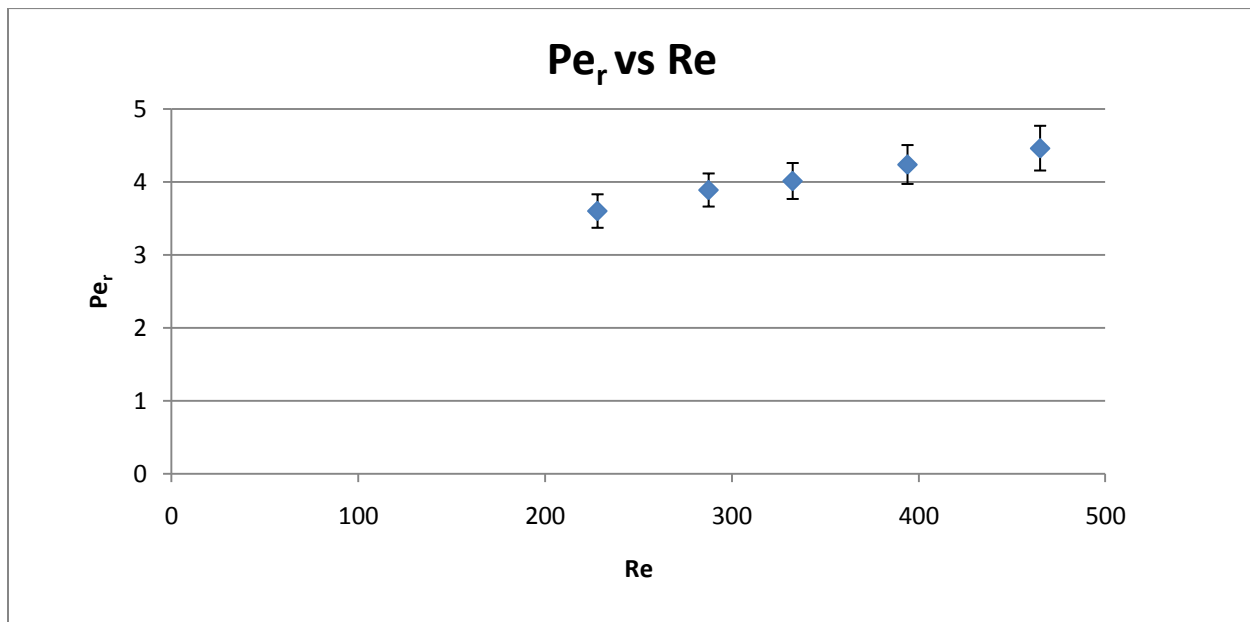


Figure 14: Radial Peclet Number with respect to Reynolds Number for  $\frac{3}{8}$ " ceramic rings in the 3 inch column

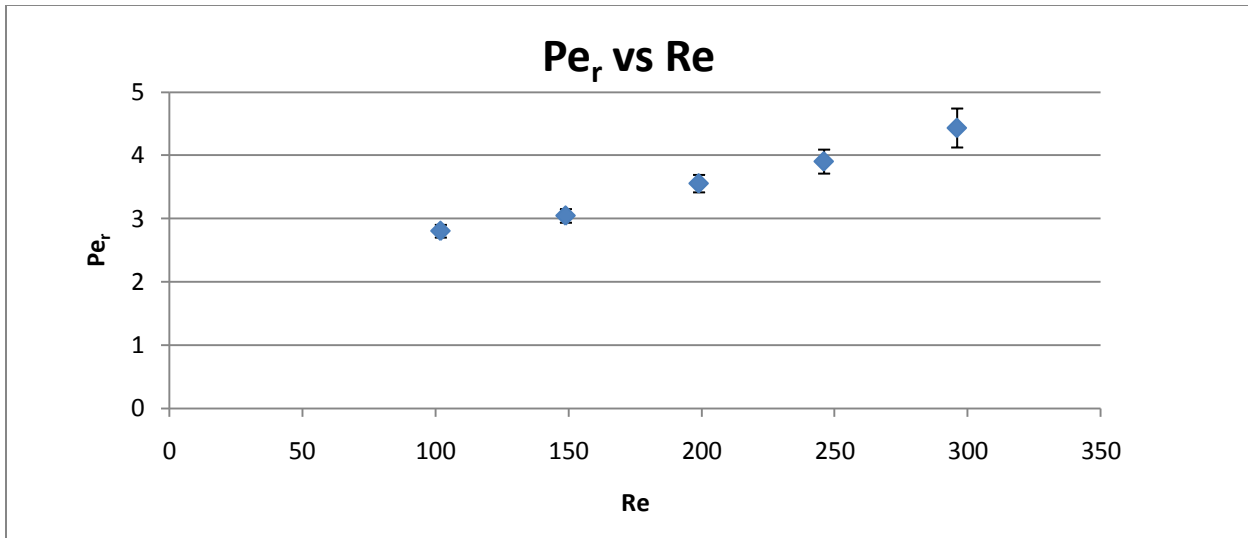


Figure 15: Radial Peclet Number with respect to Reynolds Number for  $3/8$ " ceramic rings in the 4 inch column

From Figure 13, it can be observed that  $Pe_r$  is relatively constant at approximately 4.5. Figure 15 shows that  $Pe_r$  increases with respect to Reynolds number, steadying at 4.5 at a Reynolds number of 300. Figure 14 depicts an overlap in Reynolds numbers where the Peclet number is still increasing with respect to Reynolds number but is starting to flatten out between the range of 4 and 5. These graphs agree with the previous assumption made about Peclet number, where Peclet number increases with respect to  $Re$  at low superficial velocities and flatten out at higher values of  $Re$ .

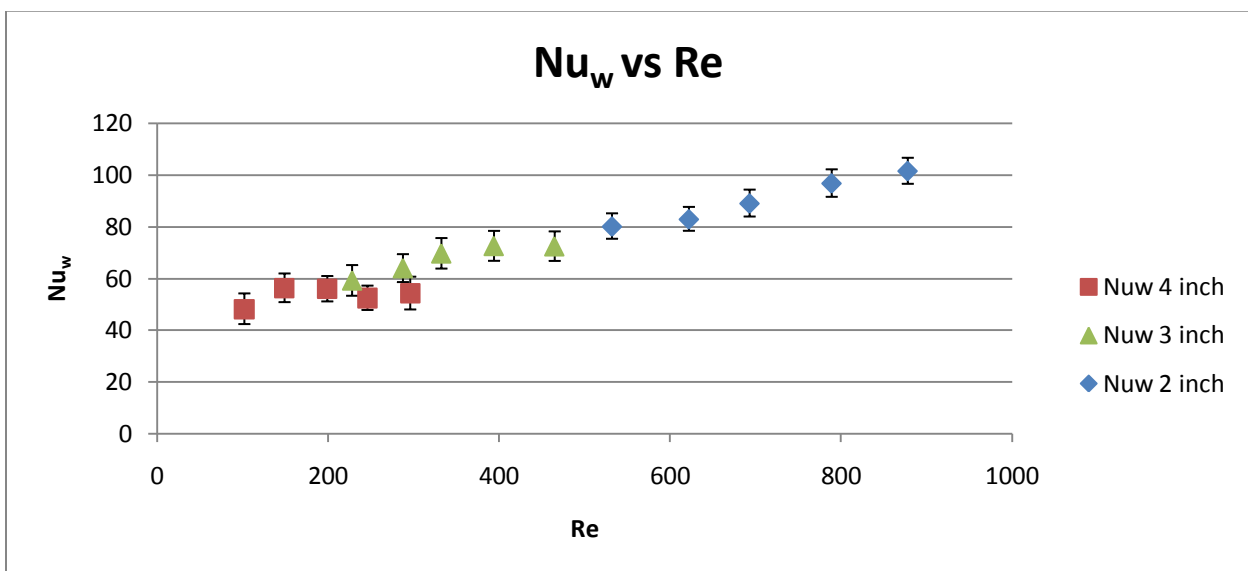


Figure 16:  $Nu_w$  with respect to Reynolds Number for  $3/8$ " ceramic rings in Various Cooled Tube Diameters

As depicted in Figure 16, wall Nusselt number increases with respect to Reynolds number. It can be observed from this graph that the results have relatively the same slope, meaning wall Nusselt number increases proportionally to  $Re$ , regardless of the tube diameter. This leads to the assertion that the wall heat transfer coefficient increases with an increase in  $Re$  or superficial velocity.

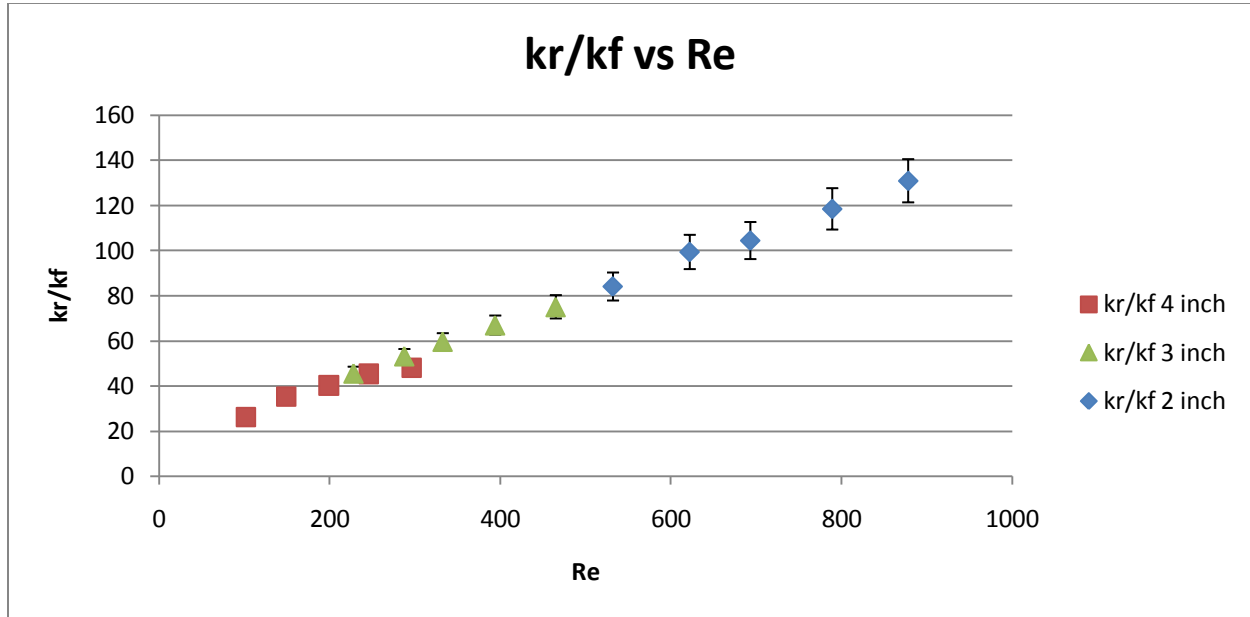


Figure 17:  $k_r/k_f$  with respect to Reynolds Number for  $3/8$ " ceramic rings in Various Cooled Tube Diameters

The ratio of effective radial thermal conductivity to effective thermal conductivity of the fluid ( $k_r/k_f$ ) increases as well, but at a much greater rate compared to  $Nu_w$ . The same assumptions can be made.  $k_r/k_f$  increases proportionally with increase in  $Re$  and superficial velocity. Because of a constant slope, as shown in Figure 17, the tube diameter and  $N$  value does not have an impact on the  $k_r/k_f$  value. The tube diameter does however change values of  $Re$  for the same flow rate used, due to changes in pressure and superficial velocity.

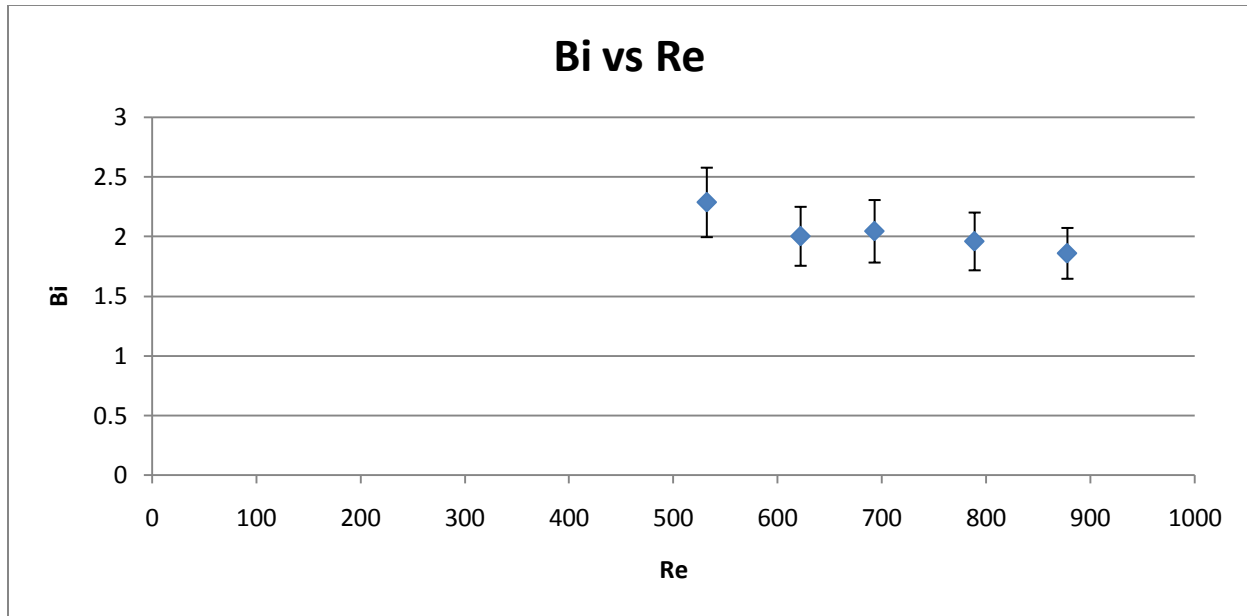


Figure 18: Biot Number with respect to Reynolds Number for  $3/8$ " ceramic rings in the 2 inch column

Because Bi is defined as,

$$Bi = \frac{h_w R}{k_r} = Nu_w \frac{R/d_p}{k_r/k_f}$$

it is possible to calculate its value using the  $k_r/k_f$  and  $Nu_w$  from the previous graphs. In addition, because  $k_r/k_f$  increases at a rate higher than  $Nu_w$ , the Biot number decreases with respect to Re as expected. This correlation is shown in Figure 18.

All of these graphs are comparable to previous experiments. Additional graphs for  $\Theta$  vs.  $y$ ,  $Pe_r$  vs. Re,  $Nu_w$  vs. Re,  $k_r/k_f$  vs. Re, and Bi vs. Re for the 3 inch and 4 inch column, showing the same trends, can be found in the Appendix.

## Experimental to CFD Temperature Profile

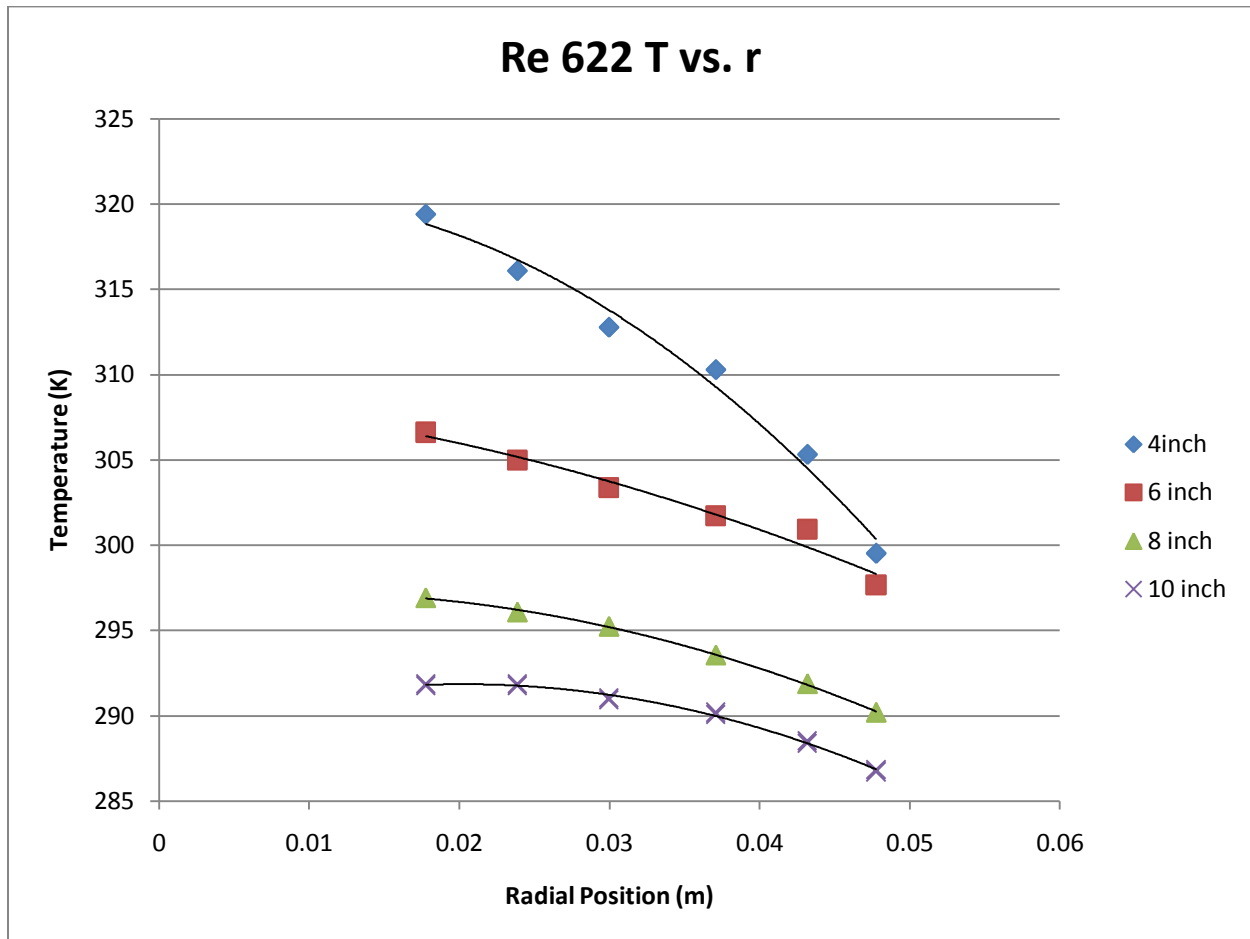


Figure 19: Temperature Profile Parabolic Fit for 3/8" ceramic rings in the 2 inch column, at various bed heights

Figure 19 portrays temperature (K) vs. radial position (m) for  $Re = 622$  in the 2 inch column. It shows the temperature profile for the various bed depths conducted experimentally. 2<sup>nd</sup> order polynomial trend lines were created for each bed height and inputted as the temperature inlet for the Air Only reaction case file in Fluent 6.3. The T-profile inlet at 4 inches can be seen in Figure 20, as the bottom wedge of the 120° cut of the packed bed. After specifying the temperature inlet at the bottom of the mesh, Fluent solves for the temperature profile at the top of the 2 inch wedge. Graphs of temperature profile for additional Re of 693 and 878 are located in the Appendix.

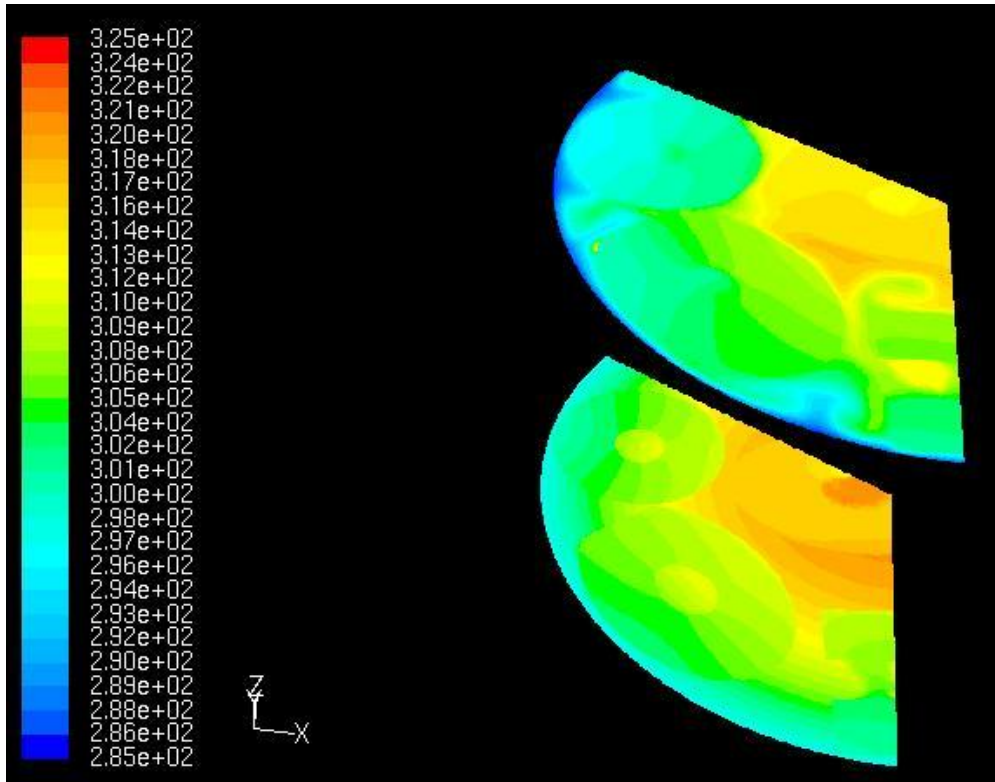


Figure 20: Temperature Contour of Top and Bottom for 4''-6'' for AirOnlyrxn.cas with No Reaction

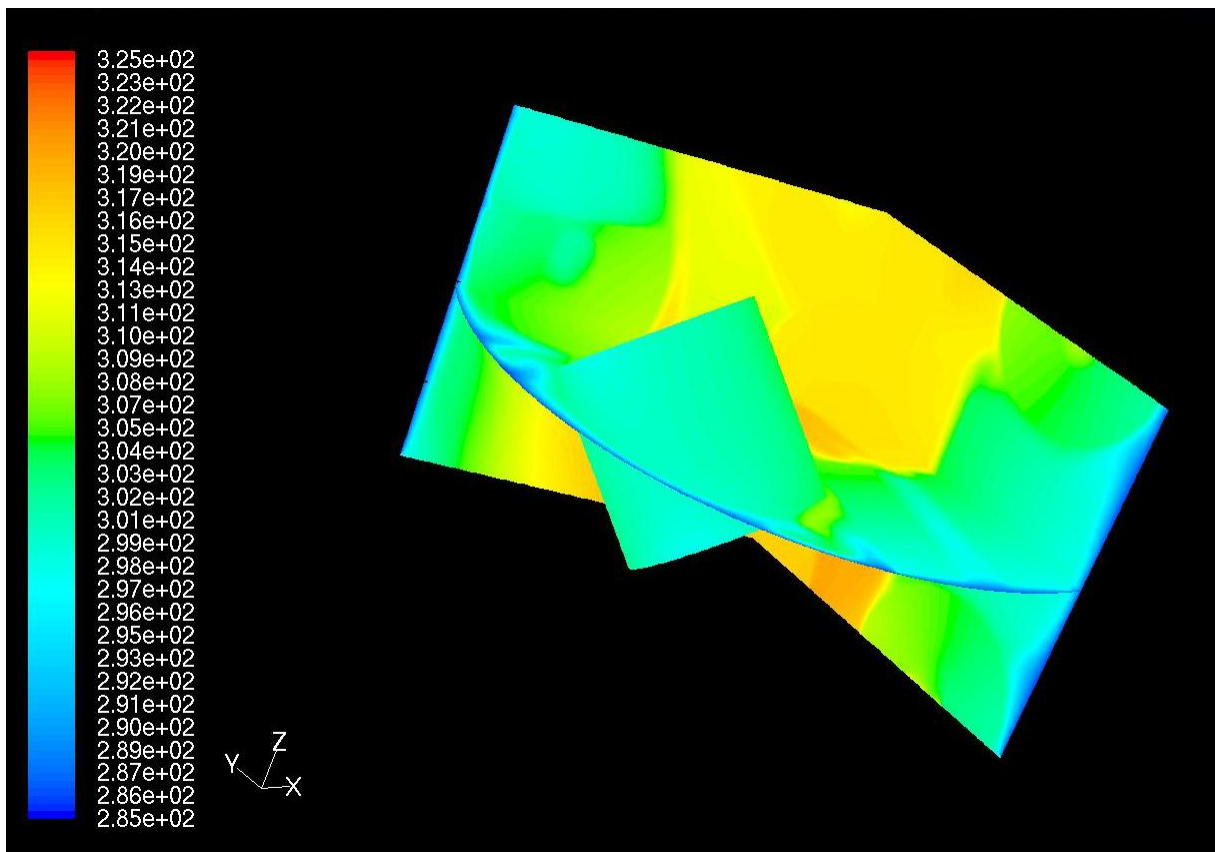


Figure 21: Temperature Contour of Particle 2 and Symmetry Boundaries for AirOnlyrxn.cas with No Reaction

The temperature contours show that the top segment is relatively cooler than the bottom due to the cooling wall. The fluid can be seen being cooled, in Figure 21, with the symmetry wall above the z-mid-plane comparatively cooler than that below. It is interesting to note that since there is no reaction occurring on the packing (particle 2) and it is quite cool compared to the center of the tube. Additional CFD temperature contours are located in the Appendix.

### Comparison of Experimental Temperature Output to CFD Output

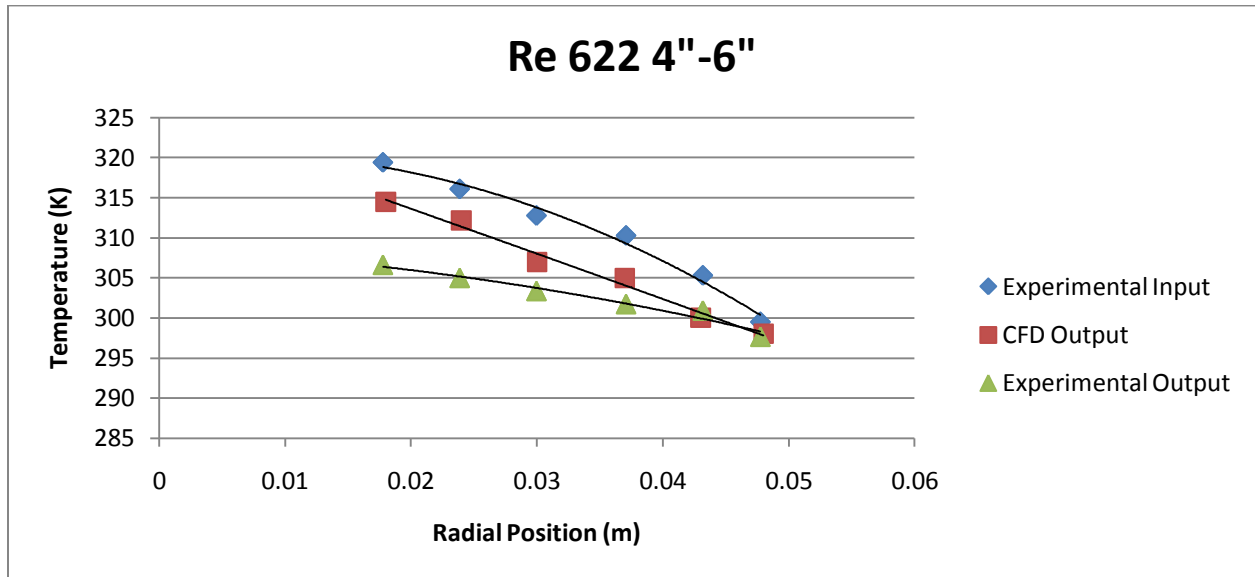


Figure 22: Temperature Profile Comparison of Experimental and CFD for the 4''- 6'' bed depth, in the 2 inch column

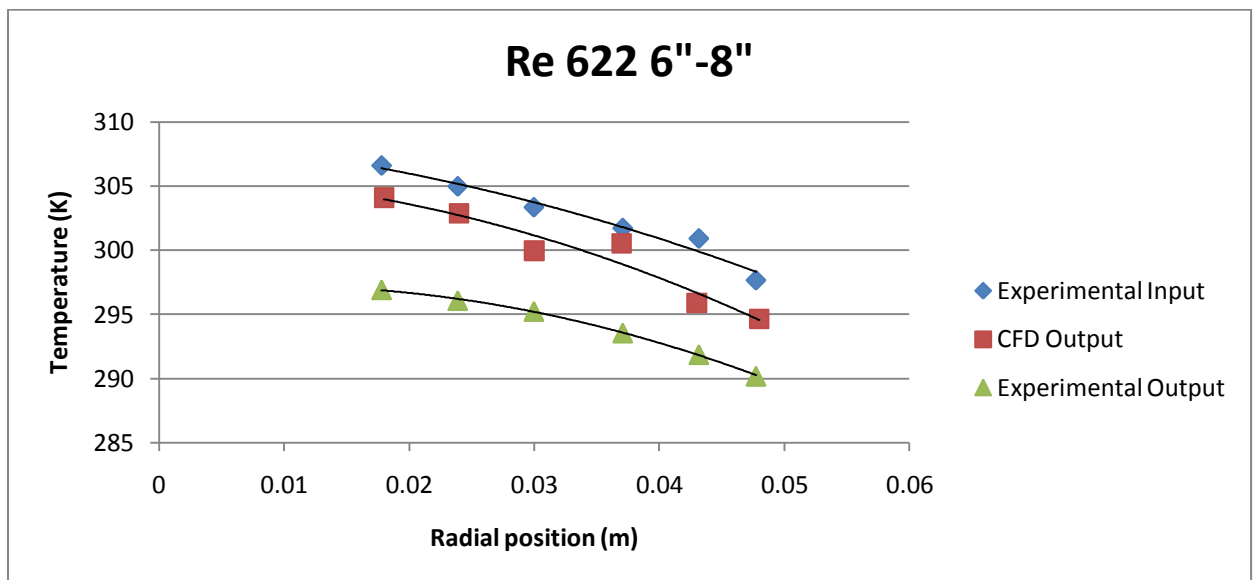


Figure 23: Temperature Profile Comparison of Experimental and CFD for the 6''- 8'' bed depth, in the 2 inch column

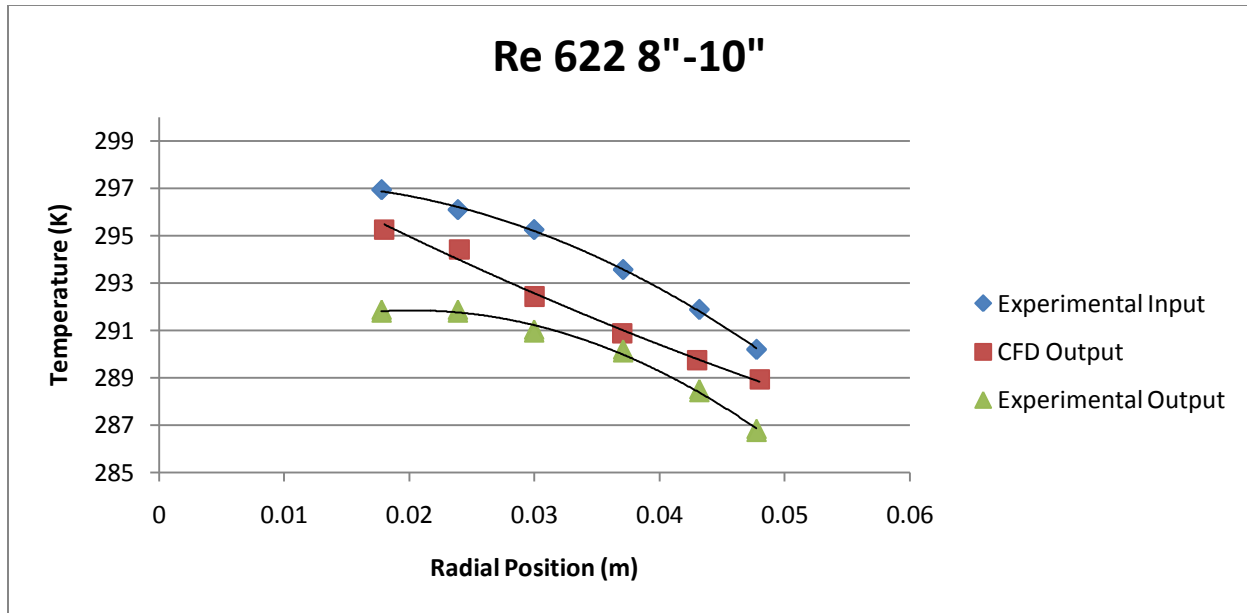


Figure 24: Temperature Profile Comparison of Experimental and CFD for the 8"-10" bed depth, in the 2 inch column

Figures 22, 23 and 24 depict the experimental temperature profiles inputted into Fluent compared with experimental and CFD results of  $T(r)$  at the next bed height. It is obvious that there is relatively less heat loss in the CFD and more heat loss in the experimental results. The temperature difference among these outputs is relatively constant with a max of approximately  $10^{\circ}\text{K}$ , and a slight overlap at a greater radial position from 4"-6". There are however slight error in the CFD results due to backflow in the meshing. A temperature for backflow was guessed and specified in Fluent to account for the error.

The difference in temperatures is understandable because of heat loss in the experiment. The CFD is more controlled and should give accurate and ideal results. In the experiment, however, the heated air stream could have lost heat to the system as it flowed through. In addition, thermocouples could have been placed slightly too high above the packing and thus temperature of the fluid recorded would be slightly lower than the actual.

Additional graphs for Reynolds number of 693 and 878 depicted similar results and are located in the Appendix of this report.

## Ethylene Oxide Reaction Results

Rates (kmol/s)	Fluent	Turton, et al.	Fluent w/ Kinetics Modified
Reaction 1	$6.18 \times 10^{-11}$	$6.16 \times 10^{-09}$	$6.75 \times 10^{-09}$
Reaction 2	$5.83 \times 10^{-14}$	$2.32 \times 10^{-10}$	$2.62 \times 10^{-10}$
Reaction 3	$3.33 \times 10^{-16}$	$5.13 \times 10^{-17}$	$6.56 \times 10^{-16}$
C2H4 consumption	$-6.18 \times 10^{-11}$	$-6.39 \times 10^{-09}$	$-7.01 \times 10^{-09}$
C2H4O production	$6.18 \times 10^{-11}$	$6.16 \times 10^{-09}$	$6.75 \times 10^{-09}$
H2O production	$1.17 \times 10^{-13}$	$4.64 \times 10^{-10}$	$5.25 \times 10^{-10}$
O2 consumption	$-3.11 \times 10^{-11}$	$-3.78 \times 10^{-09}$	$-4.16 \times 10^{-09}$
CO2 production	$1.17 \times 10^{-13}$	$4.64 \times 10^{-10}$	$5.25 \times 10^{-10}$

Table 5: Reaction Rates of Ethylene Epoxidation

Reaction was allowed to run in Fluent for approximately 1000 iterations. Using the *Execute on Demand* option in Fluent, reaction rates were able to be determined for Particle 2. Although the kinetics were inputted correctly and calculated correctly in Fluent the conversion was less than that claimed by the case study in Turton, et. al. Reaction 1 was off by a magnitude of  $10^2$  and reaction 2 by approximately 4000. Reaction 3 was off by a magnitude of  $10^{-1}$ , but its rate was so small that it was negligible.

In order to correct for this difference in results, reaction 1 was multiplied by a correction factor of  $10^{-2}$  and reaction 2 by 4000. After being iterated once again, the ethylene oxidation reaction case, provided rates that were slightly greater but to the same magnitude as those provided in Turton, et al.

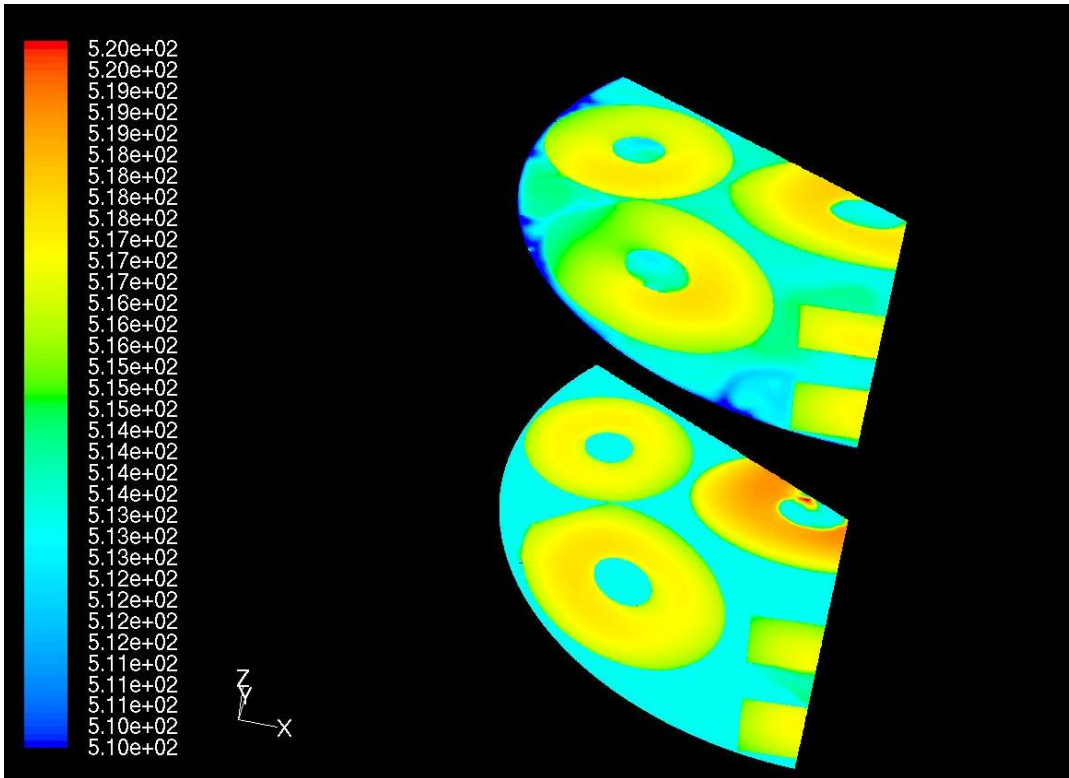


Figure 25: Temperature Contour of Top and Bottom of 2 inch packing for the EthyleneOxiderxn.cas

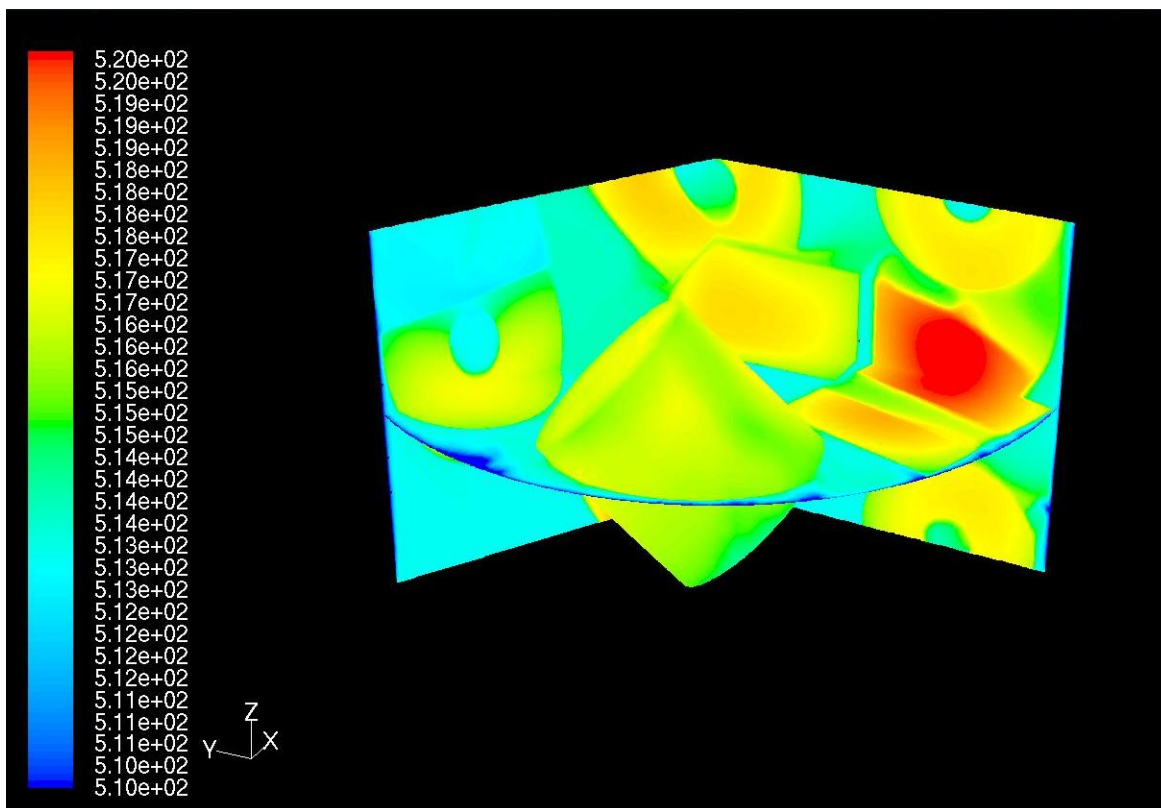


Figure 26: Temperature Contour of Particle 2 and Symmetry Boundaries for the EthyleneOxiderxn.cas

The screenshots of the temperature contours in Figures 25 and 26 do not show a significant temperature change over the 2 inch height of packing. Temperature contour of the top and the bottom of the wedge shows that the fluid is mostly isothermal, with hotter particle rings. The temperature contour of the symmetry boundaries and particle 2 displays a different view of the same results. The packing is approximately 5 degrees hotter due to the exothermic reaction of ethylene epoxidation occurring on the particle surface. The hottest particle seen (in red) is an example of the errors that occur from the mirroring of particles at the symmetry boundary.

## Conclusions

From our experiments, we have found that radial heat transfer is improved by reducing the column diameter. We believe that reducing the N value would allow for improved heat transfer. Further experiments could verify that increasing particle diameter may also improve heat transfer, by using similar column diameters and varying particle diameter.

Our simulated air flow results appear to be validated by the experimental data, though there were considerable differences in certain areas. This error could be attributed to the difference in N value between the experimental data ( $N = 5.33$ ) and the CFD model ( $N = 4$ ). Another possible factor could be difference in particle shape. Though we used one-hole cylinders in both the CFD model and our experiments, the experimental packing material was, on average, deformed, and this difference in shape could also have an effect on flow.

Our simulated ethylene epoxidation reaction created anticipated results. The particles were warmer than the fluid, as expected, since the reactions happen on their surface. The fact that reactions happen at the particle surface while the fluid remains isothermal proves that our adjusted settings were appropriate for the CFD model. This is further proved by our simulated reaction rates approximating those of the textbook model.

Using CFD simulation in place of experiments can be a useful tool for research. There is no need for expensive equipment, along with no safety concerns when running simulations. Running a simulation is also more easily repeatable than an experiment. The drawback to using a simulation is that an experiment is required to validate the CFD model; otherwise there is no evidence that the simulation is meaningful.

## Nomenclature

$A_i$	=	pre-exponential constant for reaction i or adsorption of species i
$B_i$	=	Biot number $\left(\frac{h_w R}{k_r}\right)$
$C_p$	=	heat capacity at constant pressure
$D_{Bi}$	=	Bulk diffusion coefficient of species i
$D_{ij}$	=	Binary diffusion coefficient for species i and j
$D_{Ki}$	=	Knudsen diffusion coefficient of species i
$D_{i,eff}$	=	effective diffusion coefficient of species i
$d_c$	=	particle diameter (cylindrical)
$d_p$	=	particle diameter (spherical)
$E_i$	=	activation energy for reaction i
$G$	=	gas mass flow rate
$\Delta H_i$	=	change in enthalpy for reaction i or adsorption of species i
$h_w$	=	wall heat transfer coefficient
$k_f$	=	effective thermal conductivity of the fluid
$k_i$	=	rate constant for reaction i or adsorption of species i
$k_r$	=	effective radial thermal conductivity
$MW_i$	=	molecular weight of species i
$N$	=	column diameter to particle diameter ratio
$N_j/N_i$	=	stoichiometric ratio of species j to species i
$p_i$	=	partial pressure of species i
$Pe_R$	=	Peclet number $\left(\frac{GC_p R}{k_r}\right) \left(\frac{Re * Pr}{kr/kf}\right)$
$Pr$	=	Prandtl number
$P_T$	=	total pressure
$Q$	=	heat generated by reaction
$R$	=	maximum radial position
$R_g$	=	ideal gas constant
$Re$	=	Reynolds number $\left(\frac{v_s \rho d_p}{\mu}\right)$
$r$	=	radial position
$r_i$	=	rate of reaction i

$S_i$	=	total source of species i due to reaction
$T$	=	temperature
$U$	=	overall heat transfer coefficient
$V_i$	=	specific volume of species i
$v_s$	=	superficial velocity
$x$	=	dimensionless bed depth $\left(\frac{z}{R}\right)$
$y$	=	dimensionless radial position $\left(\frac{r}{R}\right)$
$Y_i$	=	mass fraction of species i
$z$	=	bed depth

### Greek letters

$\alpha_{ij}$	=	stoichiometric coefficient of a species i in reaction j
$\varepsilon$	=	porosity
$\lambda$	=	Effective radial thermal conductivity
$\theta$	=	dimensionless temperature $\left(\frac{T-T_o}{T_w-T_o}\right)$
$\mu$	=	dynamic viscosity
$\rho$	=	density
$\tau$	=	tortuosity
$\zeta$	=	dimensionless bed depth

### Subscripts

et	=	ethylene
eto	=	ethylene oxide
0	=	inlet
w	=	wall

## Bibliography

- Ashman, Michael, Rybak, Dmitriy, Skene, William (2009). Heat Transfer Parameters of Cylindrical Catalyst Particles with Internal Voids in Fixed Bed Reactor Tubes, *WPI MQP Report*
- Borkink, J.G.H., Borman, P.C., Westerterp, K.R. (1993). Modeling of the Radial heat Transport in Wall-Cooled packed beds. *Chemical Engineering Communications*, 121, 135-155.
- Borman, P.C., Westerterp, K.R. (1992). An experimental study of the selective oxidation of ethane in a wall cooled tubular packed bed reactor. *Chemical Engineering Science*, 47, 2541-2546.
- Fulton, James W. (1986). Selecting the catalyst configuration. *Chemical Engineering*, May 12, 1986, 97-101.
- Hall, M. W., Zomerick, J. C. (1981). Technology for the Manufacture of Ethylene Oxide. *Catal. Rev. – Sci. Eng.*, 23, 163-185.
- Hoflund, Gar B., Minahan, David M. (1996). Study of Cs-Promoted ,  $\alpha$ -Alumina Supported Silver Ethylene Epoxidation Catalysts. *Journal of Catalysis* 158, 109-115.
- Lafarga, David, Al-Juaied, Mohammed A., Bondy, Christina M., Varma, Arvind (2000). Ethylene Epoxidation on Ag-Cs/ $\alpha$ -Al<sub>2</sub>O<sub>3</sub> Catalyst: Experimental Results and Strategy for Kinetic parameter Determination. *Ind Eng. Chem. Res.*, 39, 2148-2156.
- Nijemeisland, Michael (2000). Verification Studies of Computational Fluid Dynamics in Fixed Bed Heat Transfer. *WPI Master's Thesis*.
- Procelli, J. V. (1981). Ethylene Oxidation- Exploratory Research. *Catal. Rev. – Sci. Eng.*, 23, 151-162.
- Sachtler, W. M. H, Bachx, C., Van Santen, A. (1981). On the Mechanism of Ethylene Epoxidation *Catal. Rev. – Sci. Eng.*, 23, 127-149.
- Taskin, M. E, Dixon, A. G., Stitt, E. H. (2007). CFD Study of Fluid Flow and Heat Transfer in a Fixed Bed of Cylinders. *Numerical Heat Transfer, A*, 52, 203-218
- Thomeo, Joao C., Rouiller, Claudia O., Freire, Jose T. (2004), Experimental Analysis of Heat Transfer in Paced Beds with Air Flow. *Ind. Eng. Chem. Res.*, 43, 4140-4148.
- Turton, Richard, Bailie, Richard C., Whiting, Wallace B., Schaeiwitz, Joseph A. (2009) *Analysis, Synthesis, and Design of Chemical Processes*. Pearson Education, Inc., 991-1000.

## Appendix

### Ethylene Epoxidation Reaction Kinetics

$$k_1 = 1.96 * 10^{-5} * e^{\left(\frac{-10.0416}{RT}\right)}$$

$$k_1 = 1.96 * 10^{-5} * e^{\left(\frac{-10.0416}{0.0083144 * 513.15}\right)} = 1.863 * 10^{-6} \frac{\text{kmol}}{\text{m}^3 \text{s kPa}}$$

$$k_2 = 9.36 * 10^{-7} * e^{\left(\frac{-26.7776}{RT}\right)}$$

$$k_2 = 9.36 * 10^{-7} * e^{\left(\frac{-26.7776}{0.0083144 * 513.15}\right)} = 1.760 * 10^{-9} \frac{\text{kmol}}{\text{m}^3 \text{s kPa}}$$

$$k_3 = 4.2768 * 10^{-8} * e^{\left(\frac{-25.9408}{RT}\right)}$$

$$k_3 = 4.2768 * 10^{-8} * e^{\left(\frac{-25.9408}{0.0083144 * 513.15}\right)} = 9.785 * 10^{-11} \frac{\text{kmol}}{\text{m}^3 \text{s kPa}^2}$$

$$k_{et} = 9.8 * 10^{-6} * e^{\left(\frac{46.8608}{RT}\right)}$$

$$k_{et} = 9.8 * 10^{-6} * e^{\left(\frac{46.8608}{0.0083144 * 513.15}\right)} = 0.577 \text{ kPa}^{-1}$$

$$k_{eto} = 3.3 * 10^{-9} * e^{\left(\frac{88.7008}{RT}\right)}$$

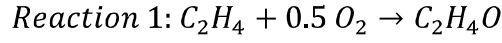
$$k_{eto} = 3.3 * 10^{-9} * e^{\left(\frac{88.7008}{0.0083144 * 513.15}\right)} = 3.527 \text{ kPa}^{-2}$$

$$DEN_{et} = 0.6 * (1 + k_{et} * p_{ethylene})$$

$$DEN_{et} = 0.6 * (1 + 0.577 * 2650 * 0.028667) = 26.900$$

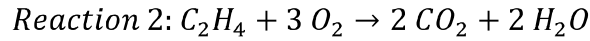
$$DEN_{eto} = 0.6 * (1 + k_{eto} * p_{ethylene\ oxide}^2)$$

$$DEN_{eto} = 0.6 * (1 + 3.527 * (2650 * 0.000278)^2) = 1.749$$



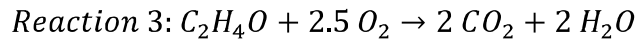
$$r_1 = \frac{k_1 * p_{ethylene}}{DEN_{et}}$$

$$r_1 = \frac{1.863 * 10^{-6} * 2650 * 0.028667}{26.900} = 5.261 * 10^{-6} \frac{kmol}{m^3(solid) s}$$



$$r_2 = \frac{k_2 * p_{ethylene}}{DEN_{et}}$$

$$r_2 = \frac{1.760 * 10^{-9} * 2650 * 0.028667}{26.900} = 4.970 * 10^{-9} \frac{kmol}{m^3(solid) s}$$



$$r_3 = \frac{k_3 * p_{ethylene\ oxide}^2}{DEN_{eto}}$$

$$r_3 = \frac{9.785 * 10^{-11} * (2650 * 0.000278)^2}{1.749} = 3.036 * 10^{-11} \frac{kmol}{m^3(solid) s}$$

$$S_i = MW_i \sum_{j=1}^3 \alpha_{ij} r_j$$

$$S_{ethylene} = 28.05 * ((-1 * 5.261 * 10^{-6}) + (-1 * 4.970 * 10^{-9}) + (0 * 3.036 * 10^{-11}))$$

$$= -1.477 * 10^{-4} \frac{kg}{m^3(solid) s}$$

$$\frac{dP_{ethylene}}{dY_{ethylene}} = P * \frac{MW_{average}}{MW_{ethylene}} * \left( 1.0 - Y_{ethylene} * \frac{MW_{average}}{MW_{ethylene}} \right)$$

$$\frac{dP_{ethylene}}{dY_{ethylene}} = 2650 * \frac{28.731}{28.05} * \left( 1.0 - 0.028667 * \frac{28.731}{28.05} \right) = 2634.6$$

$$\frac{dr_1}{dp_{ethylene}} = \frac{k_1}{DEN_{et}} - \frac{p_{et} * k_1 * k_{et} * 0.6}{DEN_{et}^2}$$

$$\frac{dr_1}{dp_{ethylene}} = \frac{1.863 * 10^{-6}}{26.900} - \frac{2650 * 0.028667 * 1.863 * 10^{-6} * 0.577 * 0.6}{26.900^2} = 1.545 * 10^{-9}$$

$$\frac{dr_2}{dp_{ethylene}} = \frac{k_2}{DEN_{et}} - \frac{p_{et} * k_2 * k_{et} * 0.6}{DEN_{et}^2}$$

$$\frac{dr_2}{dp_{ethylene}} = \frac{1.760 * 10^{-9}}{26.900} - \frac{2650 * 0.028667 * 1.760 * 10^{-9} * 0.577 * 0.6}{26.900^2} = 1.459 * 10^{-12}$$

$$\frac{dr_3}{dp_{ethylene}} = 0$$

$$\frac{dS_i}{dY_i} = \frac{dP_i}{dY_i} MW_i \sum_{j=1}^3 \left( \alpha_{ij} \frac{dr_j}{dP_i} \right)$$

$$\frac{dS_{et}}{dY_{et}} = 2634.6 * 28.05 * (-1 * 1.545 * 10^{-9} - 1 * 1.459 * 10^{-12}) = -1.143 * 10^{-8}$$

## Reaction Enthalpy

$$Q = \Delta H_1 * r_1 + \Delta H_2 * r_2 + \Delta H_3 * r_3$$

$$Q = 105140000 * 5.261 * 10^{-6} + 1323158000 * 4.970 * 10^{-9} + 1218018000 * 3.036$$

$$* 10^{-11} = 559.75 \frac{J}{m^3(solid) s}$$

$$\frac{dDEN_{et}}{dT} = - \frac{0.6 * p_{et} * 9.8 * 10^{-6} * 46.8608}{RT^2} * e^{\frac{46.8608}{RT}}$$

$$\frac{dDEN_{et}}{dT} = - \frac{0.6 * 2650 * 0.028667 * 9.8 * 10^{-6} * 46.8608}{0.0083144 * 513.15^2} * e^{\frac{46.8608}{0.0083144 * 513.15}} = -0.563$$

$$\frac{dDEN_{eto}}{dT} = - \frac{0.6 * p_{eto}^2 * 3.3 * 10^{-9} * 88.7008}{RT^2} * e^{\frac{88.7008}{RT}}$$

$$\frac{dDEN_{eto}}{dT} = - \frac{0.6 * (2650 * 0.000278)^2 * 3.3 * 10^{-9} * 88.7008}{0.0083144 * 513.15^2} * e^{\frac{88.7008}{0.0083144 * 513.15}} = -0.047$$

$$\frac{dk_1}{dT} = k_1 * - \frac{10.0416}{RT^2}$$

$$\frac{dk_1}{dT} = 1.863 * 10^{-6} * - \frac{10.0416}{0.0083144 * 513.15^2} = -8.545 * 10^{-9}$$

$$\frac{dk_2}{dT} = k_2 * - \frac{26.7776}{RT^2}$$

$$\frac{dk_2}{dT} = 1.760 * 10^{-9} * - \frac{26.7776}{0.0083144 * 513.15^2} = -2.153 * 10^{-11}$$

$$\frac{dk_3}{dT} = k_3 * - \frac{25.9408}{RT^2}$$

$$\frac{dk_3}{dT} = 9.785 * 10^{-11} * -\frac{25.9408}{0.0083144 * 513.15^2} = -1.159 * 10^{-12}$$

$$\frac{dr_1}{dT} = \frac{p_{et} \left( DEN_{et} * \frac{dk_1}{dT} - k_1 * \frac{dDEN_{et}}{dT} \right)}{DEN_{et}^2}$$

$$\frac{dr_1}{dT} = \frac{2650 * 0.028667(26.900 * -8.545 * 10^{-9} - 1.863 * 10^{-6} * -0.563)}{26.900^2} = 8.598 * 10^{-8}$$

$$\frac{dr_2}{dT} = \frac{p_{et} \left( DEN_{et} * \frac{dk_2}{dT} - k_2 * \frac{dDEN_{et}}{dT} \right)}{DEN_{et}^2}$$

$$\frac{dr_2}{dT} = \frac{2650 * 0.028667(26.900 * -2.153 * 10^{-11} - 1.760 * 10^{-9} * -0.563)}{26.900^2}$$

$$= 4.322 * 10^{-11}$$

$$\frac{dr_3}{dT} = \frac{p_{eto}^2 \left( DEN_{eto} * \frac{dk_3}{dT} - k_3 * \frac{dDEN_{eto}}{dT} \right)}{DEN_{eto}^2}$$

$$\frac{dr_3}{dT} = \frac{(2650 * 0.000278)^2(1.749 * -1.159 * 10^{-12} - 9.785 * 10^{-11} * -0.047)}{1.749^2}$$

$$= 4.563 * 10^{-13}$$

$$\frac{dQ}{dT} = \Delta H_1 * \frac{dr_1}{dT} + \Delta H_2 * \frac{dr_2}{dT} + \Delta H_3 * \frac{dr_3}{dT}$$

$$\frac{dQ}{dT} = 105140000 * 8.598 * 10^{-8} + 1323158000 * 4.322 * 10^{-11} + 1218018000 * 4.563$$

$$* 10^{-13} = 9.098$$

## Diffusivity

$$D_{AB} = \frac{10^{-3} * T^{1.75} * \left(\frac{MW_A + MW_B}{MW_A * MW_B}\right)^{0.5}}{P * \left(V_A^{\frac{1}{3}} + V_B^{\frac{1}{3}}\right)^2}$$

$$D_{et-eto} = \frac{10^{-3} * 513.15^{1.75} * \left(\frac{28.05 + 44.05}{28.05 * 44.05}\right)^{0.5}}{26.5 * \left(40.92^{\frac{1}{3}} + 62.84^{\frac{1}{3}}\right)^2} = 9.156 * 10^{-3} \frac{cm^2}{s}$$

$$D_{Ki} = 9700 * 1000 * 10^{-8} * \left(\frac{T}{MW_i}\right)^{0.5}$$

$$D_{K,et} = 9700 * 1000 * 10^{-8} * \left(\frac{513.15}{28.05}\right)^{0.5} = 0.415 \frac{cm^2}{s}$$

$$D_{Bi} = \frac{1}{\frac{\sum_j \left(\frac{y_j - y_i * N_j/N_i}{D_{ij}}\right)}{1 - y_i \sum_j (N_j/N_i)}}$$

$$D_{B,et} = \frac{1}{\frac{0.0002 - 0.0294 * \frac{-1}{2}}{9.156 * 10^{-3}} + \frac{0.0009 - 0.0294 * \frac{-1}{2}}{0.019} + \frac{0.1776 - 0.0294 * \frac{7}{4}}{0.015} + \frac{0.0009 - 0.0294 * \frac{-1}{2}}{0.012}}$$

$$= 0.072 \frac{cm^2}{s}$$

$$D_{i\_eff} = \frac{\varepsilon}{\tau} * \frac{1}{\left(\frac{1}{D_{Ki}}\right) + \left(\frac{1}{D_{Bi}}\right)} * 10^{-4}$$

$$D_{et\_eff} = \frac{0.44}{3.54} * \frac{1}{\left(\frac{1}{0.415}\right) + \left(\frac{1}{0.072}\right)} * 10^{-4} = 7.657 * 10^{-7} \frac{m^2}{s}$$

## Spherical Particle Diameter

$$d_p = 2 * \left( \frac{3L \left( \frac{d_c}{2} \right)^2}{4} \right)^{\frac{1}{3}}$$

$$d_p = 2 * \left( \frac{3 * \frac{11}{32} \text{ in} \left( \frac{3/8 \text{ in}}{2} \right)^2}{4} \right)^{\frac{1}{3}} = 0.417 \text{ in}$$

## Reynolds Number

2 inch

$$Re = 380(d_p)SCFM$$

$$SCFM = (\%Reading) * (Max Flow) * (14.7 + Pressure)/14.7$$

$$SCFM = .6 * 2.6 * \frac{14.7 + 37.5}{14.7} = 5.54$$

$$Re = 380 * .417 * 5.54 = 878$$

3 inch

$$Re = 169(d_p)SCFM$$

$$SCFM = (\%Reading) * (Max Flow) * (14.7 + Pressure)/14.7$$

$$SCFM = .7 * 2.39 * \frac{14.7 + 47}{14.7} = 6.52$$

$$Re = 169 * .417 * 6.52 = 460$$

4 inch

$$Re = 95(d_p)SCFM$$

$$SCFM = (\%Reading) * (Max Flow) * (14.7 + Pressure)/14.7$$

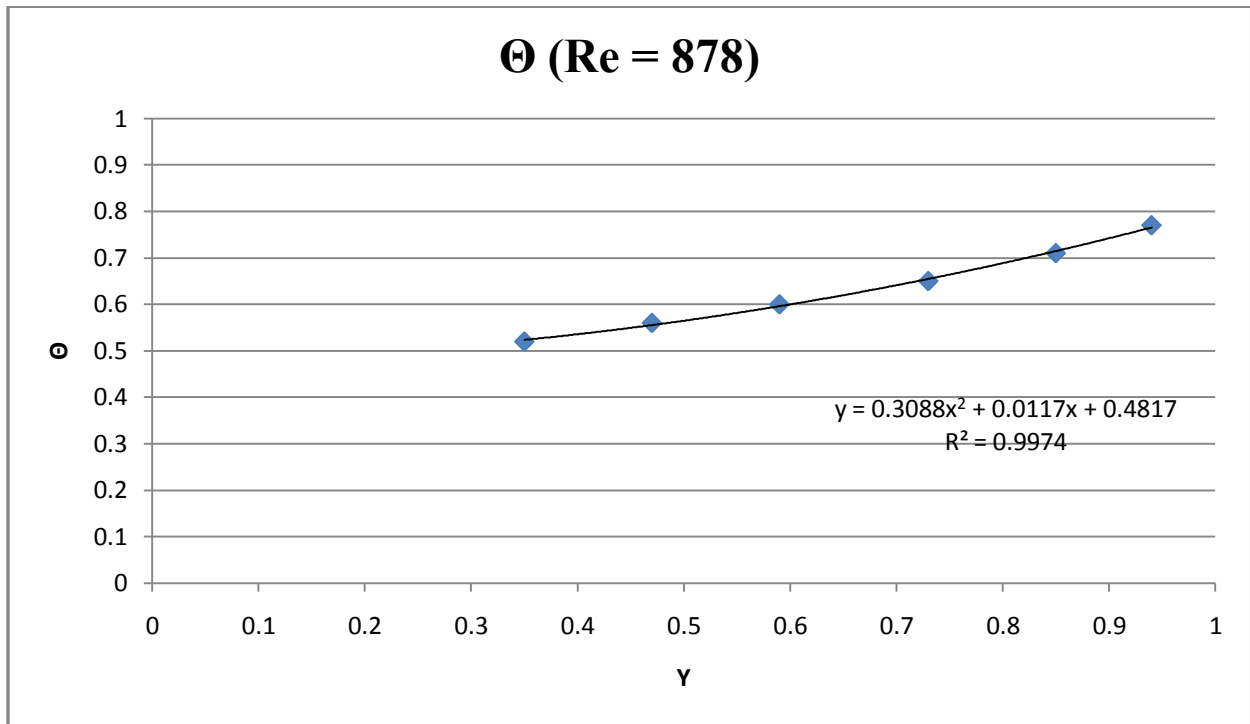
$$SCFM = .7 * 2.25 * \frac{14.7 + 55}{14.7} = 7.47$$

$$Re = 95 * .417 * 7.47 = 296$$

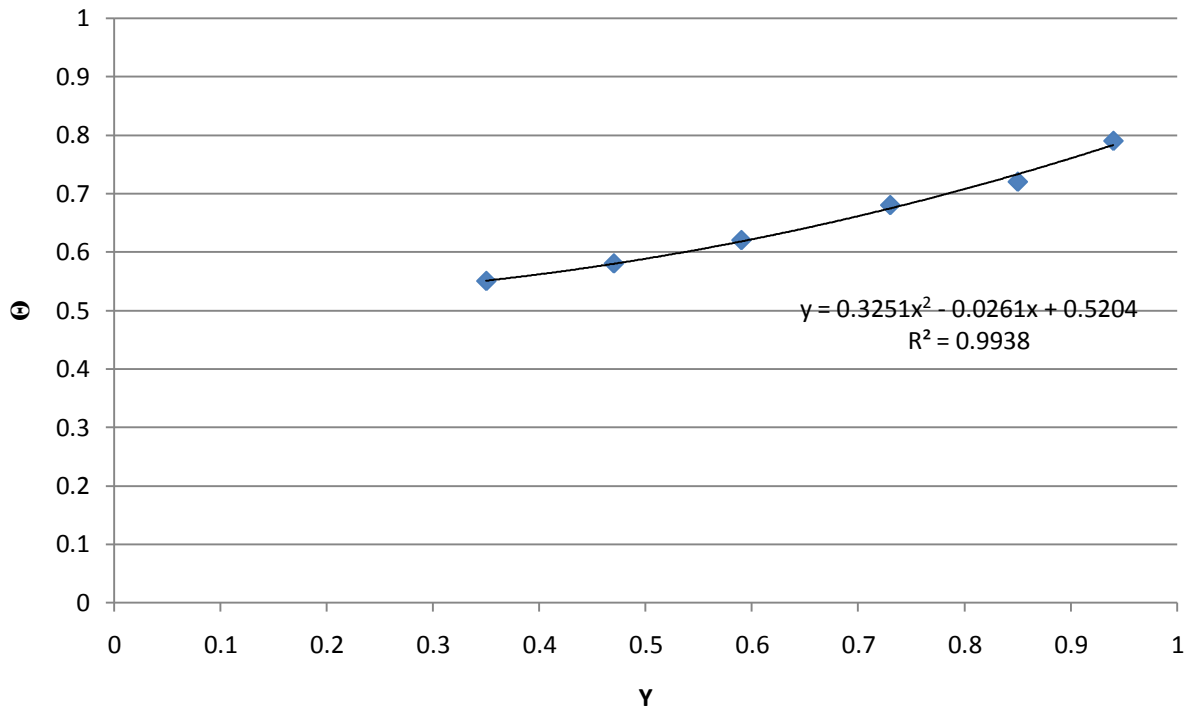
## Dimensionless Temperature vs. Dimensionless Radial Position

### First Bed Height

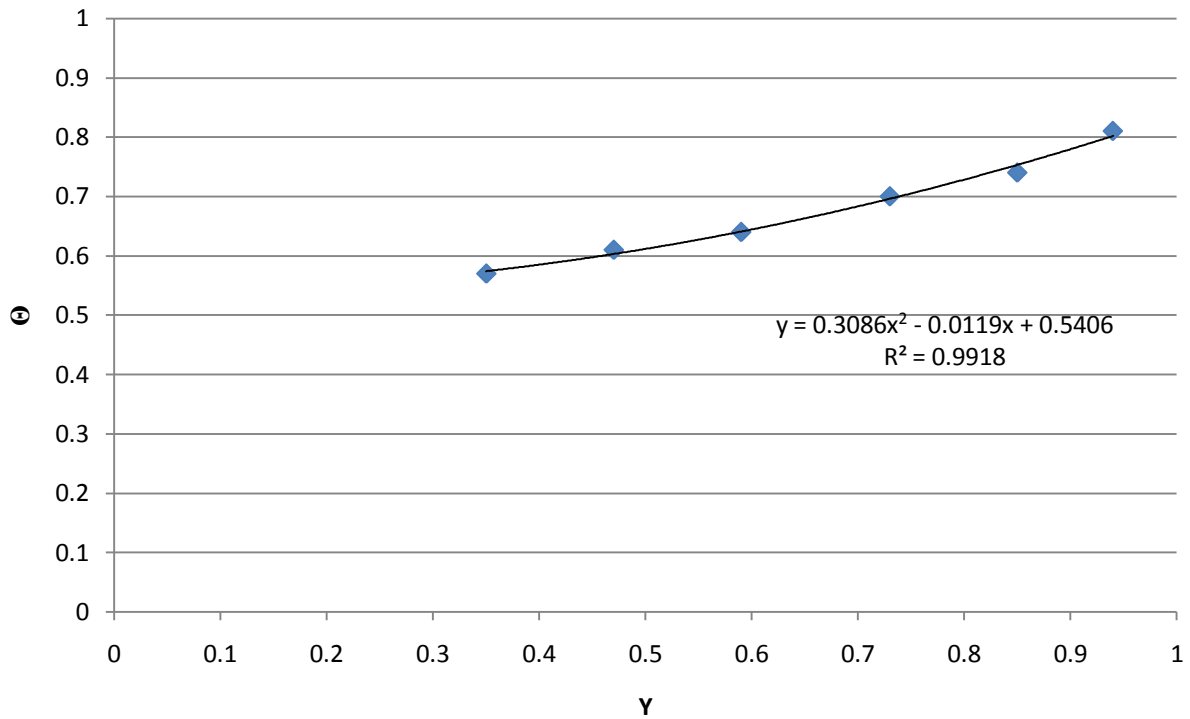
#### 2inch Tube



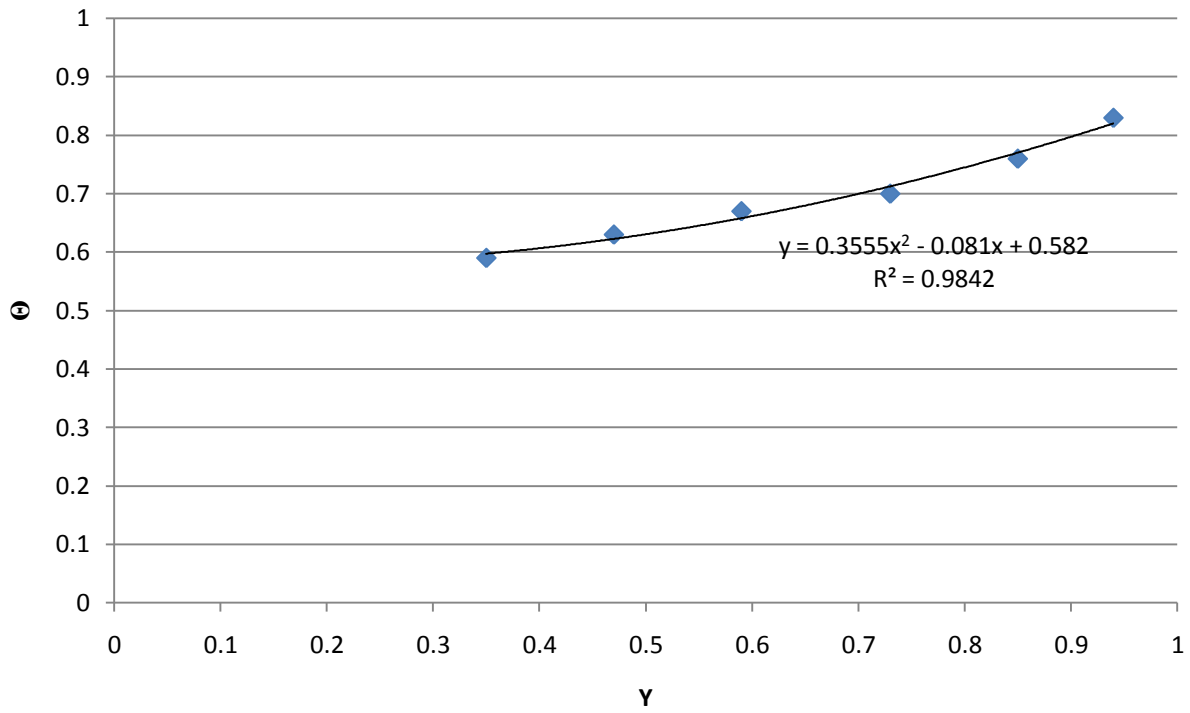
**$\Theta$  (Re = 789)**



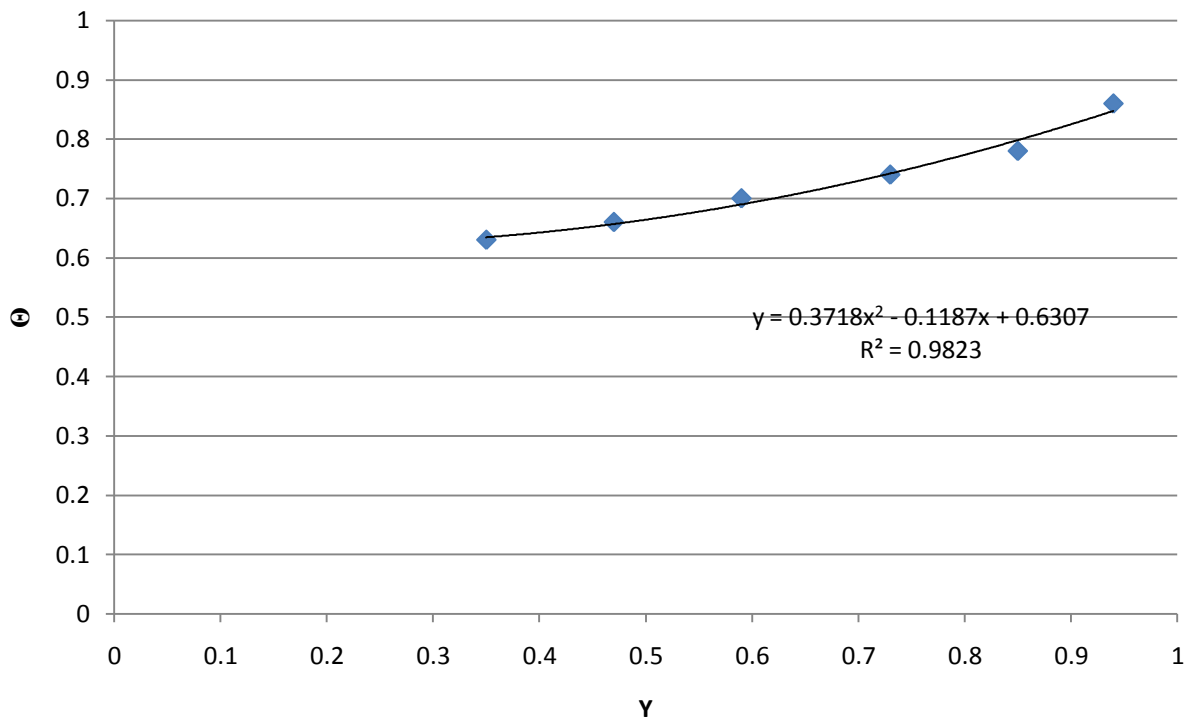
**$\Theta$  (Re = 693)**



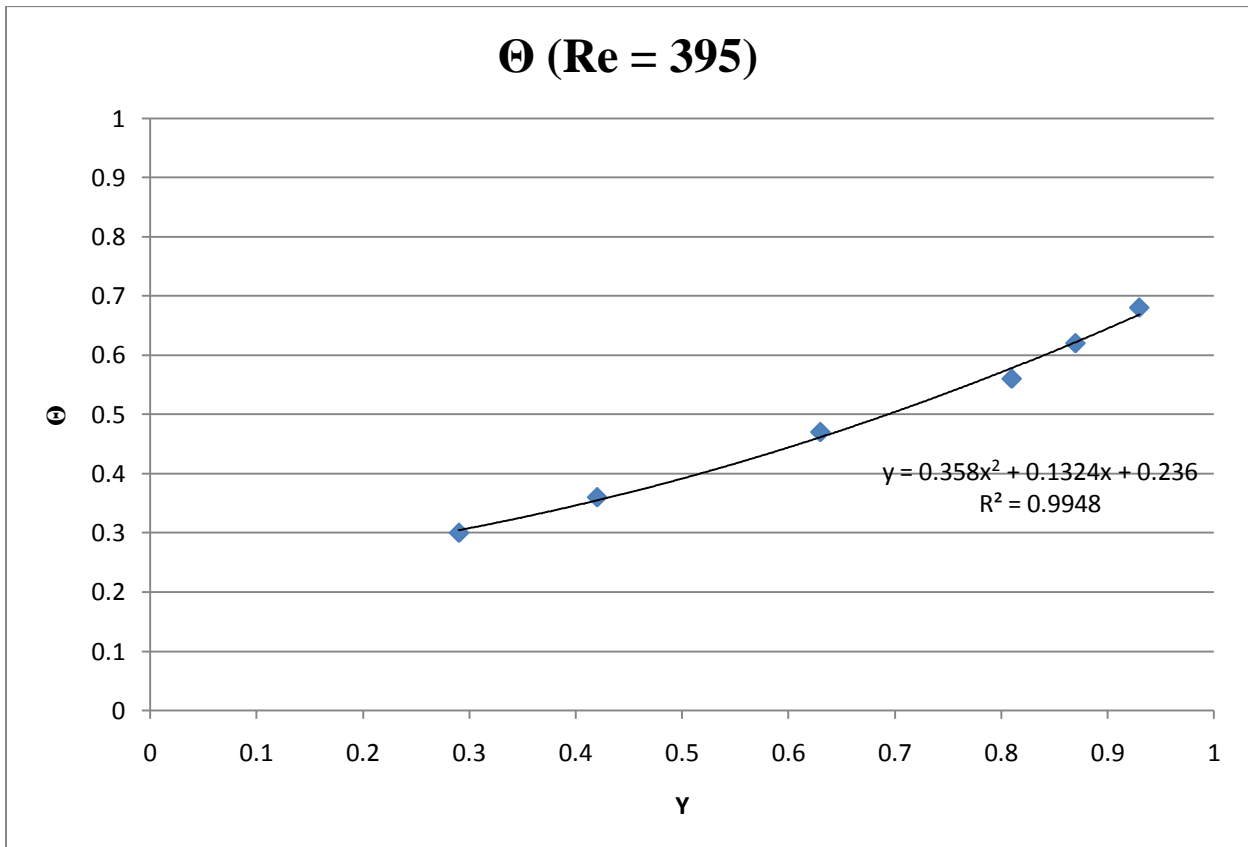
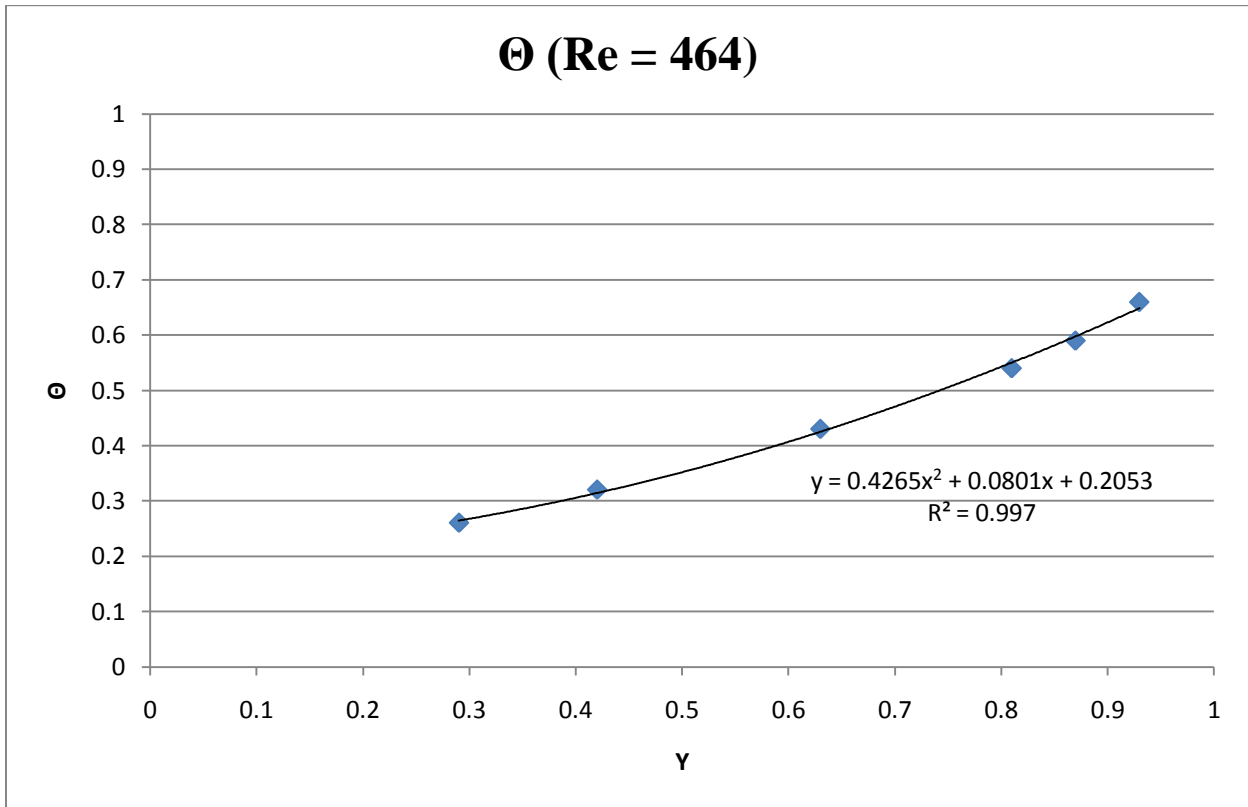
### $\Theta$ (Re = 622)



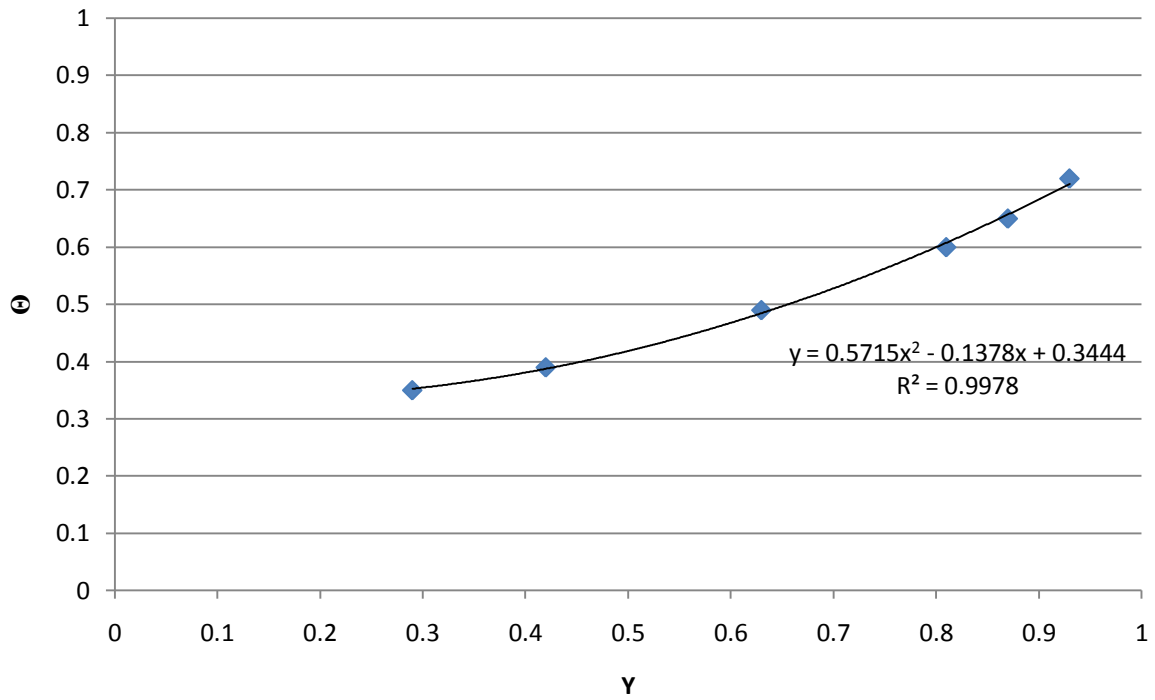
### $\Theta$ (Re = 532)



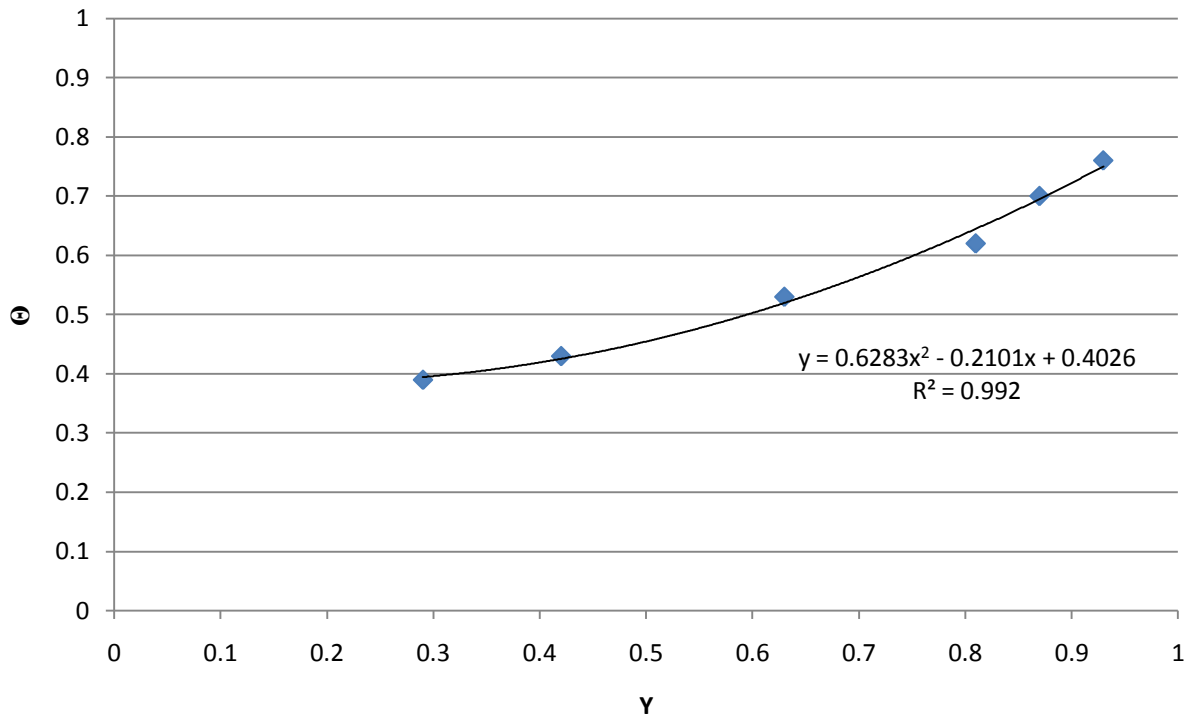
3 inch Tube

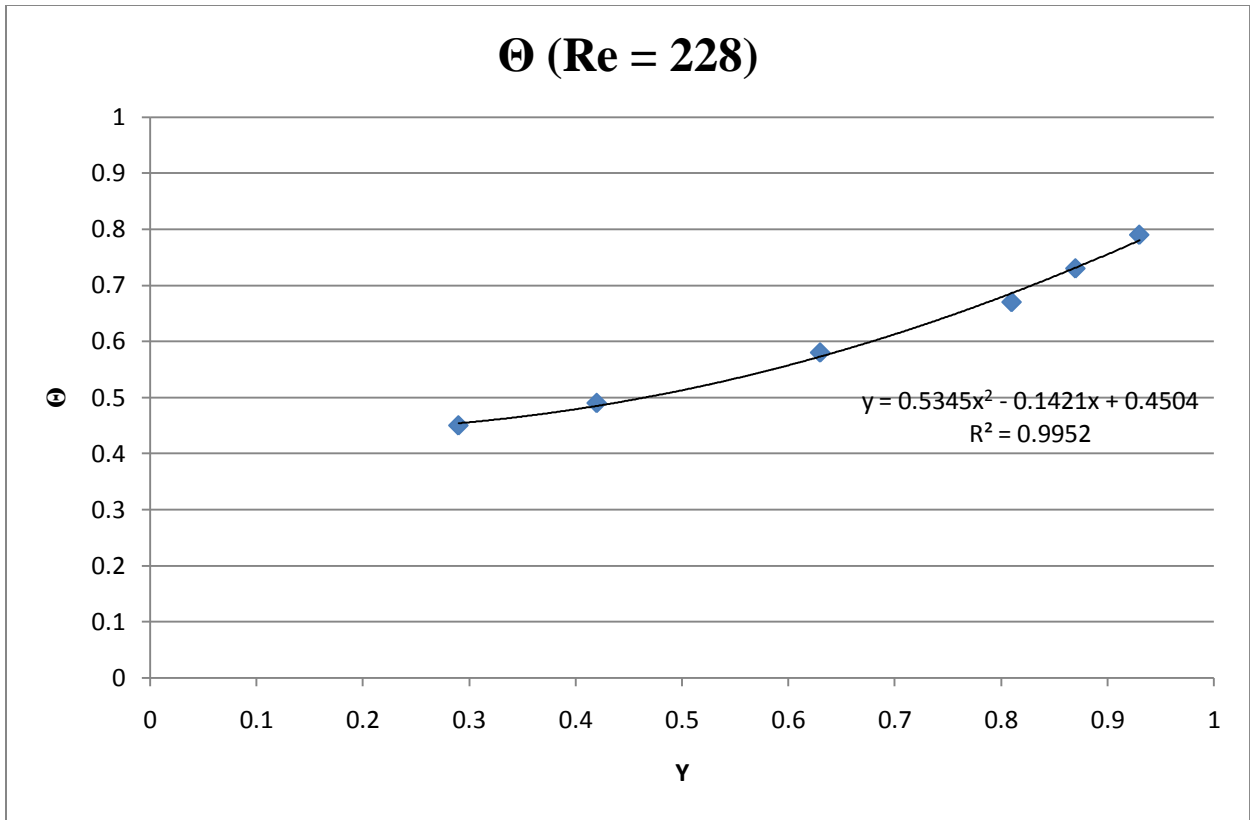


### $\Theta$ (Re = 330)

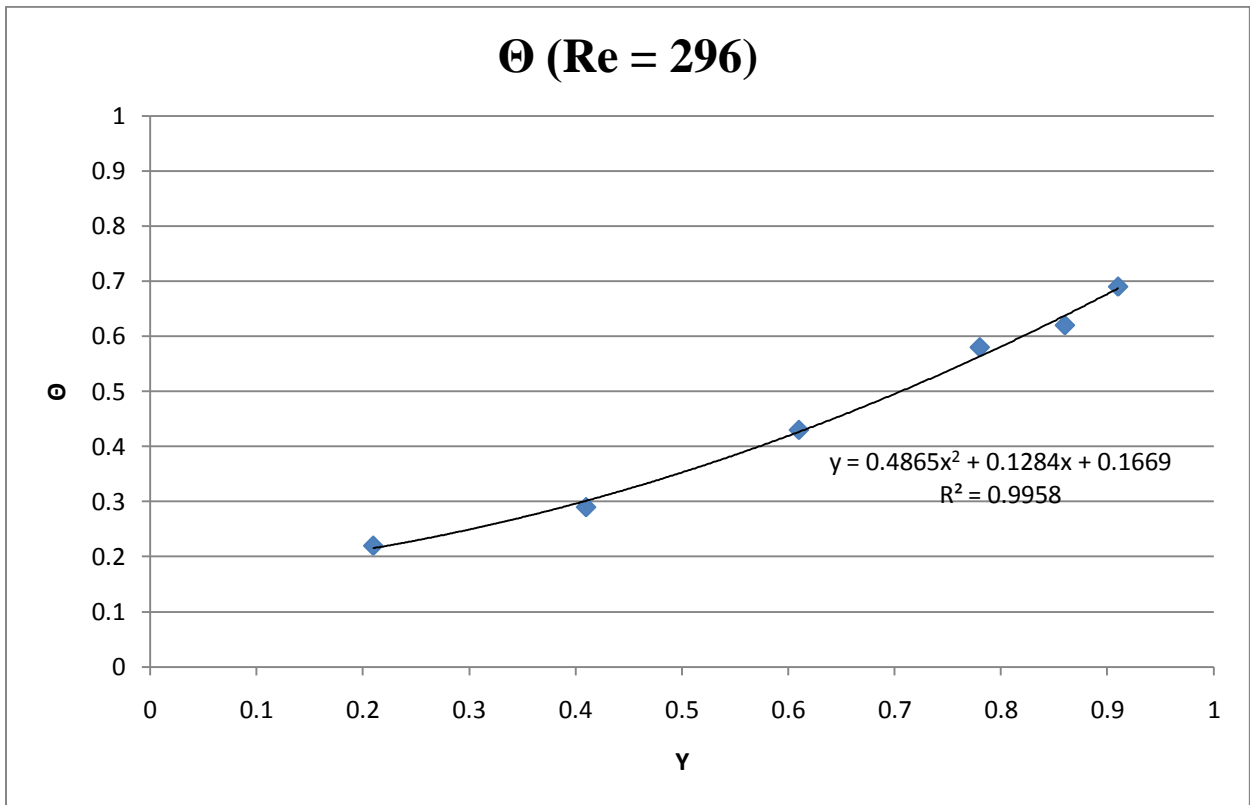


### $\Theta$ (Re = 286)

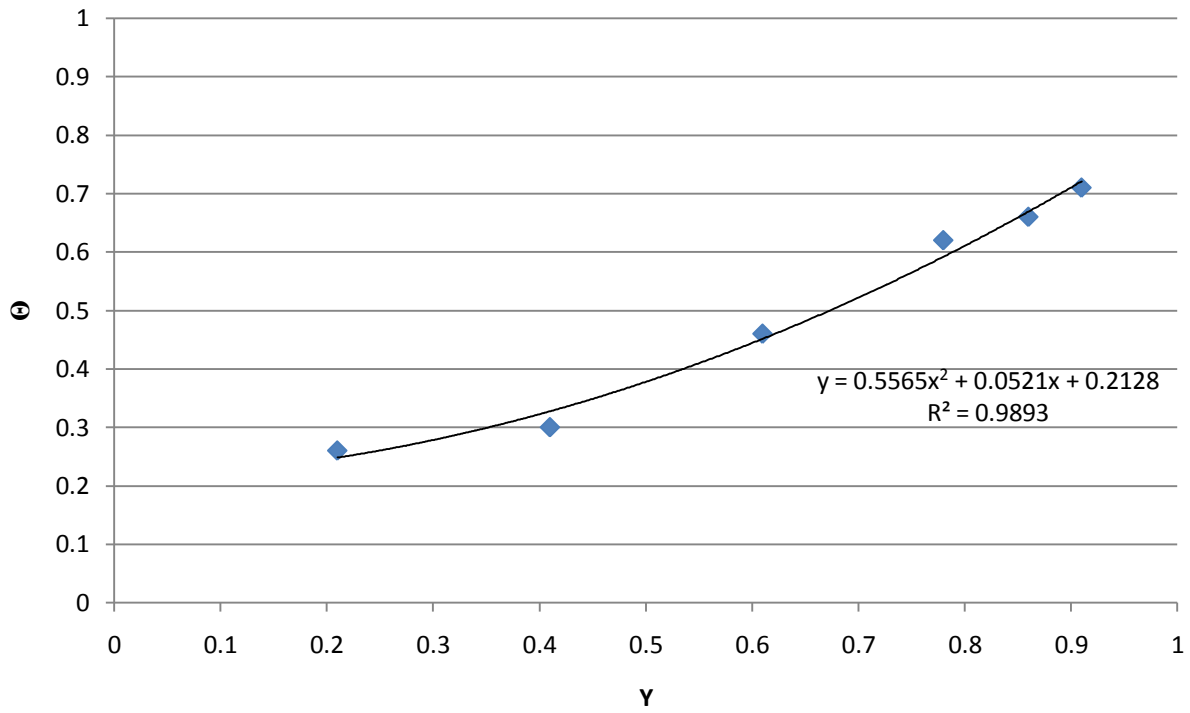




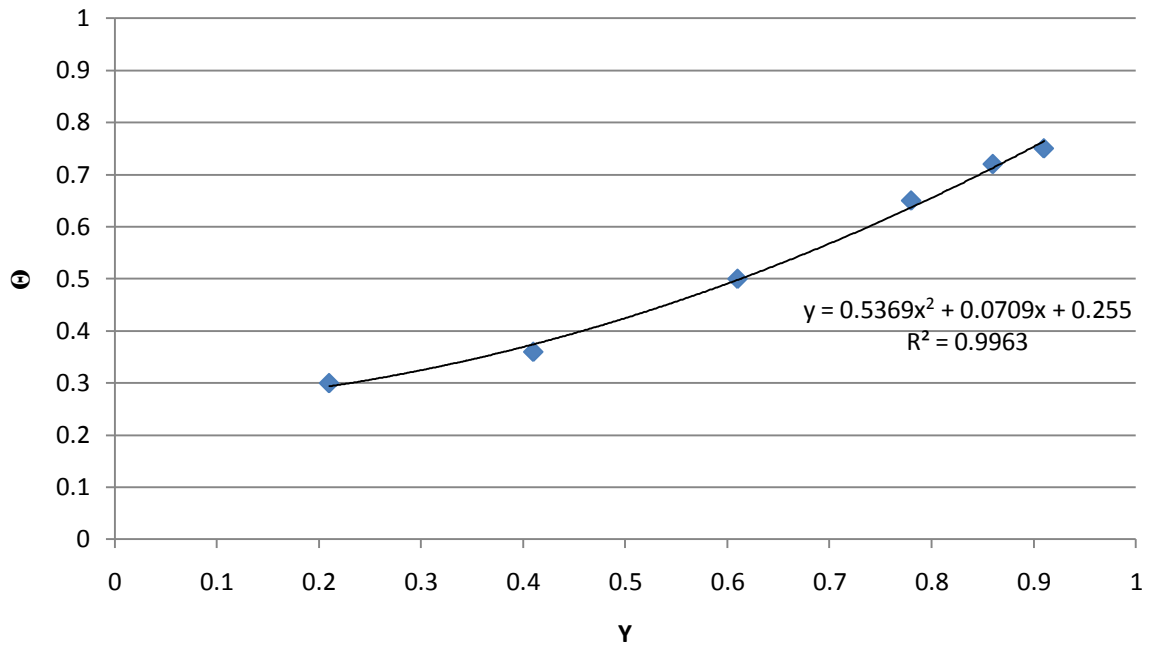
*4 inch Tube*



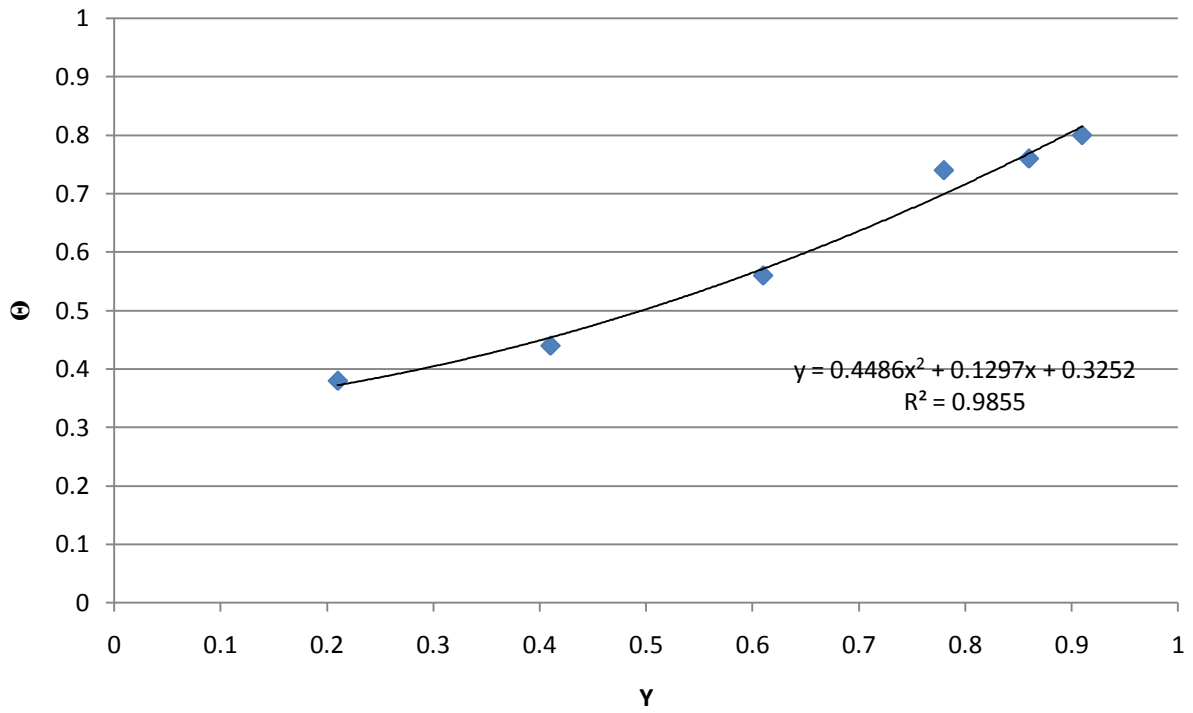
### $\Theta$ (Re = 246)



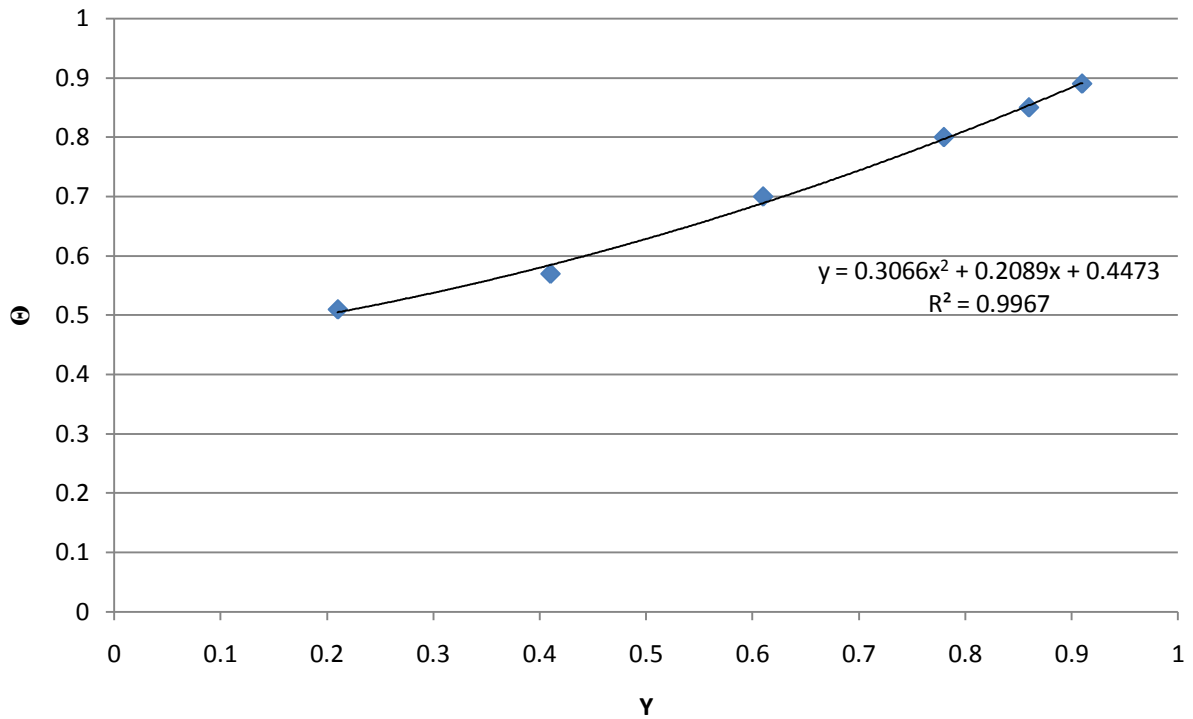
### $\Theta$ (Re = 199)



### $\Theta$ (Re = 149)

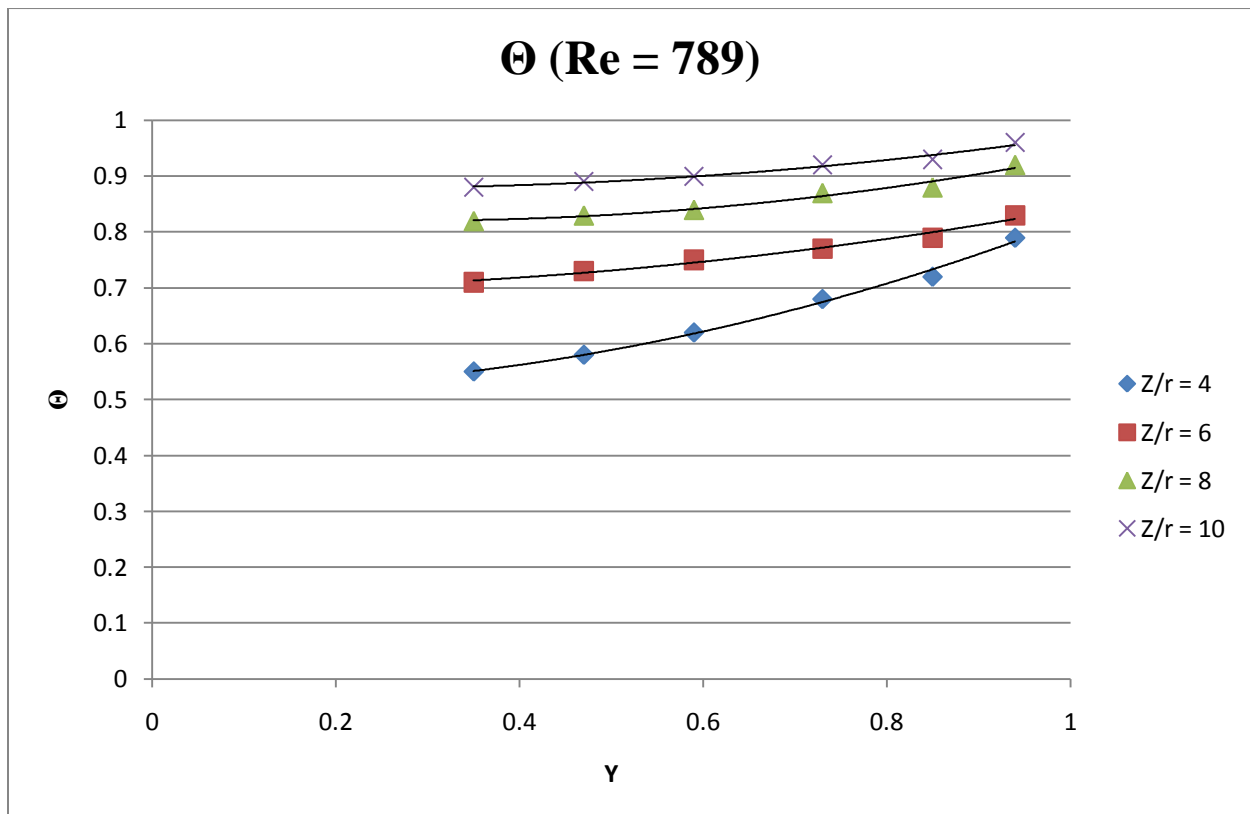
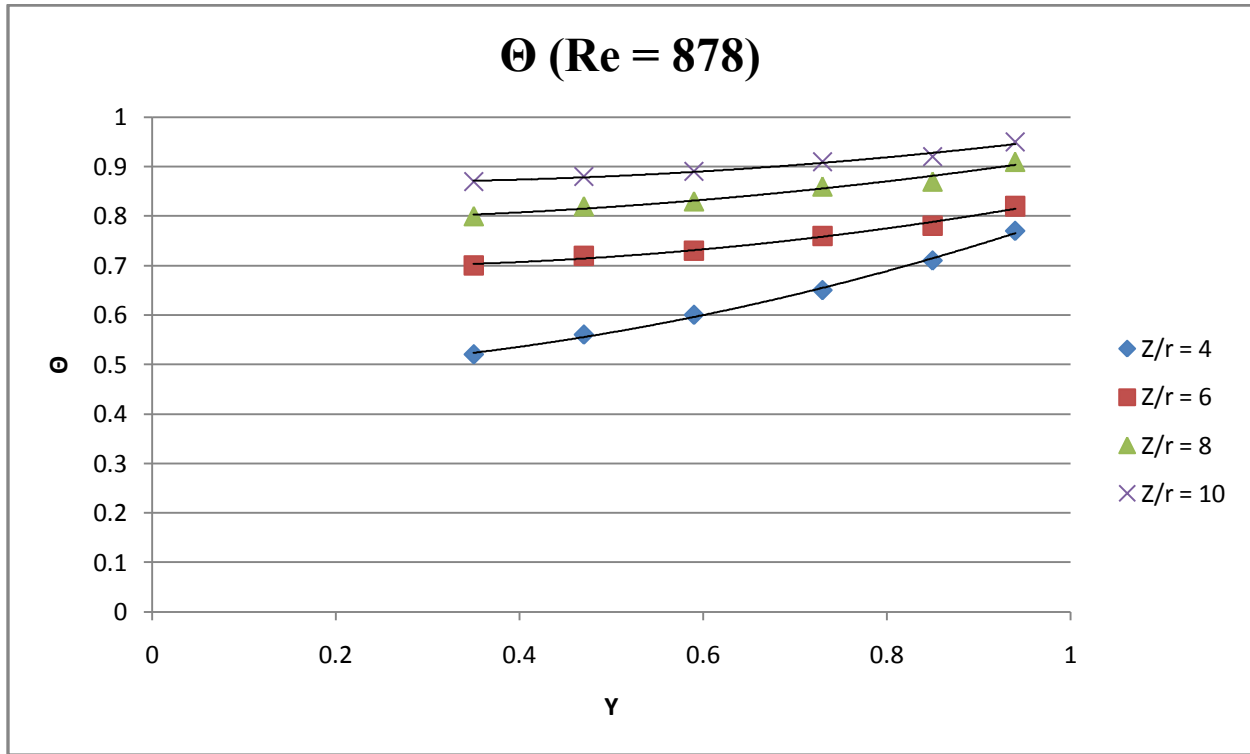


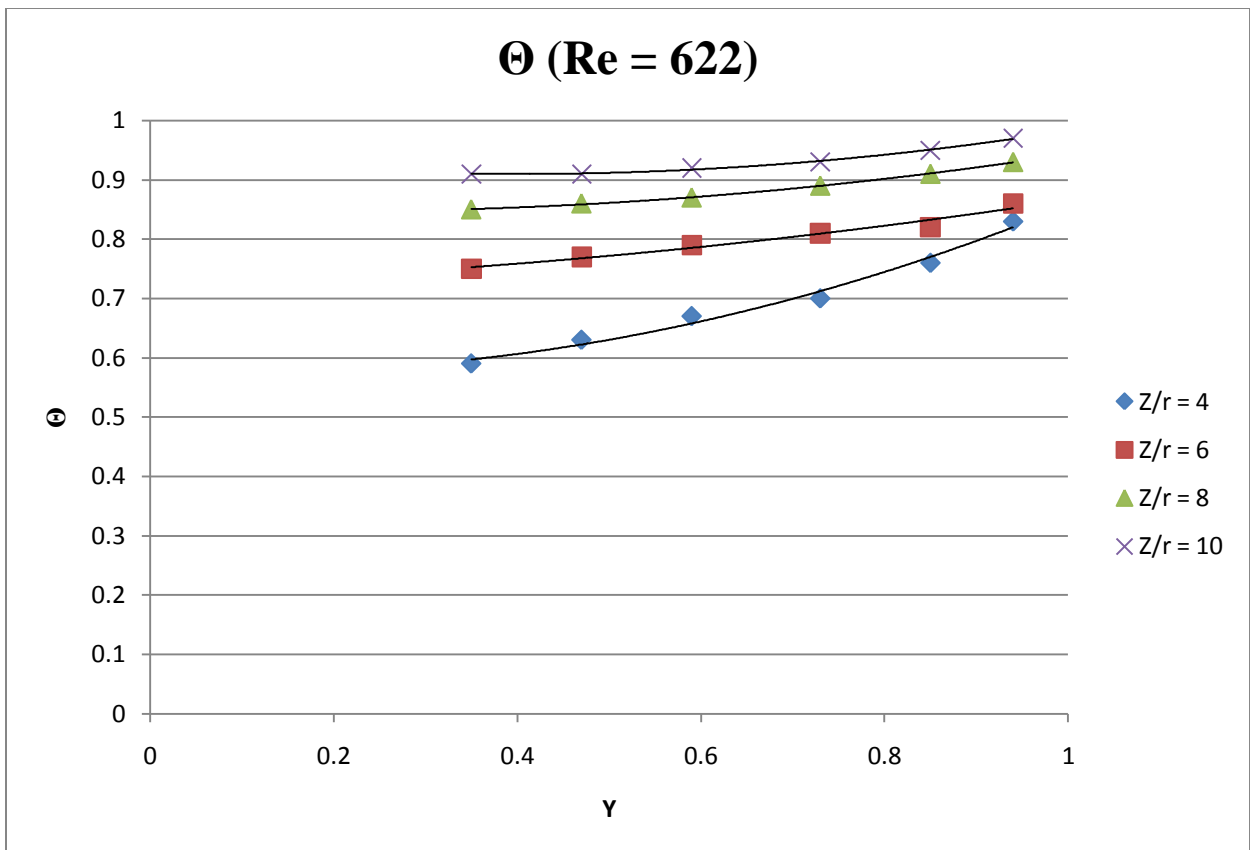
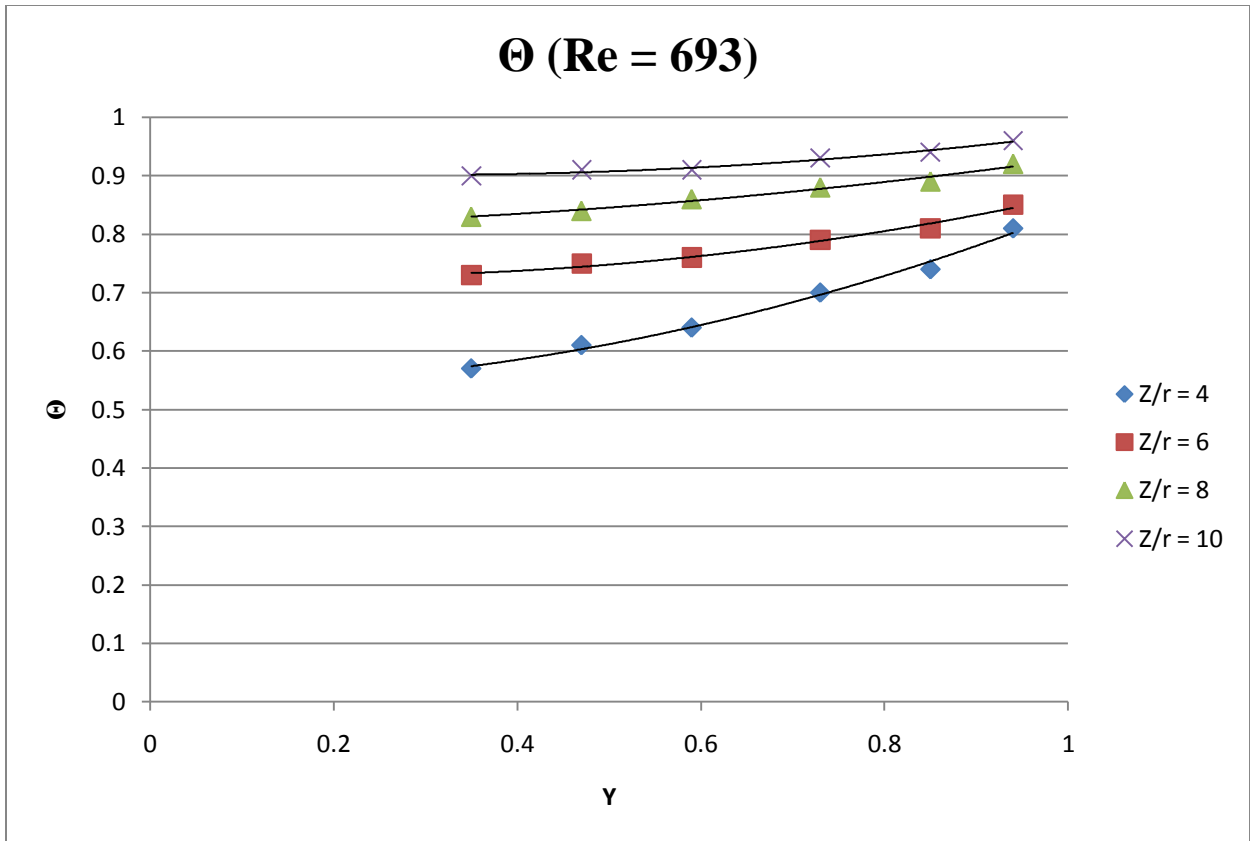
### $\Theta$ (Re = 102)

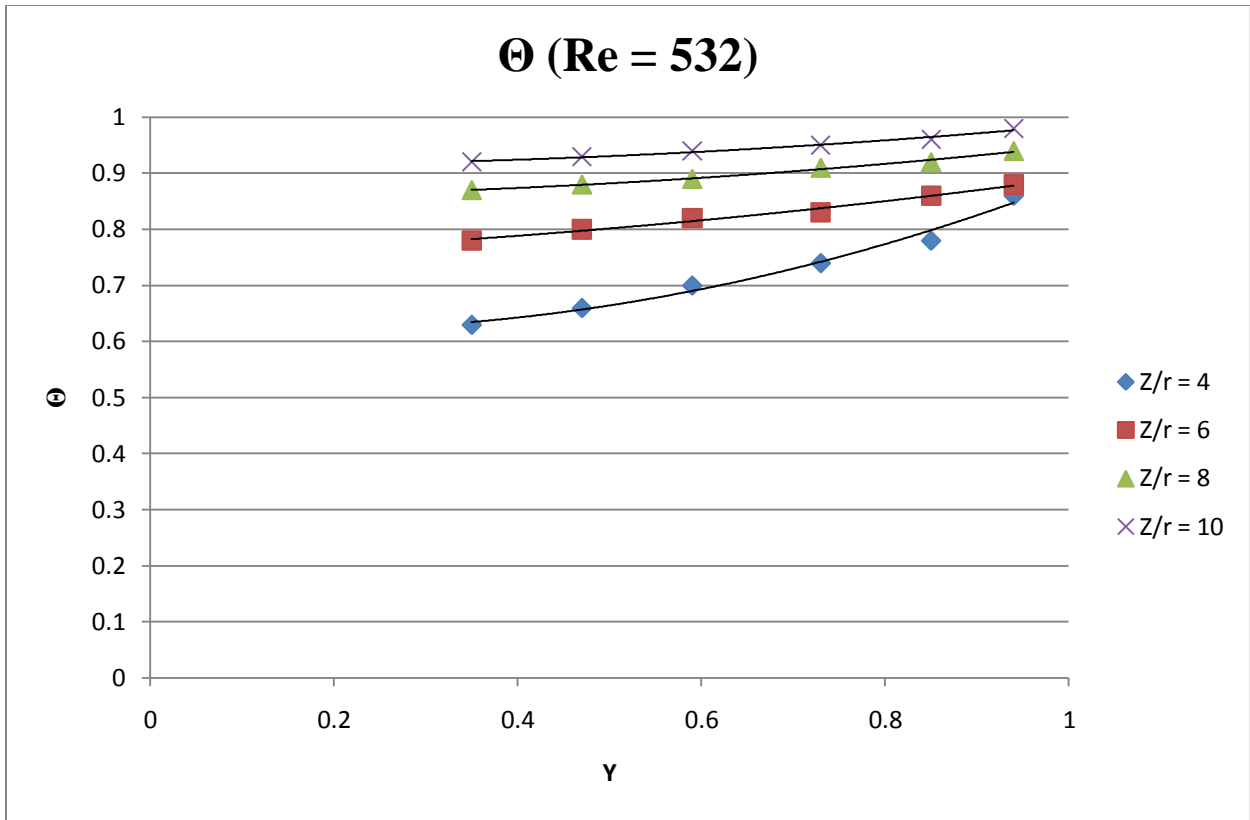


## All Bed Heights

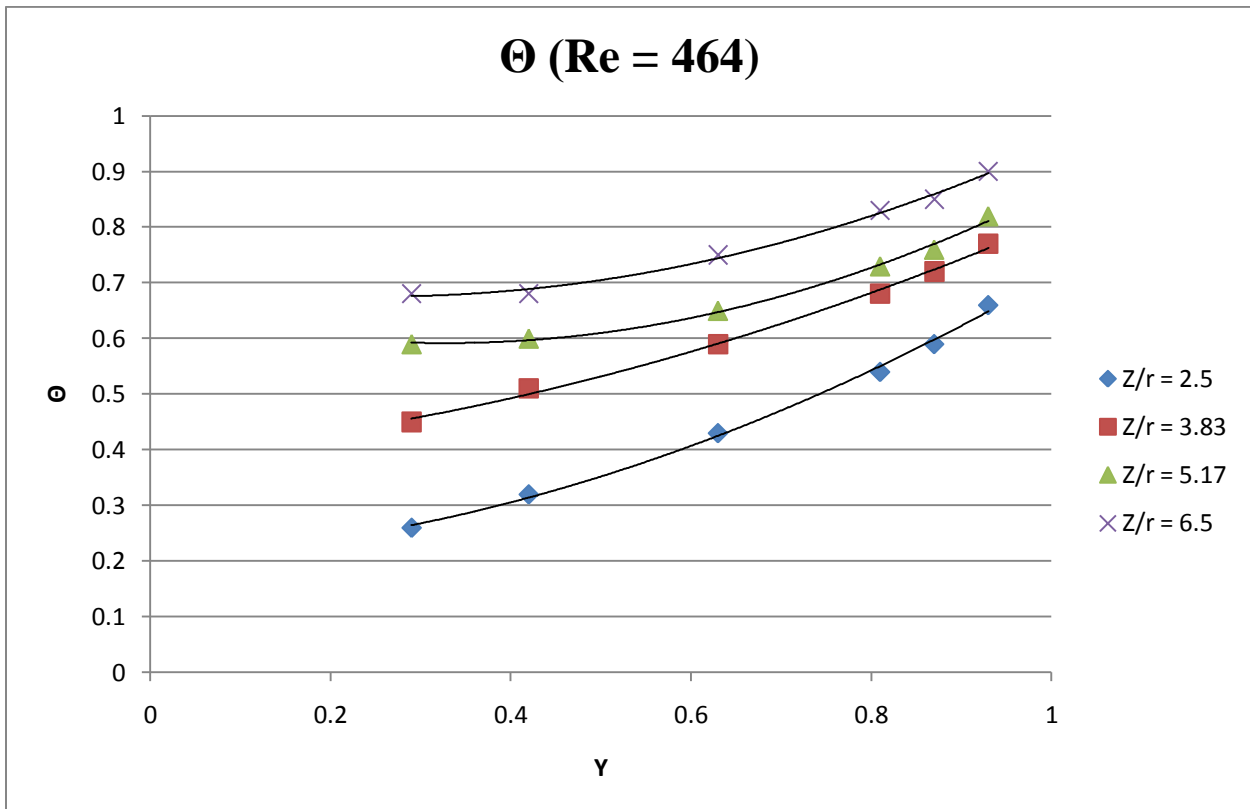
### 2inch Tube

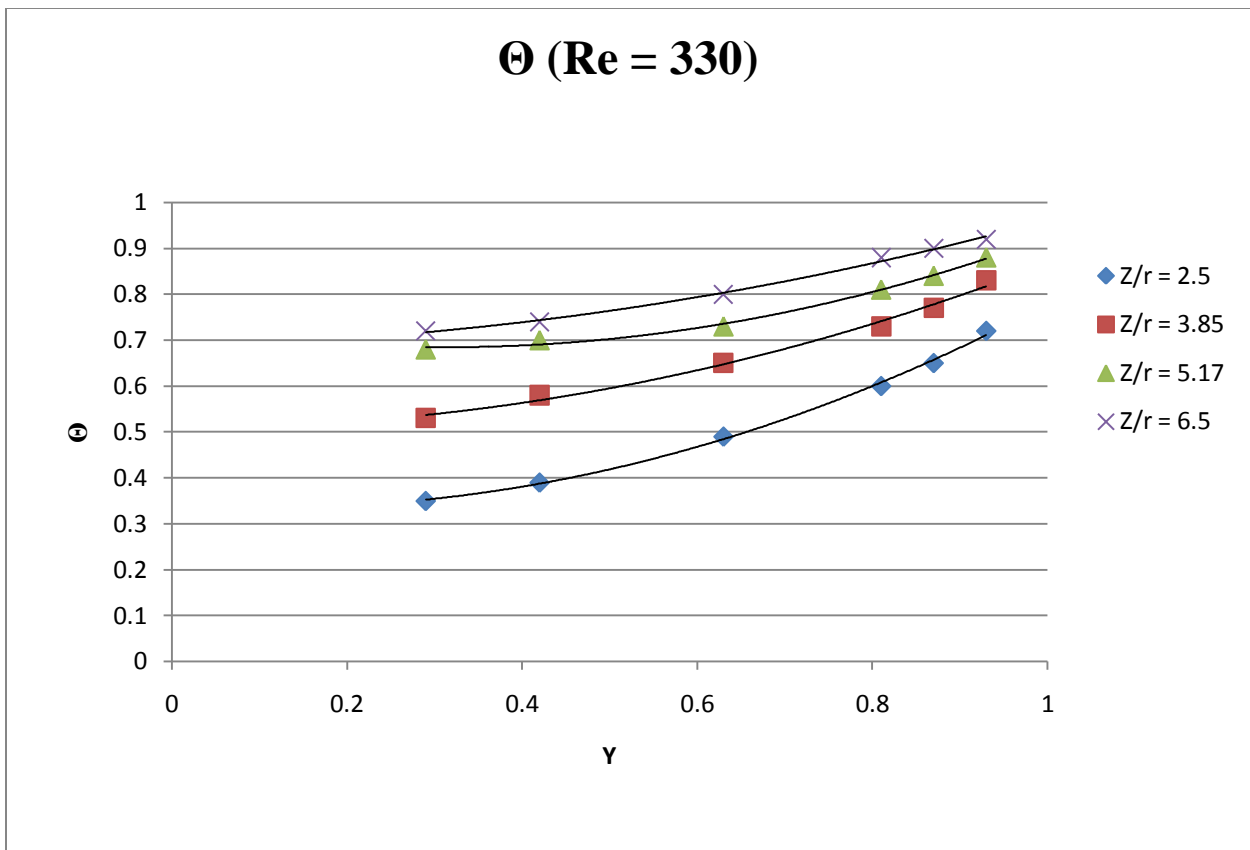
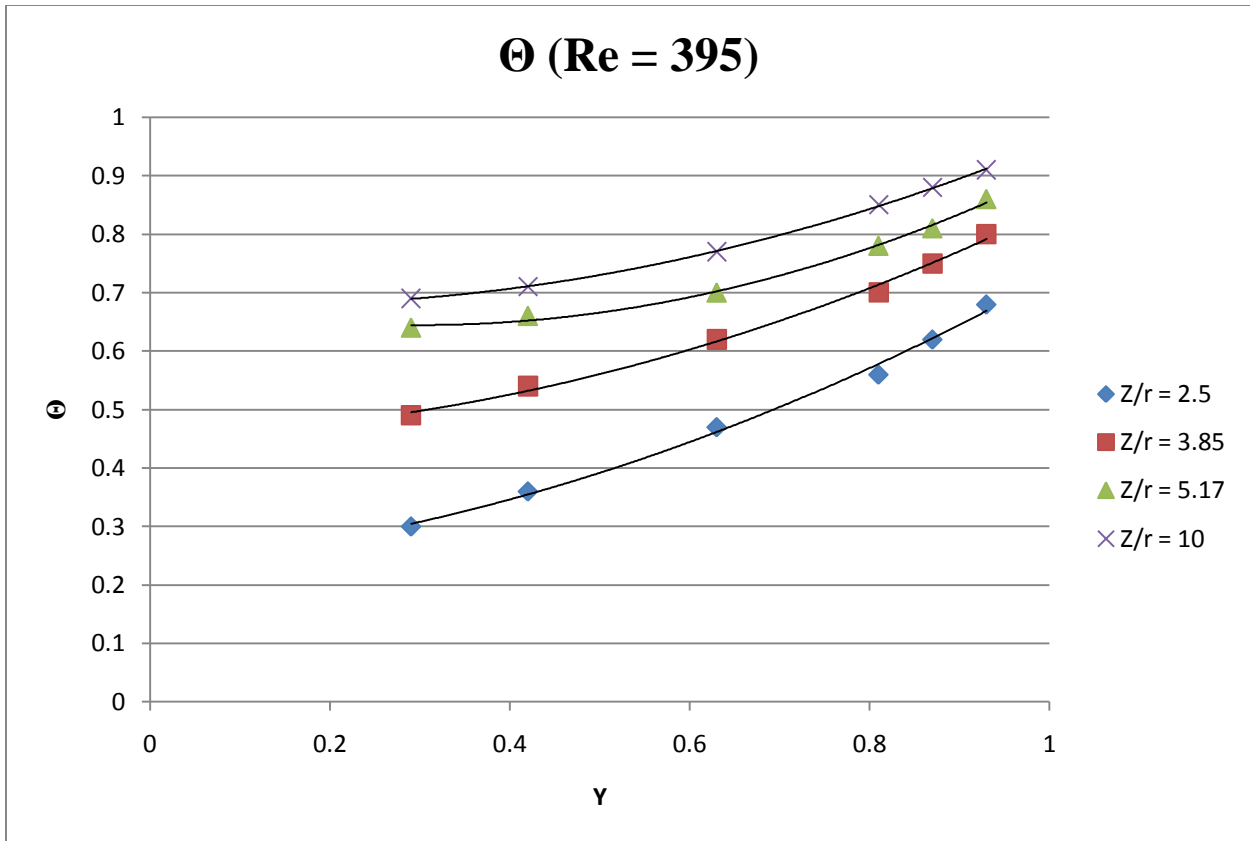


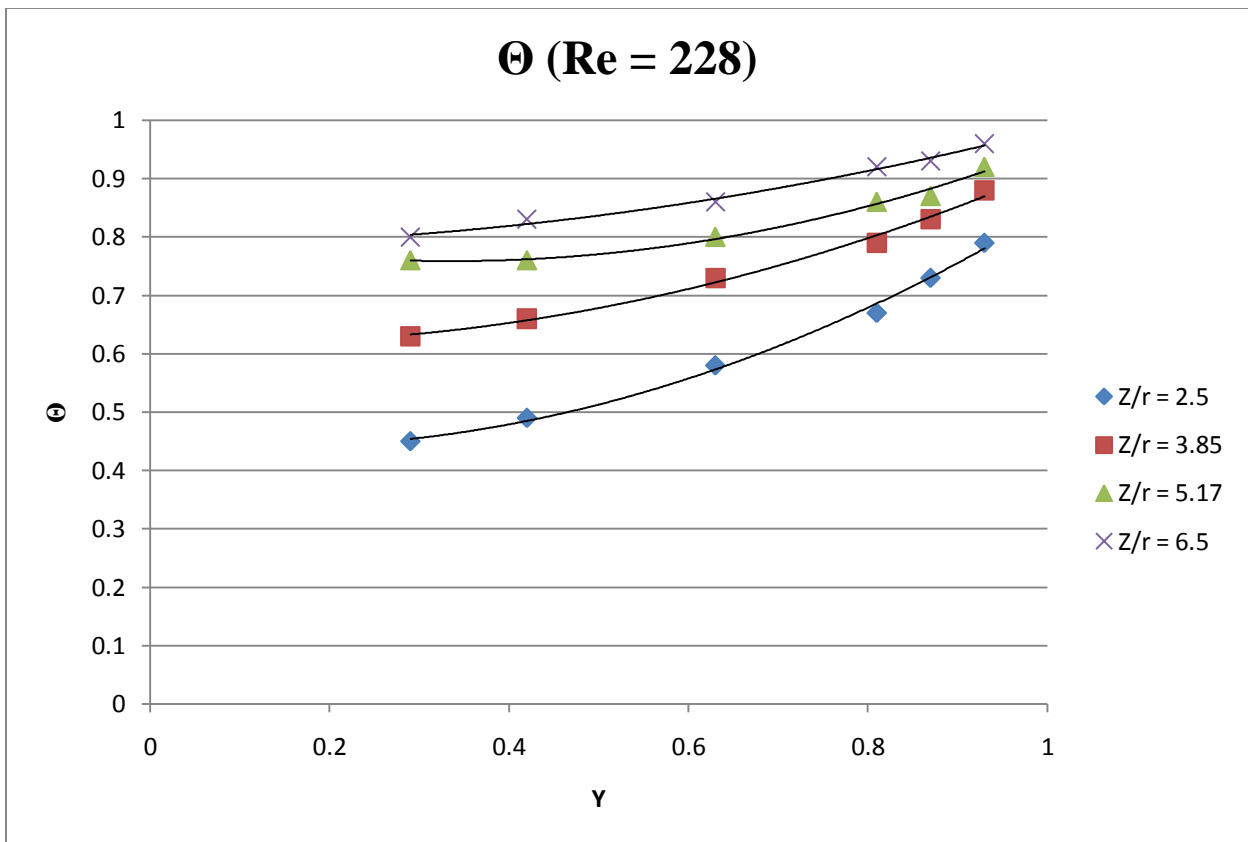
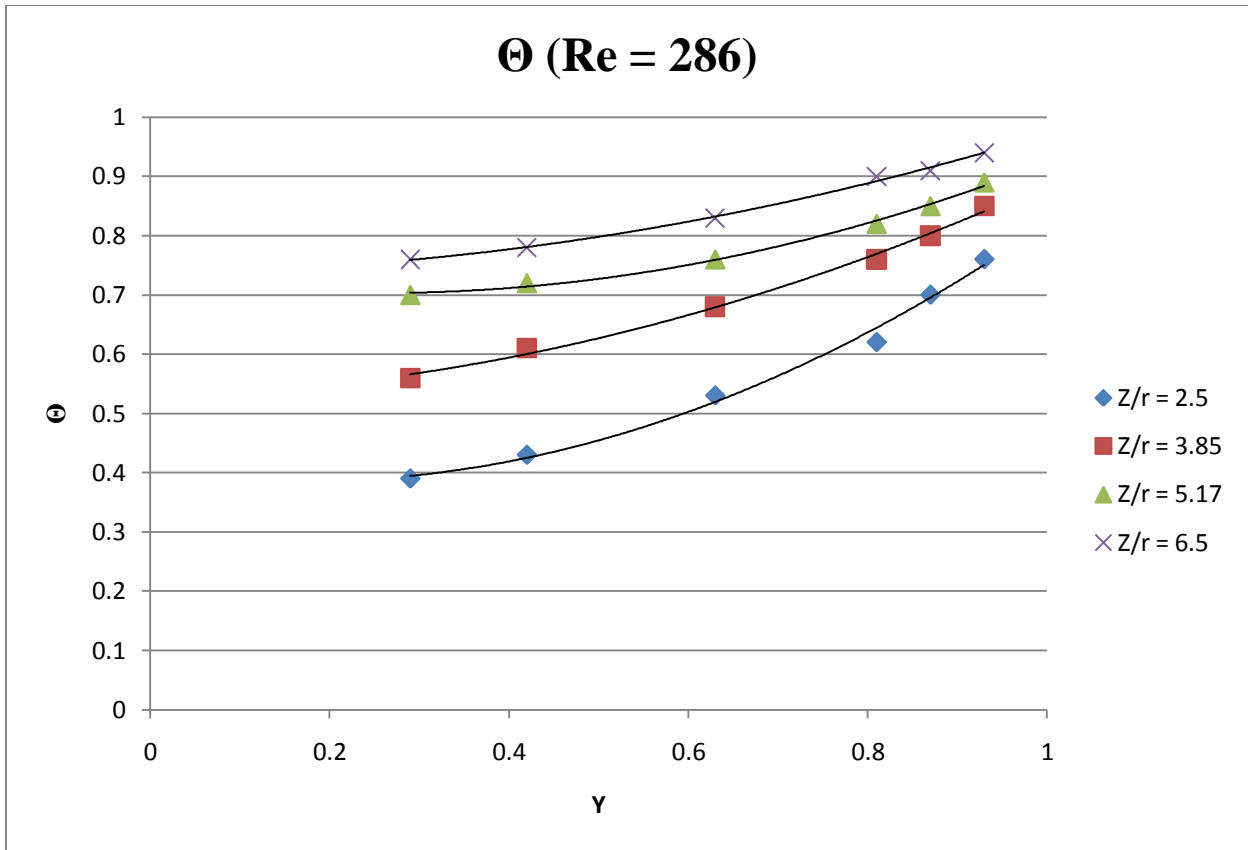




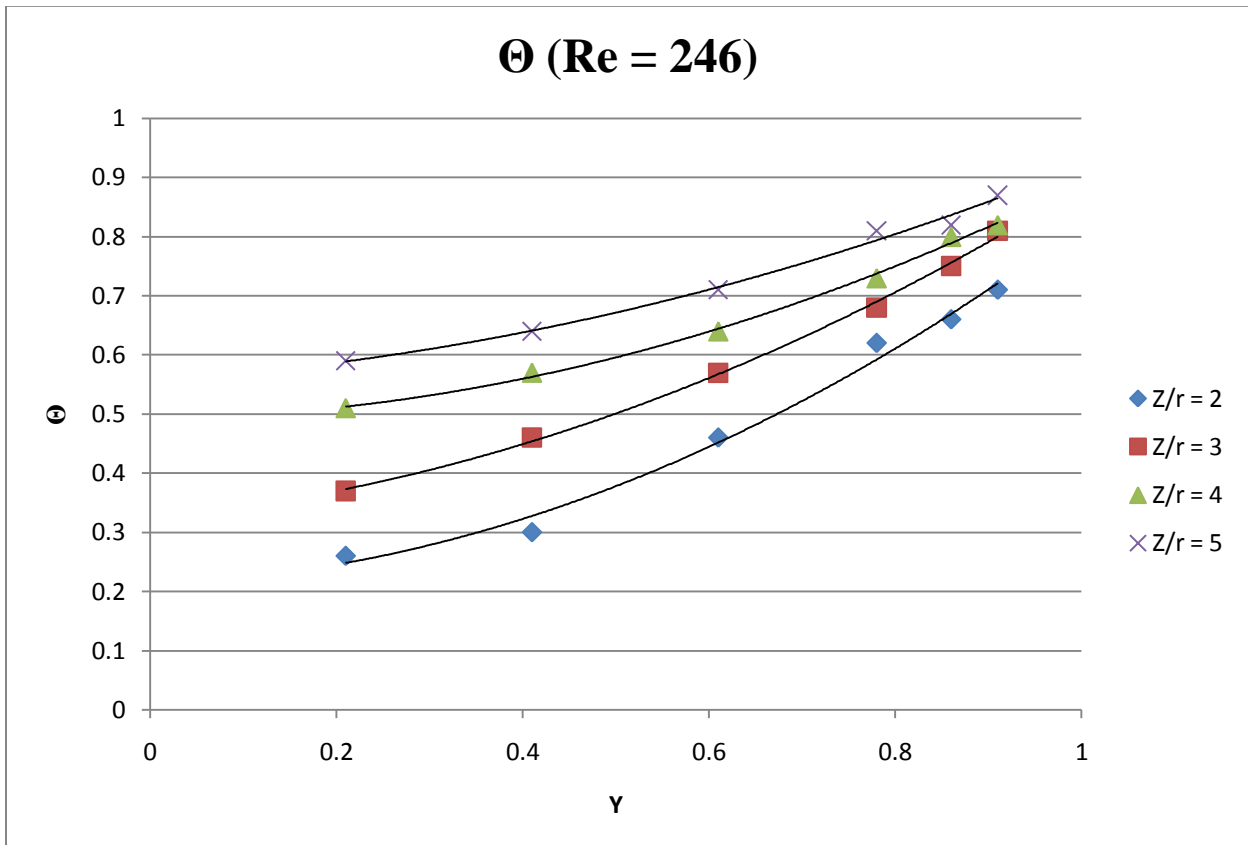
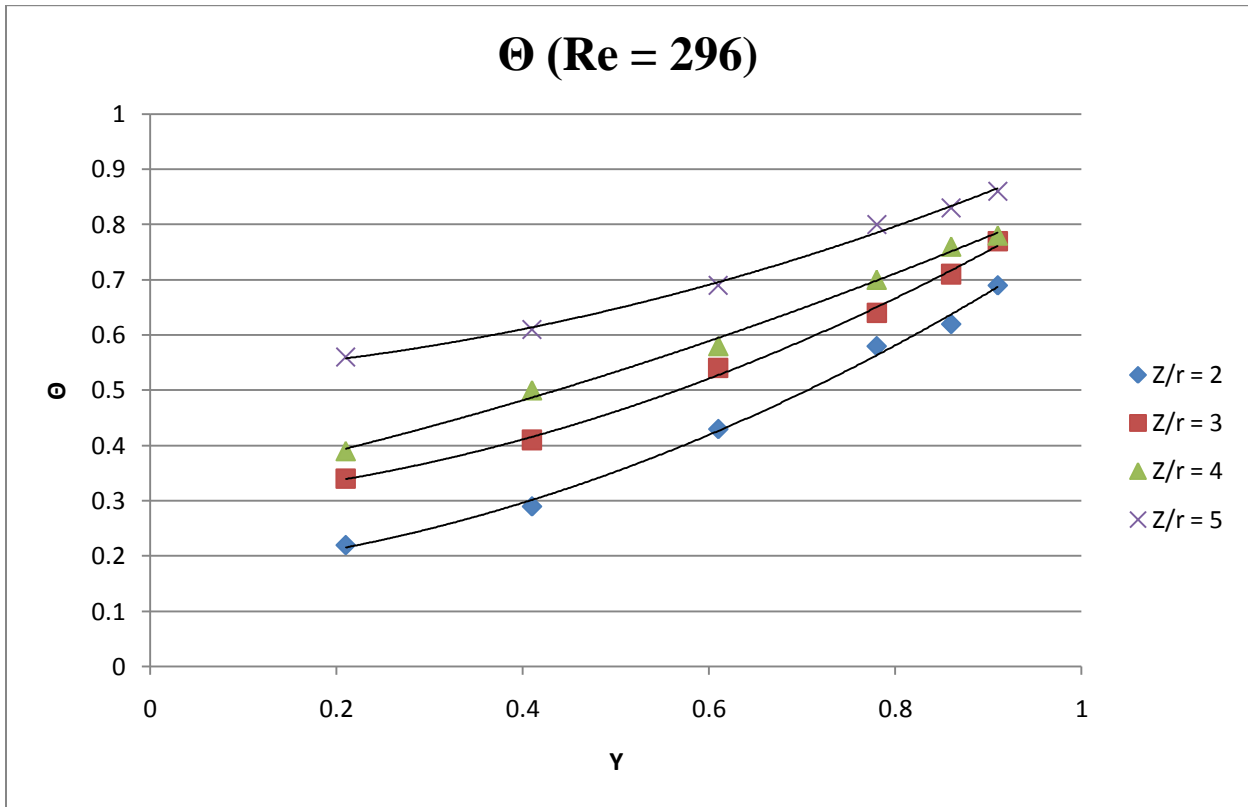
*3 inch Tube*



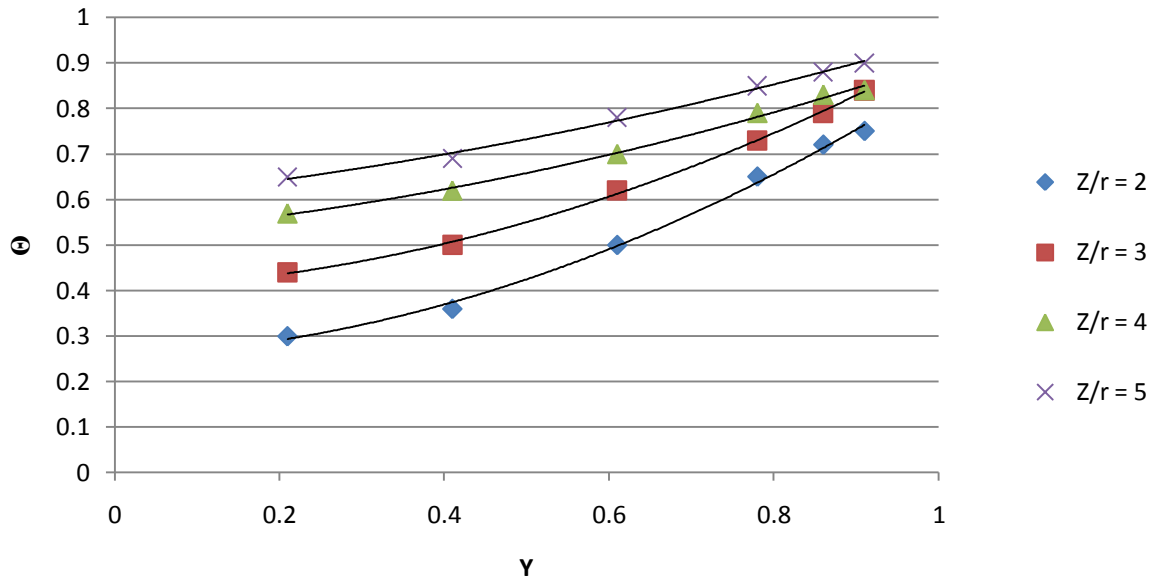




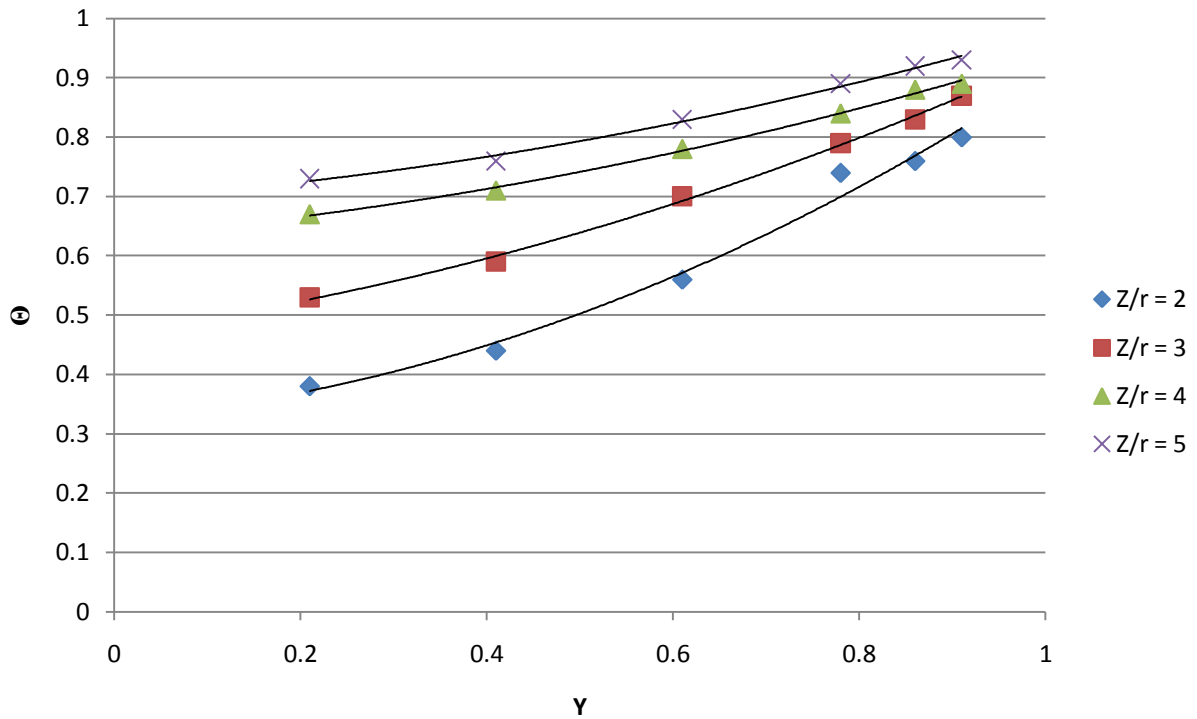
4 inch Tube

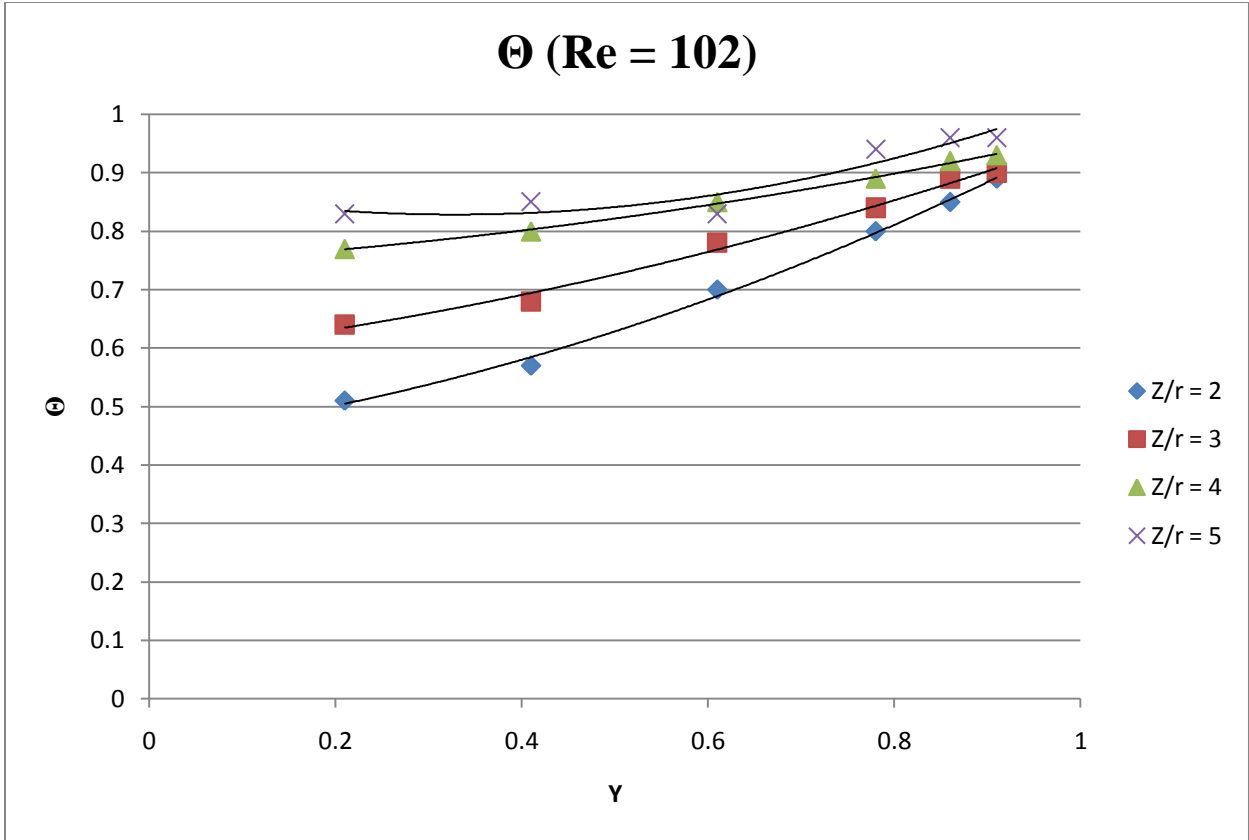


### $\Theta$ (Re = 199)



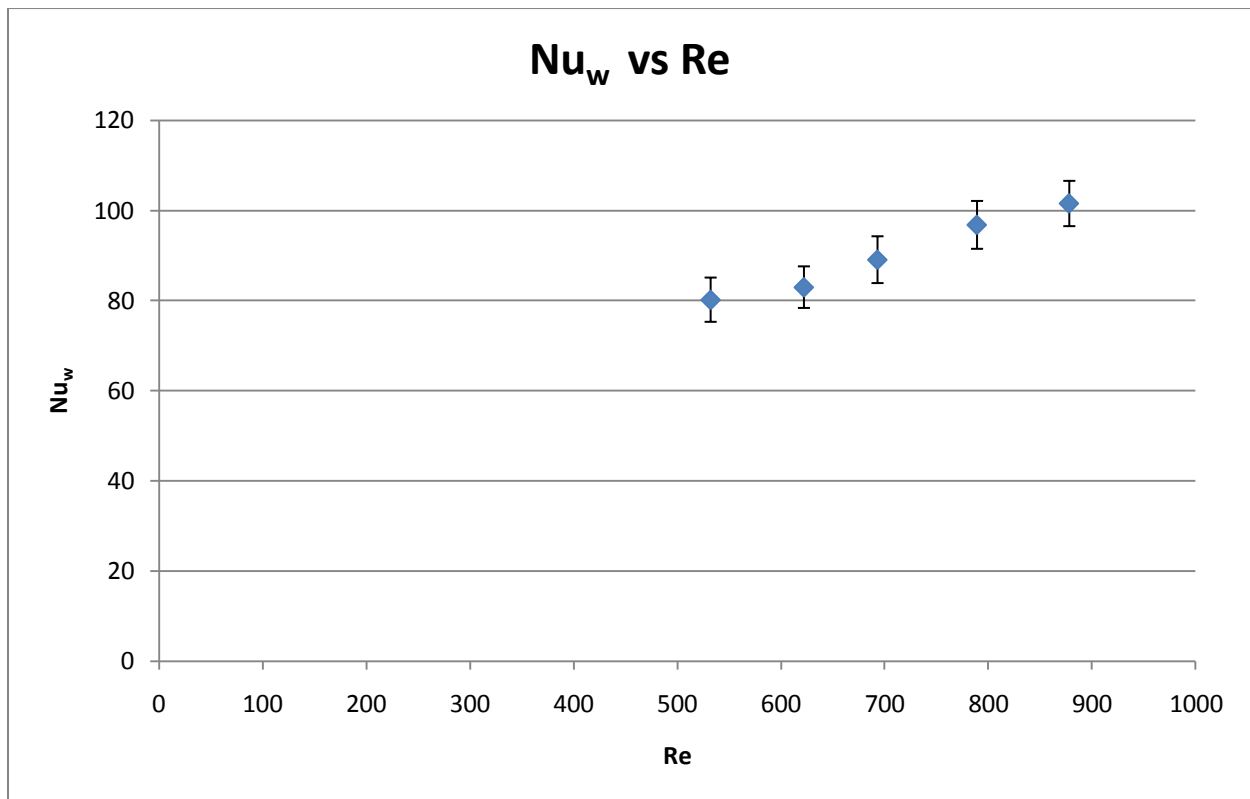
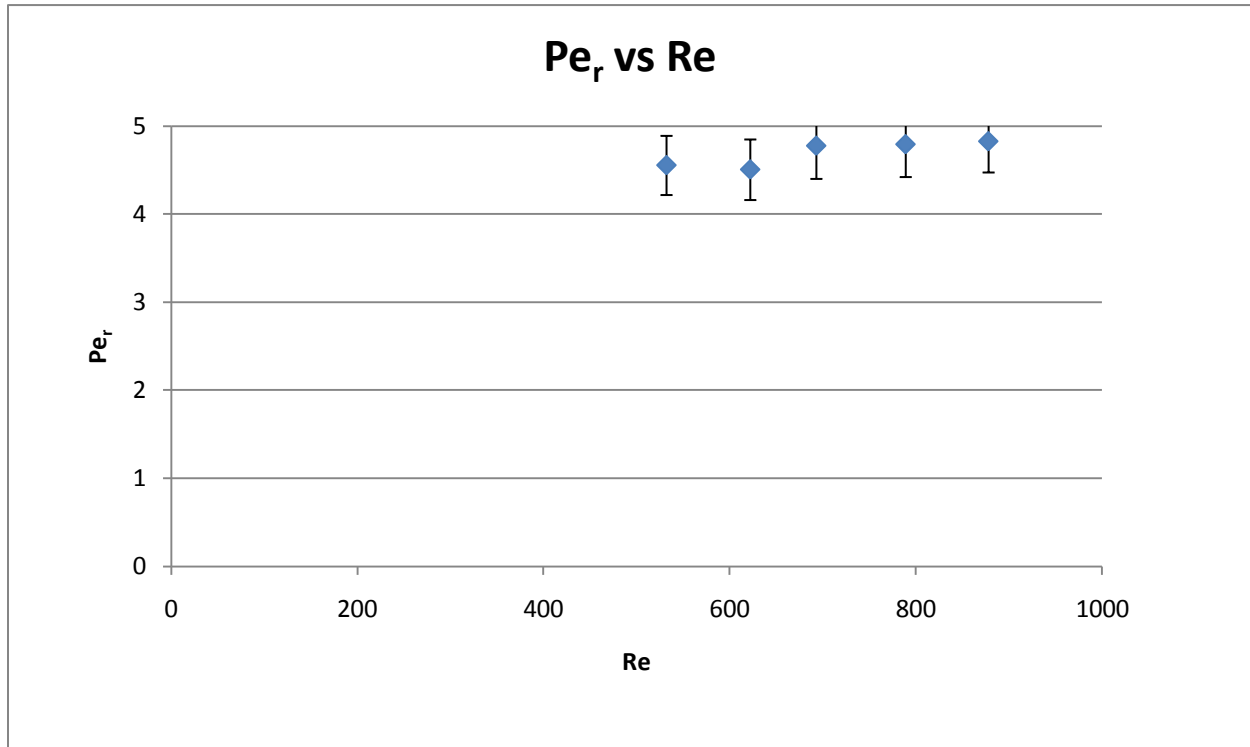
### $\Theta$ (Re = 149)

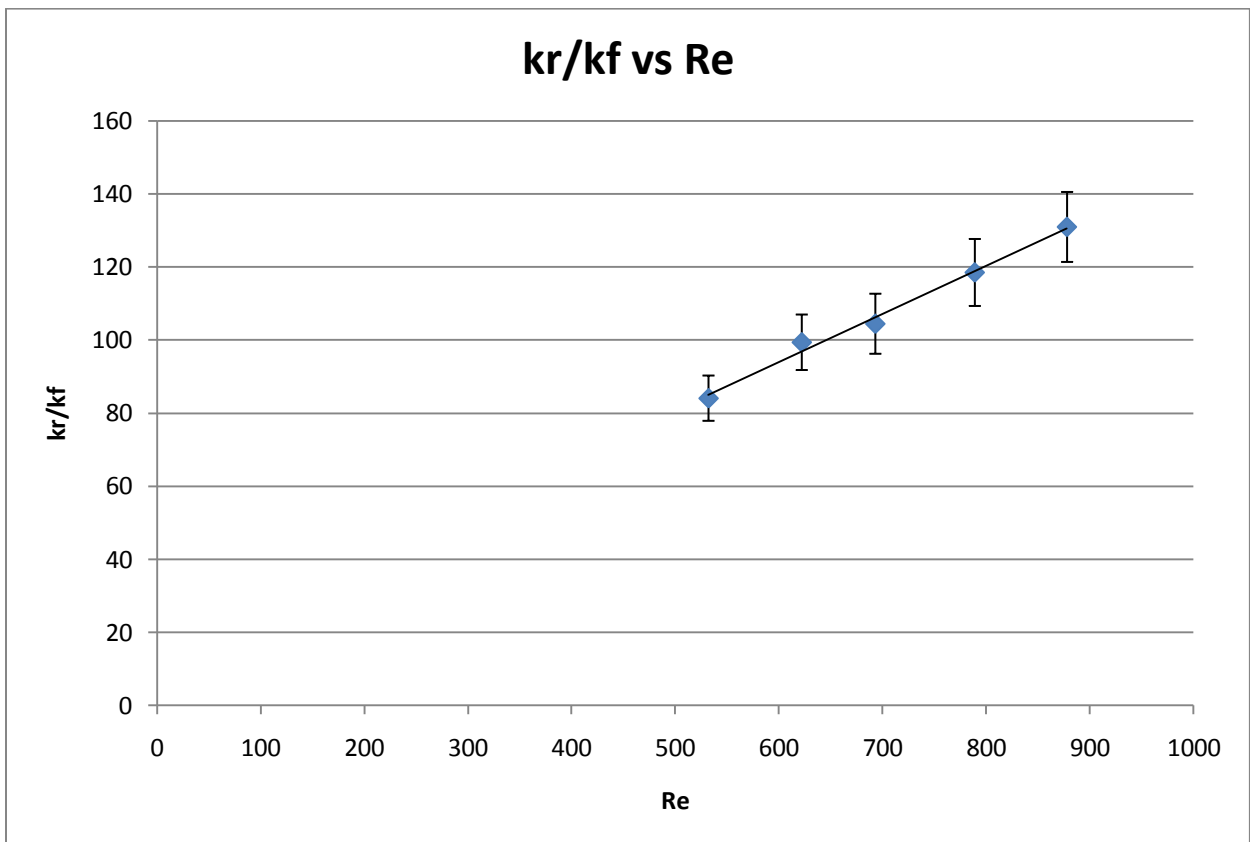
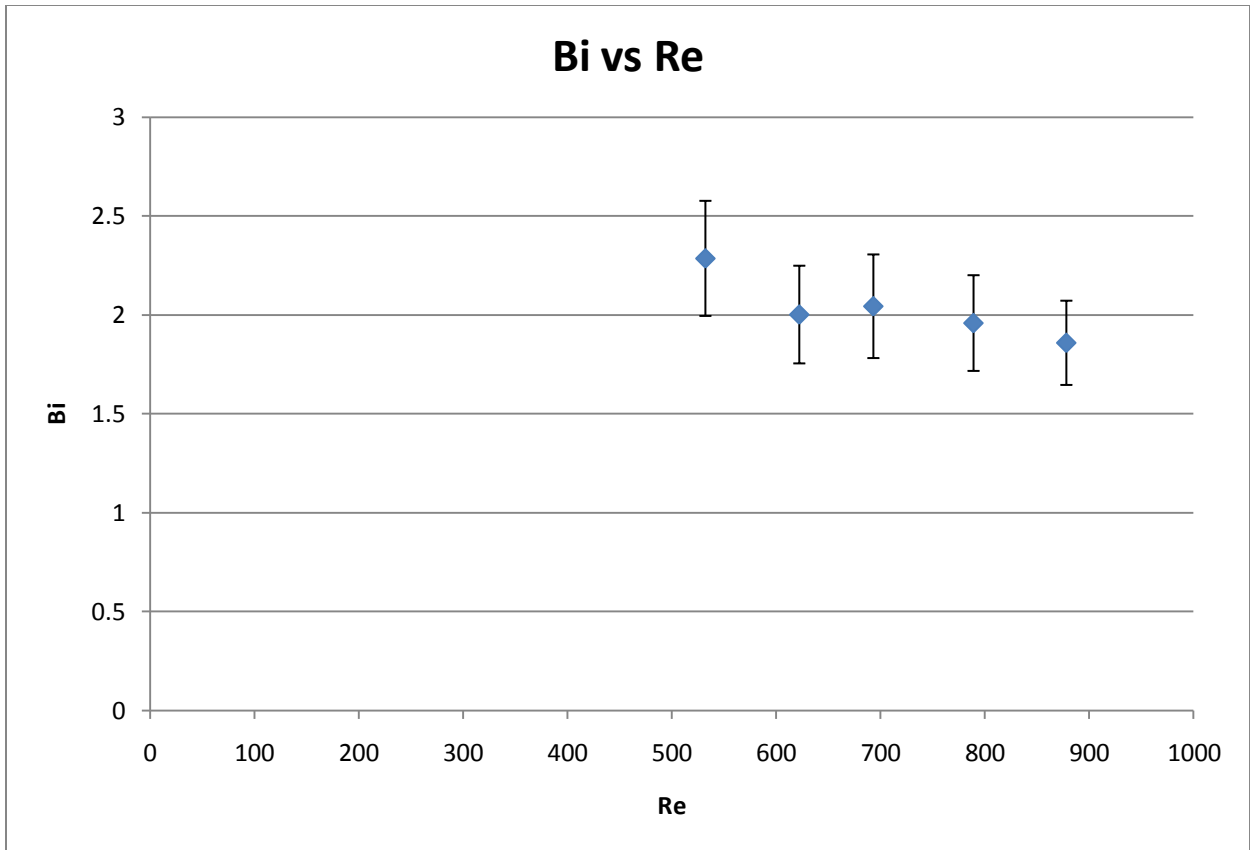




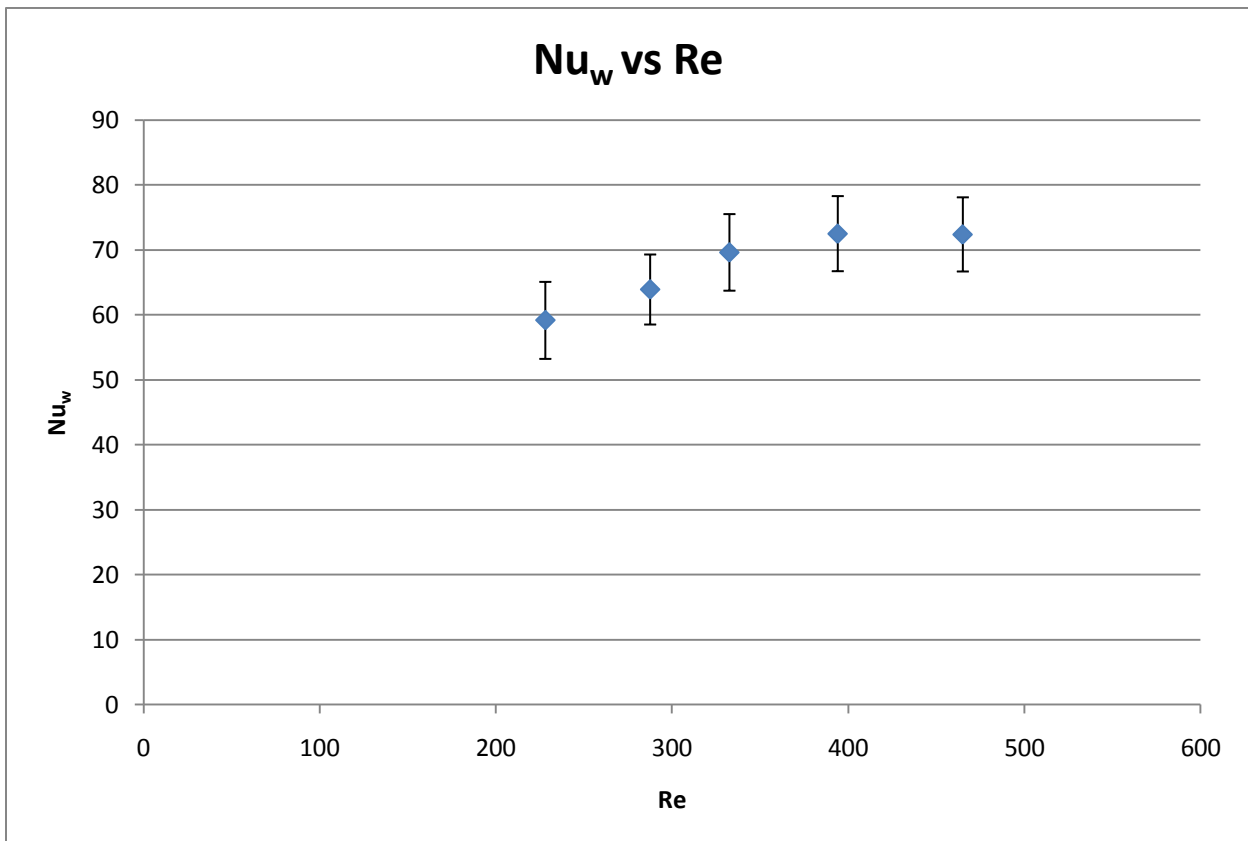
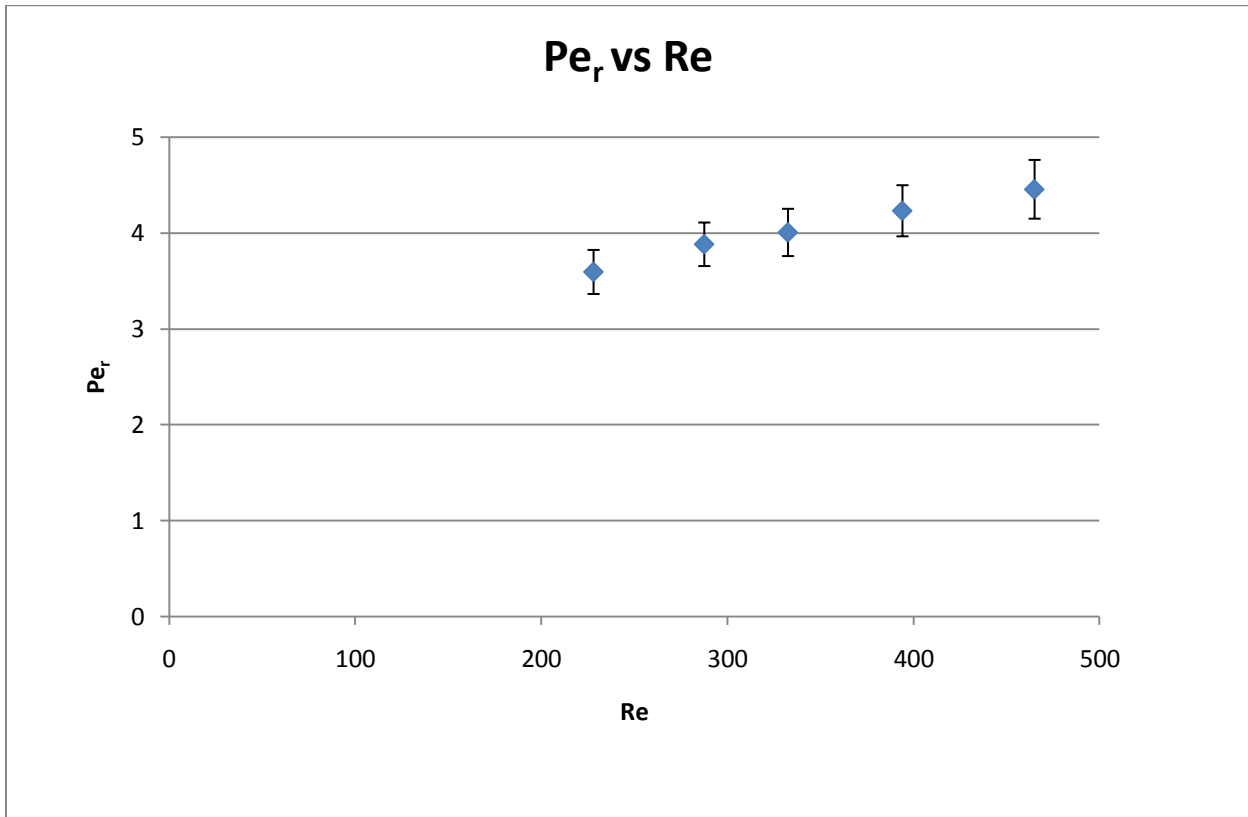
## Heat Transfer Parameters vs. Re

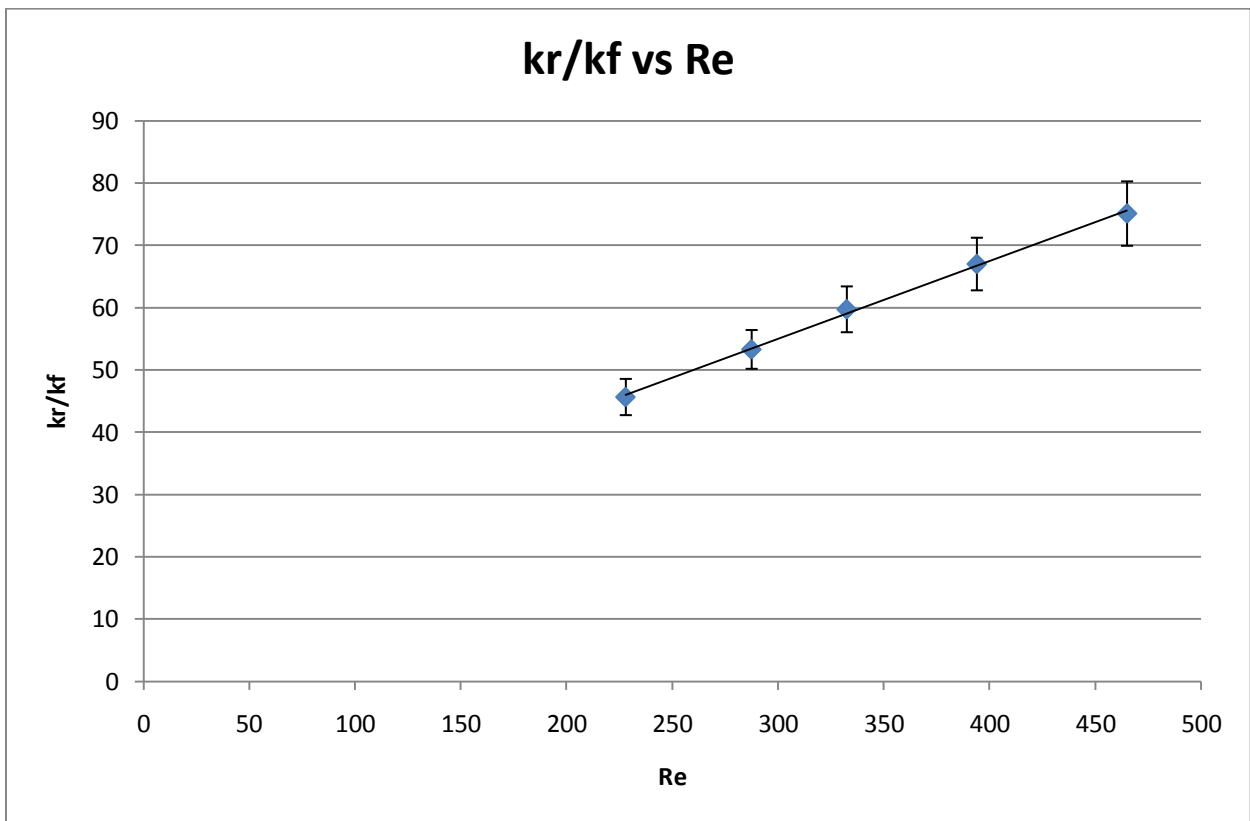
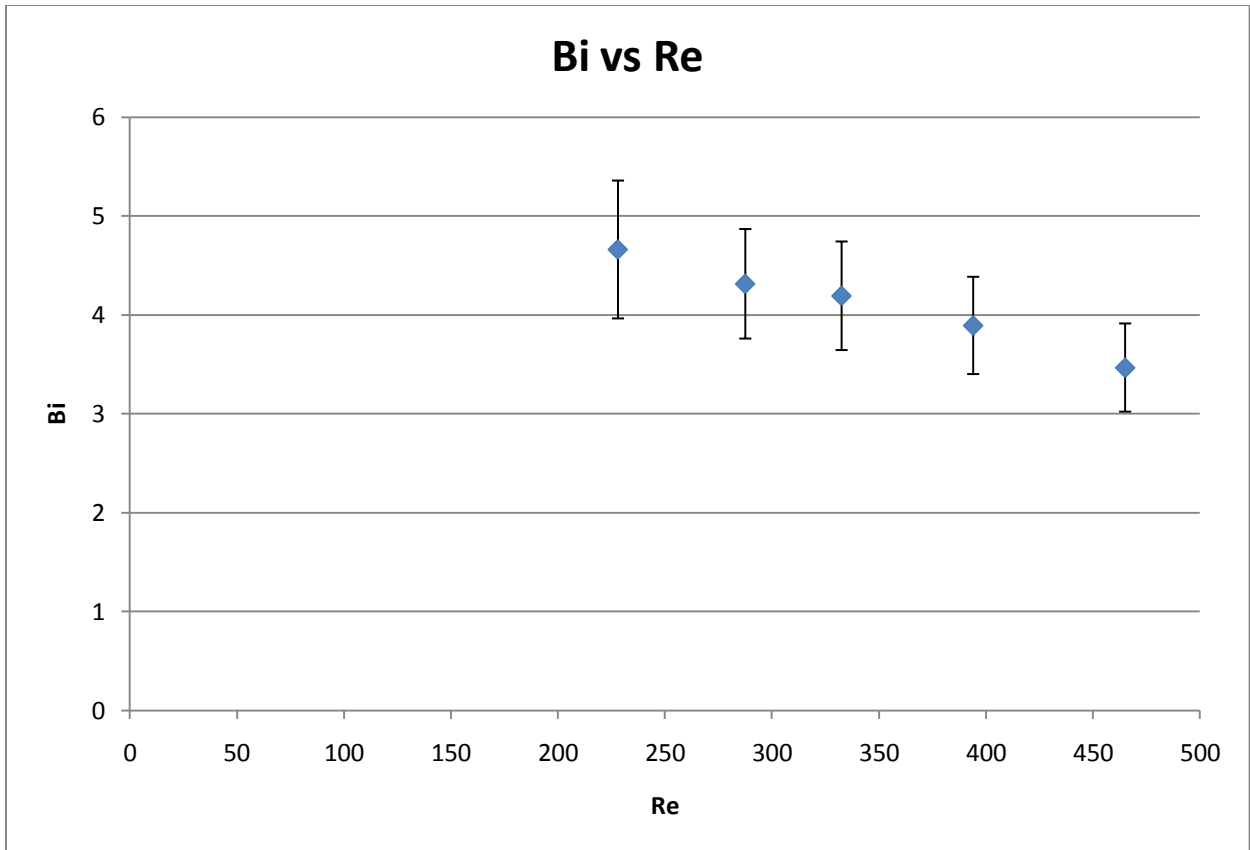
### 2 inch Tube



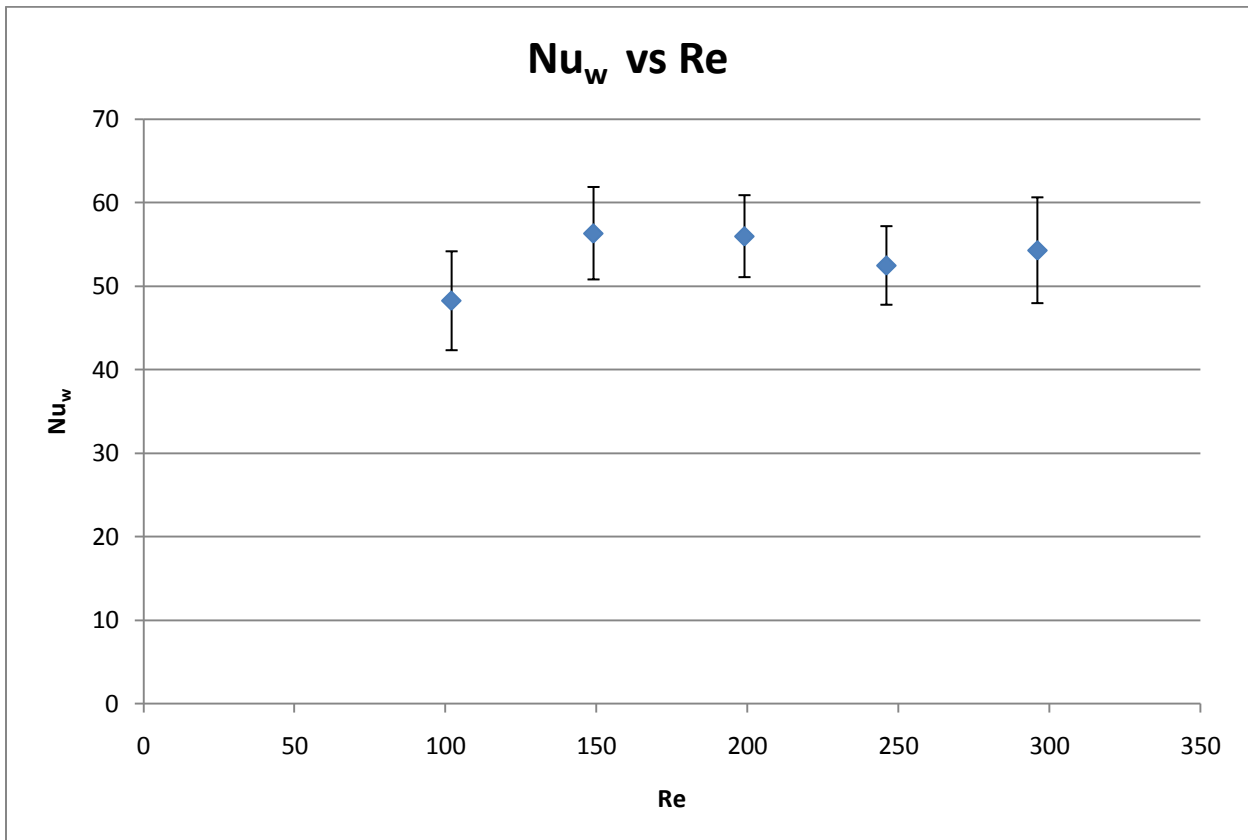
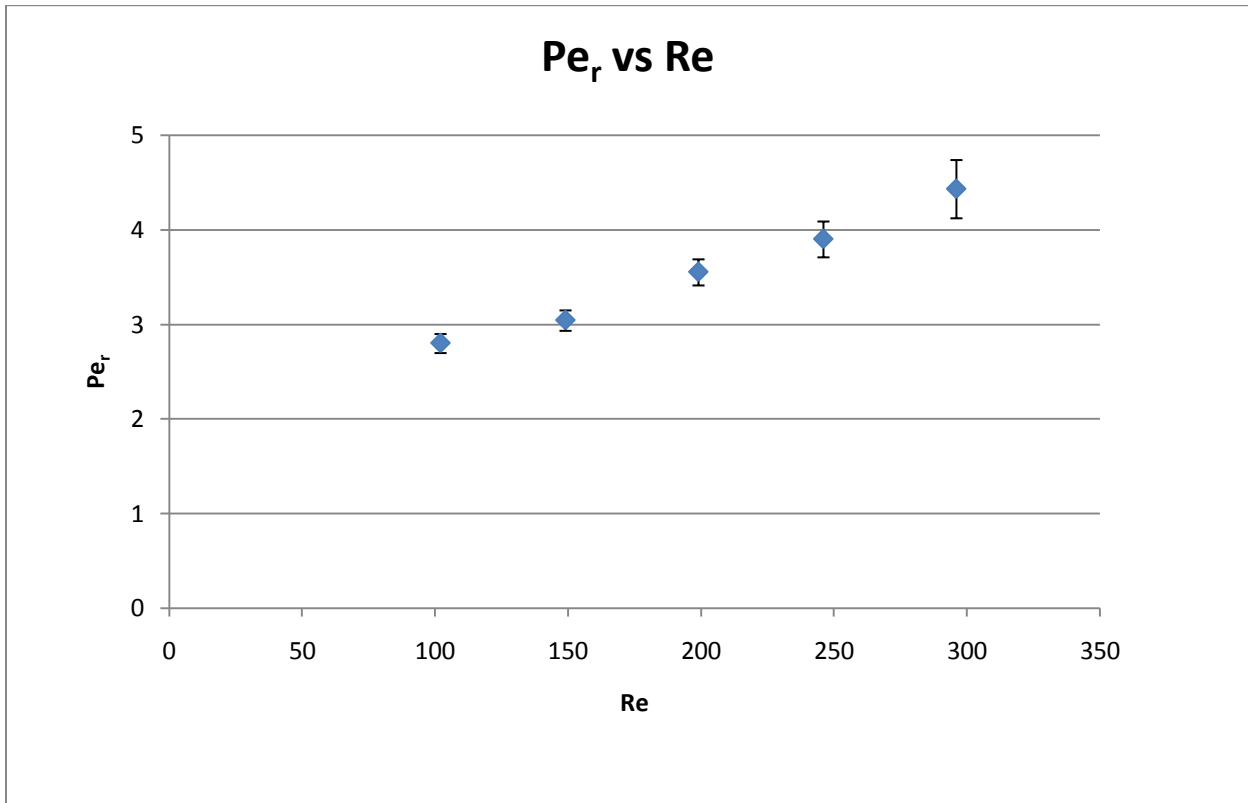


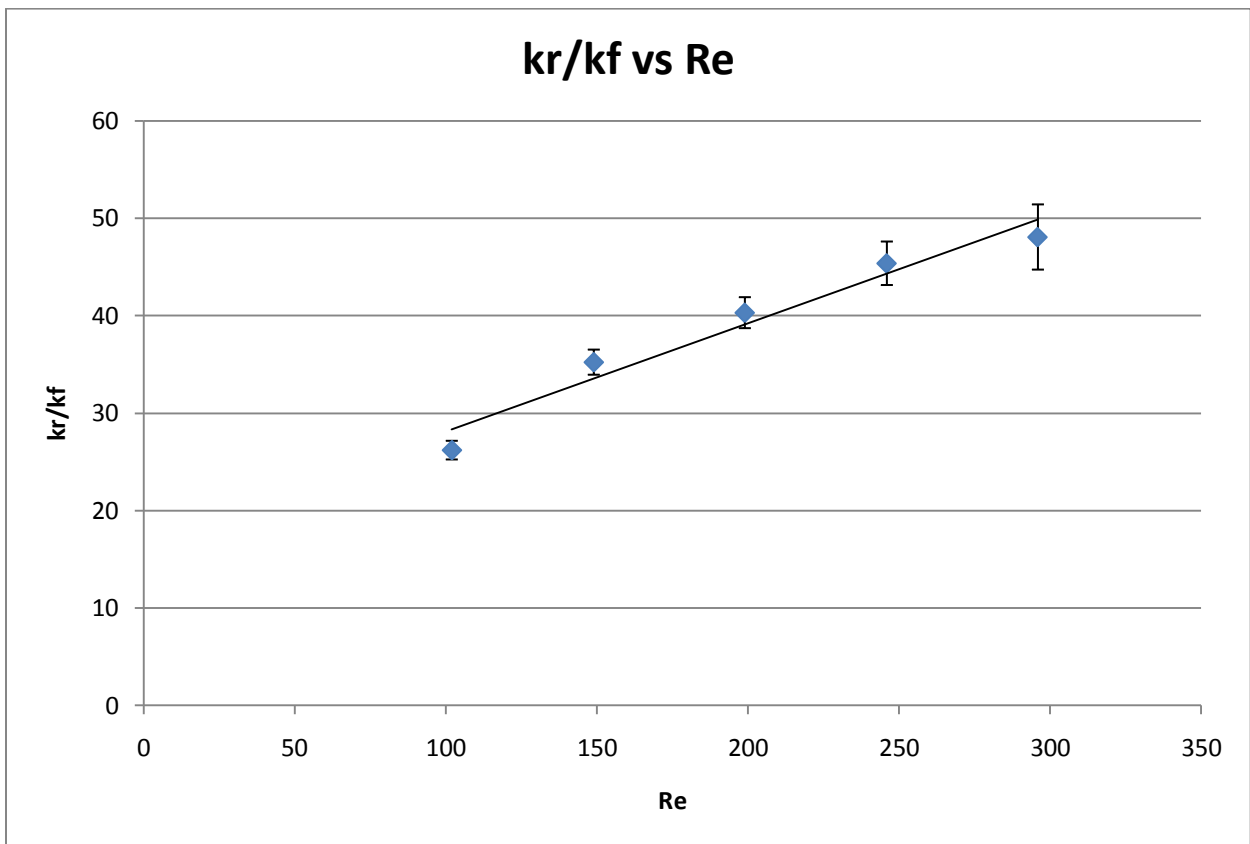
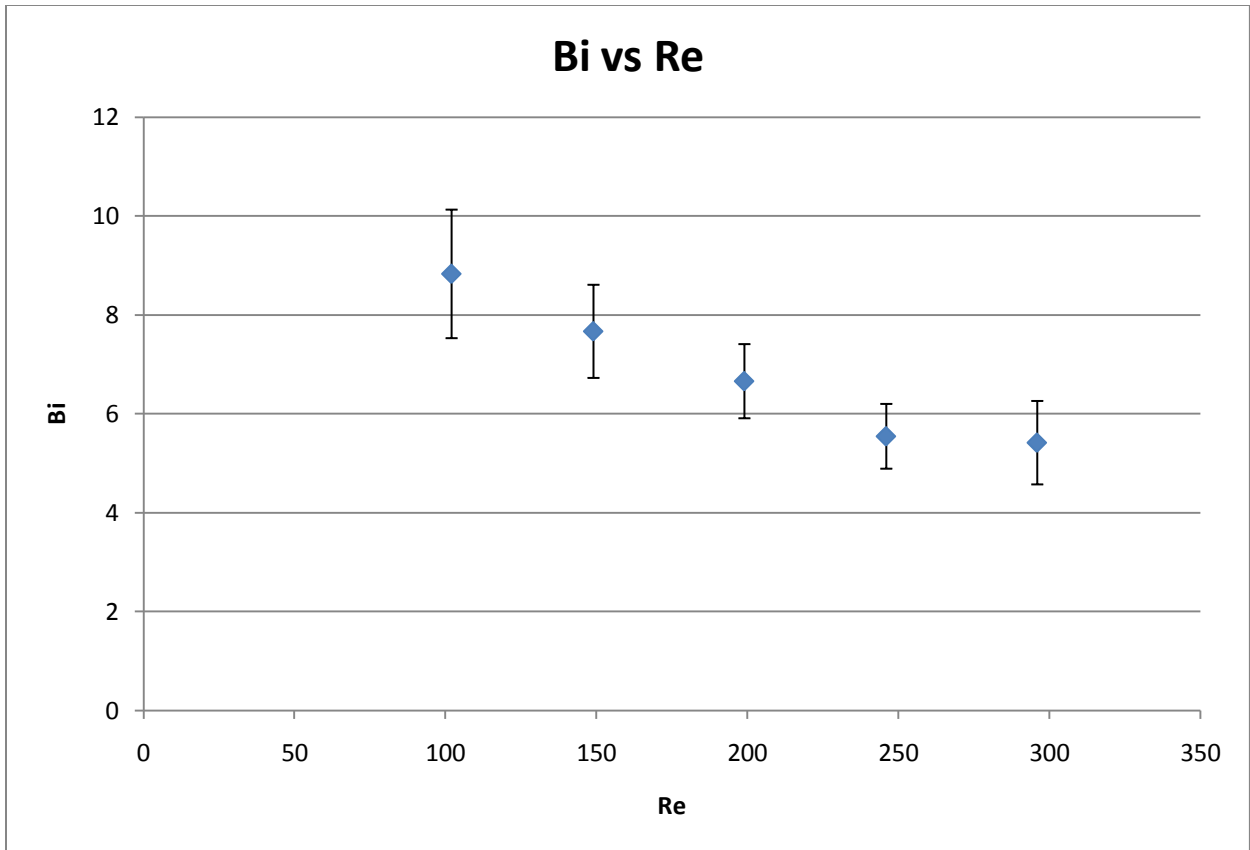
3 inch Tube



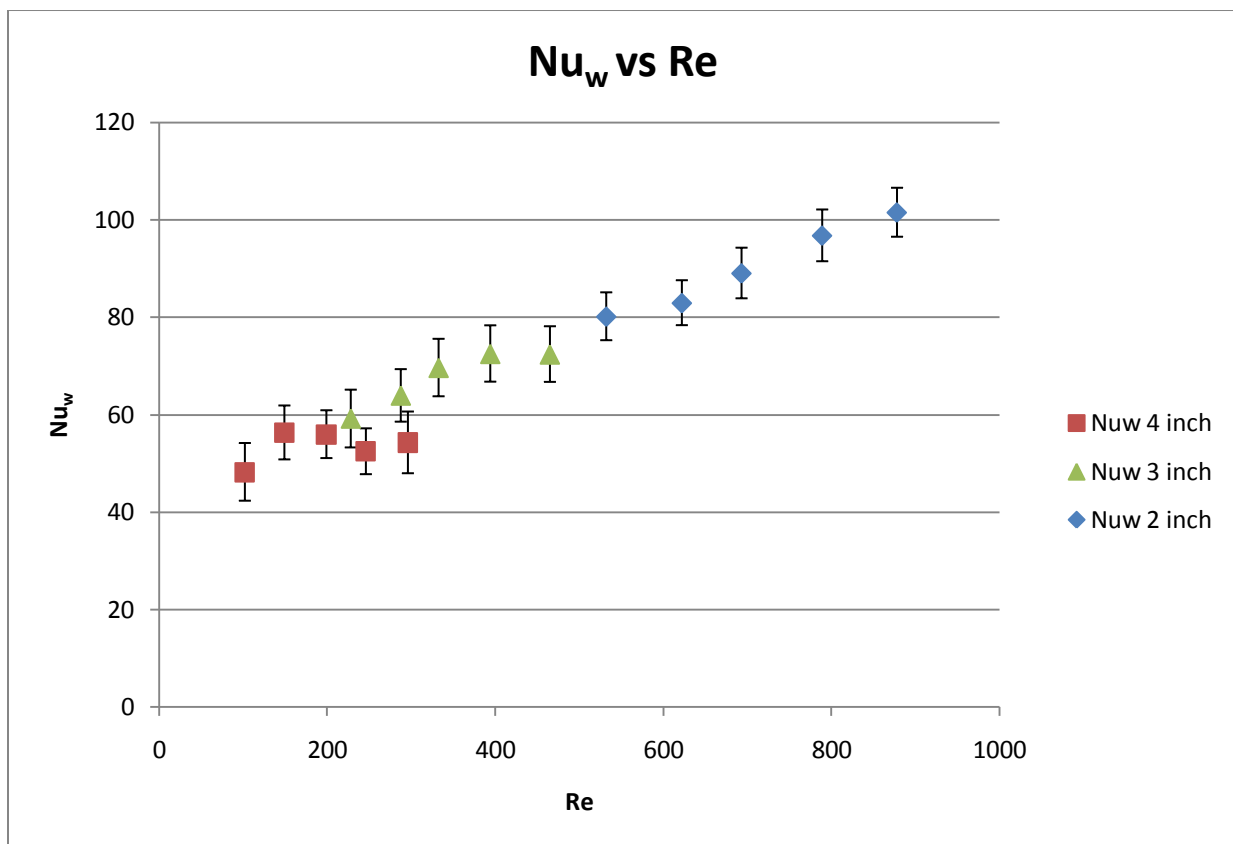
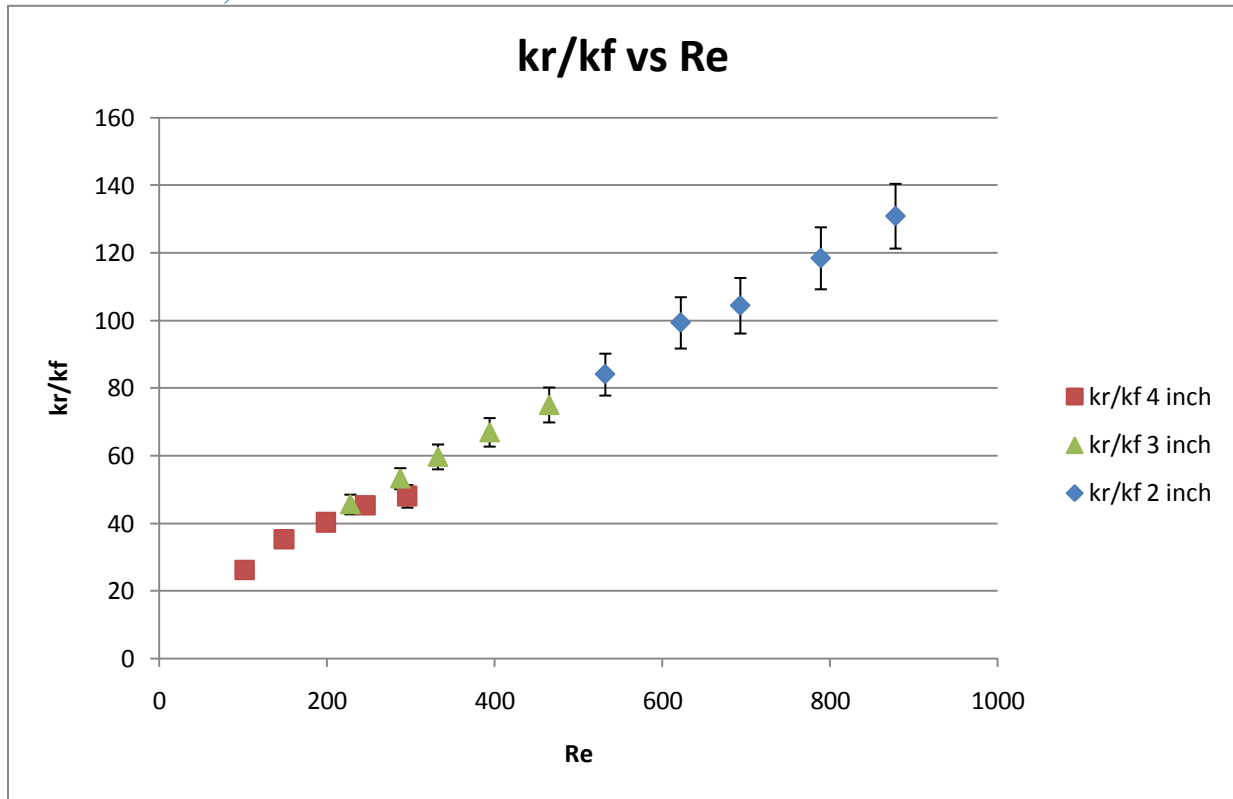


4 inch Tube

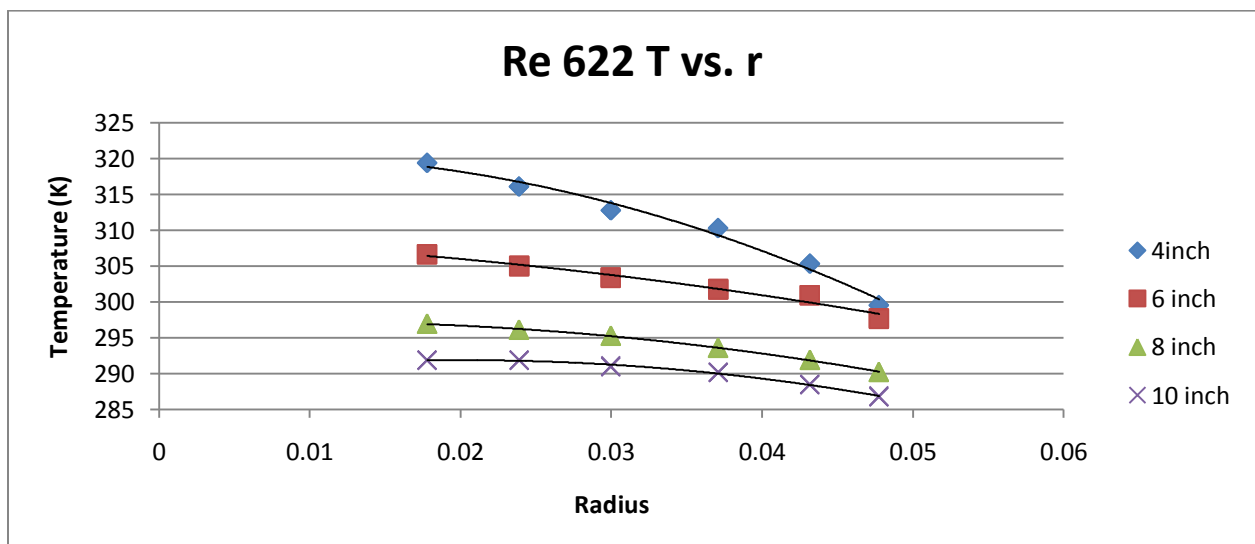
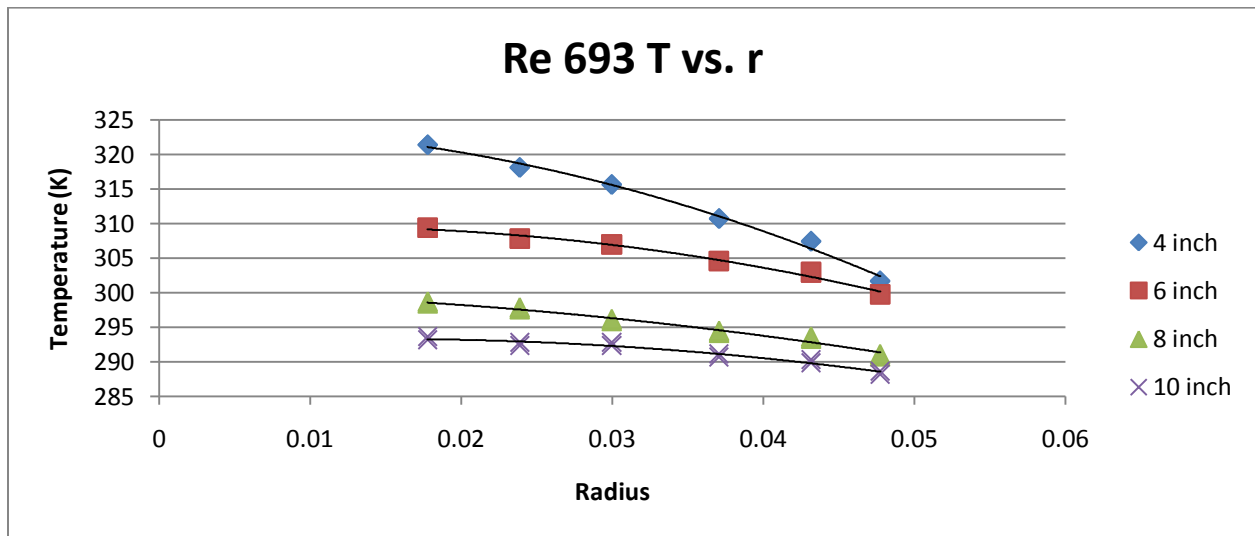
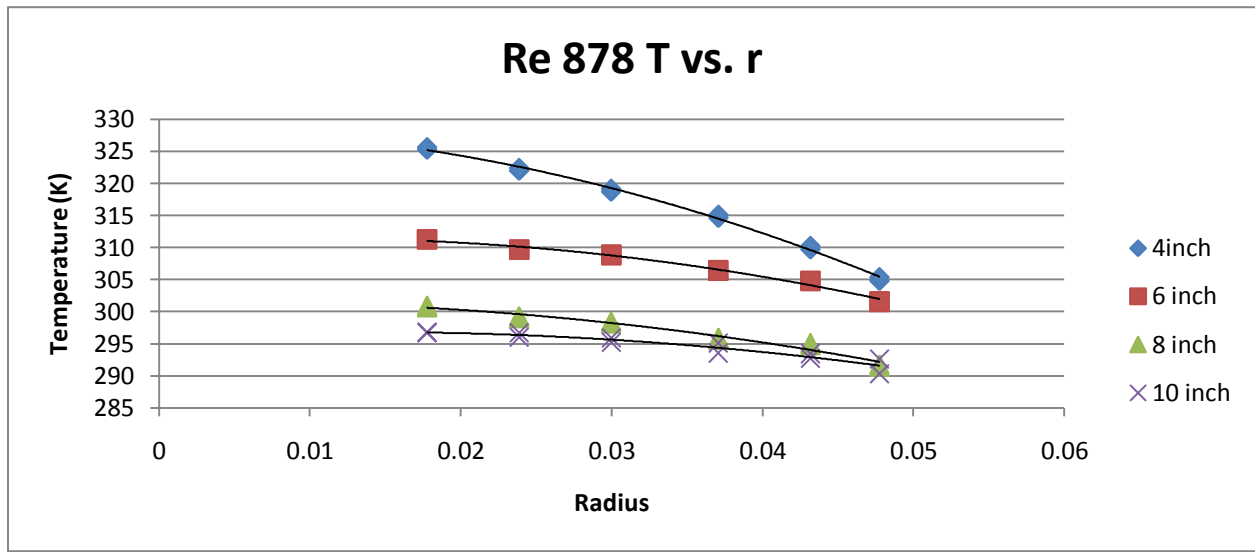




### Combined $kr/k_f$ , $Nu_w$



## Experimental Temperature Profile



## Comparison of Experimental T-Profile to CFD

